SANDIA REPORT

SAND2015-1746
Unlimited Release
Printed March 2015

Analysis of Dust Samples Collected from an Unused Spent Nuclear Fuel Interim Storage Container at Hope Creek, Delaware

Charles R. Bryan and David G. Enos

Prepared by
Sandia National Laboratories
Albuquerque, New Mexico 87185 and Livermore, California 94550

Sandia National Laboratories is a multi-program laboratory managed and operated by Sandia Corporation, a wholly owned subsidiary of Lockheed Martin Corporation, for the U.S. Department of Energy's National Nuclear Security Administration under contract DE-AC04-94AL85000.

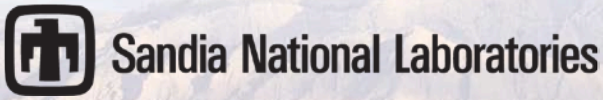

Issued by Sandia National Laboratories, operated for the United States Department of Energy by Sandia Corporation.

Available to DOE and DOE contractors from
U.S. Department of Energy
Office of Scientific and Technical Information
P.O. Box 62
Oak Ridge, TN 37831

Telephone: (865) 576-8401
Facsimile: (865) 576-5728
E-Mail: reports@adonis.osti.gov
Online ordering: http://www.osti.gov/bridge

Available to the public from
U.S. Department of Commerce
National Technical Information Service
5285 Port Royal Rd.
Springfield, VA 22161

Telephone: (800) 553-6847
Facsimile: (703) 605-6900
E-Mail: orders@ntis.fedworld.gov
Online order: http://www.ntis.gov/help/ordermethods.asp?loc=7-4-0#online

SAND2015-1746
Unlimited Release
Printed March 2015

Analysis of Dust Samples Collected from an Unused Spent Nuclear Fuel Interim Storage Container at Hope Creek, Delaware

Charles R. Bryan
Storage and Transportation Technologies Department
Sandia National Laboratories
P.O. Box 5800
Albuquerque, New Mexico 87185-MS0779

David G. Enos
Materials Reliability Department
Sandia National Laboratories
P.O. Box 5800
Albuquerque, New Mexico 87185-MS0888

Abstract

In July, 2014, the Electric Power Research Institute and industry partners sampled dust on the surface of an unused canister that had been stored in an overpack at the Hope Creek Nuclear Generating Station for approximately one year. The foreign material exclusion (FME) cover that had been on the top of the canister during storage, and a second recently-removed FME cover, were also sampled. This report summarizes the results of analyses of dust samples collected from the unused Hope Creek canister and the FME covers.

Both wet and dry samples of the dust/salts were collected, using SaltSmart™ sensors and Scotch-Brite™ abrasive pads, respectively. The SaltSmart™ samples were leached and the leachate analyzed chemically to determine the composition and surface load per unit area of soluble salts present on the canister surface. The dry pad samples were analyzed by X-ray fluorescence and by scanning electron microscopy to determine dust texture and mineralogy; and by leaching and chemical analysis to determine soluble salt compositions. The analyses showed that the dominant particles on the canister surface were stainless steel particles, generated during manufacturing of the canister. Sparse environmentally-derived silicates and aluminosilicates were also present. Salt phases were sparse, and consisted of mostly of sulfates with rare nitrates and chlorides. On the FME covers, the dusts were mostly silicates/aluminosilicates; the soluble salts were consistent with those on the canister surface, and were dominantly sulfates. It should

be noted that the FME covers were washed by rain prior to sampling, which had an unknown effect of the measured salt loads and compositions.

Sulfate salts dominated the assemblages on the canister and FME surfaces, and included Ca-SO_4, but also Na-SO_4, K-SO_4, and Na-Al-SO_4. It is likely that these salts were formed by particle-gas conversion reactions, either prior to, or after, deposition. These reactions involve reaction of carbonate, chloride, or nitrate salts with atmospheric SO_2, sulfuric acid, or ammonium sulfate to form sulfate minerals. The Na-Al-SO_4 phase is unusual, and may have formed by reaction of Na-Al containing phases in aluminum smelter emissions with SO_2, also present in smelter emissions. An aluminum smelter is located in Camden, NJ, 40 miles NE of the Hope Creek Site.

ACKNOWLEDGMENTS

This work was carried out as part of a Cooperative Research and Development Agreement with the Electric Power Research Institute. EPRI directed and funded sample collection activities at the fuel storage installations and provided the samples to Sandia for analysis and interpretation. Sampling was performed by Laszlo Zsidai and personnel from Holtec International, with support from personnel of the Hope Creek Nuclear Power Plant. At Sandia, Mark Rodriguez performed XRF and XRD analyses, and Amy Allen provided SEM/EDS support. Kirsten Norman helped with sample preparation.

CONTENTS

FIGURES

TABLES

NOMENCLATURE

DOE	Department of Energy
EDS	energy dispersive [X-ray] spectroscopy
EPRI	Electric Power Research Institute
FME	foreign material exclusion [cover]
IC	ion chromatography
ICP-OES	inductively coupled plasma-optical emission spectroscopy
ISFSI	independent spent fuel storage installation
SCC	stress corrosion cracking
SEM	scanning electron microscope
SNF	spent nuclear fuel
SNL	Sandia National Laboratories
XRD	X-ray diffraction
XRF	X-ray fluorescence

1. INTRODUCTION

When spent nuclear fuel (SNF) storage pools at commercial nuclear reactors become filled to capacity, it is necessary to shift SNF to dry storage systems. Modern dry storage systems consist of a stainless steel canister within an overpack that protects the canister from the weather. Decay heat from the waste drives convective airflow through an annulus between the overpack and the canister, cooling the container. Over time, dust, drawn into the overpacks with the circulating air, is deposited on the surfaces of containers within the storage systems. Salts within the dust will deliquesce as heat production declines over time and the packages cool, and it is possible that deliquescence-induced corrosion of the stainless steel waste container could lead to penetration of the container walls by chloride-induced stress corrosion cracking (SCC). To address this concern, the Electrical Power Research Institute (EPRI) has instituted a sampling program for the dust on the surface of in-service SNF storage canisters. The first samples were collected from a NUHOMS horizontal storage system at the Calvert Cliffs Independent Spent Fuel Storage Installation (ISFSI) in June 2012, 15.6 years after waste emplacement (Calvert Cliffs Nuclear Power Plant, 2012). In November 2013, the second set of samples was collected at Hope Creek, from canisters in storage for 7 years; and in January, 2014, a third set was collected from Diablo Canyon, from canisters in storage for 2-4 years. The Calvert Cliffs samples were analyzed in part by an external lab contracted by EPRI, and in part by Sandia National Laboratories (SNL) and are reported elsewhere (Calvert Cliffs Nuclear Power Plant, 2013; DOE, 2013). The samples from the Hope Creek and Diablo Canyon sites were characterized by SNL (Bryan and Enos, 2014).

In July, 2014, EPRI went back to the Hope Creek facility and sampled dust on the surface of an unused canister that had been stored in an overpack at the site for approximately one year. Since the canister was empty and had no heat load, convective airflow through the overpack was very limited, and it was anticipated that dust loads on the canister surface would be very light. The dust compositional data for a cold, unused canister complements that from dust on the hot in-service canisters, potentially allowing evaluation of the effects of temperature on the salt compositions. The foreign material exclusion (FME) cover that had been on the top of the canister during storage, and a second recently-removed FME cover, were also sampled. The sampling was done for several reasons. First, it offered the opportunity to assess the potential effects of heating on dust deposited on an in-service canister relative to dust deposited under ambient conditions on the unused canister. Second, it could be done easily, since the empty canister was not emitting high levels of radiation. Finally, if offered an additional opportunity to collect and analyze dust deposited on a vertical steel surface at the Hope Creek site.

This report summarizes the results of the analyses of the dust samples collected from the unused Hope Creek canister and FME covers. The sample types collected were similar to those described previously for the Hope Creek and Diablo Canyon sampling episodes (Bryan and Enos, 2014). Both wet and dry samples of the dust/salts were collected, using two different devices:

- The wet samples were collected using SaltSmart™ sensors (Louisville Solutions, Inc.). However, since there was not radiation field around the canister, these were collected by hand, rather than with a remote sampling tool.

- Dry dust samples were collected with a sampling tool consisting of a rectangular piece of a abrasive Scotch-Brite™ abrasive pad, backed with a stainless steel plate. However, the Scotch-Brite™ pads used to sample the in-service canisters at Hope Creek and Diablo Canyon contained a great deal of talc filler, and several soluble salt components leached readily from the matrix of the pads, interfering with compositional analysis. For this reason, a different pad, similar to that used in the original Calvert Cliffs testing, was used. The abrasive pads were Scotch-Brite™ Type 7440 pads, made by 3M Company. The material safety data sheet for the pads indicates that the pads are nylon fibers (5-15 wt%), with aluminum oxide as the abrasive (45-65 wt%),bound together with a cured mixed-polymer resin (15-40 wt%). A small amount of titanium oxide (0.5-2.75 wt%) is present; later analysis showed that it was primarily present in the white letters stenciled onto the surface of the pads. Note that for samples 387-009, 387-011, and 389-015, white lettering was observed on the surface of the sampling pad.

First, the wet samples were analyzed by chemical analysis to determine the composition and surface load per unit area of soluble salts present. Each of the Scotch-Brite™ pads was removed from its stainless steel backing plate and analyzed by X-ray fluorescence (XRF) to obtain bulk chemical compositions. Then, each pad was sectioned, and a small portion of the sponge was removed and retained for Scanning Electron Microscopy (SEM) imaging and energy dispersive system (EDS) element mapping. The remaining pad was washed thoroughly with deionized water and the leachate collected, filtered, and analyzed for soluble salts. A tiny amount of insoluble residue was collected during the washing process; however, the sample size was so small that bulk analysis was not attempted. It is important to note that the soluble salt data from the dry pad leachate cannot be used to determine the surface load of salts on the canister surface, as it is unknown what area of the surface was contacted when the pad was brushed across the surface, and because the efficiency of collection of dust by the dry pad is unknown, and is likely to be much less than 100%.

Sampling and analytical methods, and a list of the samples collected, are provided in Section 2 of this report. Section 3 summarizes the results of the different analyses (complete sets of SEM/EDS and XRF analyses are provided in Appendices A and B), and Section 4 provides conclusions.

As discussed in the following sections, the dust samples from the surface of the unused canister at Hope Creek were dominantly particles of stainless steel. Terrestrially-derived silicate/aluminosilicate dust particles and salts were also present, but at much lower abundances. The salts were dominantly sulfates, with rare chlorides and nitrates. The FME covers had been stored in the open for a few days prior to sampling, and a rainstorm had washed them. Sampling showed that despite the rain, dust and salts remained on the surface; however, the degree to which these salts represent what was there prior to the rain is unknown. The FME dusts were almost entirely silicates/aluminosilicates, but sulfate salts were also abundant; nitrate and chloride salts were rare, as were stainless steel particles. The abundance of stainless steel particles on the canister surface and the relative paucity of stainless steel particles relative to environmentally-derived particles on the FME cover strongly suggest that the stainless steel particles were created during the canister manufacturing process and were not deposited after relocation of the canister to the Hope Creek Site.

Sulfate salts dominated the assemblages on the canister and FME surfaces, and included Ca-SO_4, Na-SO_4, K-SO_4, and Na-Al-SO_4. It is likely that these salts were formed by particle-gas conversion reactions, either prior to, or after, deposition. These involve reaction of carbonate, chloride, or nitrate salts with atmospheric SO_2, sulfuric acid, or ammonium sulfate to form sulfates. The Na-Al-SO_4 phase is unusual, and may have formed by reaction of particles or gasses in aluminum smelter emissions; an aluminum smelter is located in Camden, NJ, 40 miles NE of the Hope Creek Site.

While SaltSmart™ chemical analyses, SEM/EDS analyses, and XRF analysis are consistent in indicating that sulfates are the dominant salts present, the leachates from the dry pad samples differed, and were rich in chloride. It is likely that the high chloride concentrations are artifacts due to leaching from the pad matrices; however, no definitive conclusion can be reached.

2. SAMPLES AND METHODS

2.1. Samples

Unlike the sampling of the in-service canisters at Hope Creek where extensive tooling was required to acquire dust samples, the unused canister, MPC-387, was removed from its overpack and the SaltSmart™ and Scotch-Brite™ samples were collected by hand. Samples were collected from three locations on the side of the canister. The sampling plan called for then sampling dust on the Foreign Material Exclusion (FME) cover on top of the canister; however, the FME cover was inadvertently removed and placed outdoors inan exposed location, and the top of the canister sampled instead. When the error was discovered, the sampling team returned to the site and collected samples from the FME cover. An adjacent FME cover (MPC-389), also in exposed storage, was also sampled. Unfortunately, in the intervening few days, a thunderstorm had thoroughly washed the FME covers, probably removing most of the soluble salts.

Table 1 lists the samples that were collected, and provides the sampling location. The SaltSmart™ sensors are referred to as wet samples, because the salts were leached off the storage canister surface by water passing through the wick. The abrasive pads collected dust without the aid of water, and are referred to as dry samples.

Upon delivery to Sandia, the samples were examined and a description was recorded. No discoloration was visible on any samples; salt and dust loads on the Saltsmart™ wicks and the Scotch-Brite™ pads were too light to be seen. When the SaltSmart™ samples were disassembled to extract the soluble salts, the condition of the wick and the reservoir pad was also noted; no discoloration was observed. It should be noted that some of the Scotch-Brite™ pads (samples 387-009, 387-011, and 389-015) had white stenciled numbers on the surface, which consist largely of titanium oxide.

2.2. Methods

The methods and equipment used to characterize the samples are identical to those used previously for the in-service canisters are provided in summary below. A more detailed discussion of each method is presented in Bryan and Enos (2014). The methods include:

- *XRF analysis*. This method was implemented as a microbeam technique, allowing chemical mapping of the dry dust samples on the surface of the collection pads, with a resolution of ~25 µm. It provides semi-quantitative chemical analyses. However, one limitation is that elements lighter than sodium (e.g. oxygen, nitrogen, carbon) cannot be detected, and sensitivity to sodium is low.

- *SEM imaging and EDS element mapping. SEM/EDS analysis of the dry dust samples* provides textural and mineralogical information of dust/dust components, and allows visual identification of organic matter (floral/faunal fragments).

- *Chemical analyses of the dust and soluble salts.* The soluble salts were leached from the components of the SaltSmart™ sensors and analyzed. For the dry samples, the Scotch-Brite™ pad was washed thoroughly with deionized water and the leachate collected and filtered. The leachate was then analyzed for soluble salts.

Table 1. Hope Creek Samples from Unused Storage Canister MPC-387

Sample #	Sample Type	Sample location
387-001	Dry pad	Canister side, 1 foot from base
387-002	SaltSmart	Canister side, 1 foot from base
387-003	Dry pad	Canister side, 1 foot from top
387-004	SaltSmart	Canister side, 1 foot from top
387-005	Dry pad	Canister lid, 1 foot from edge
387-006	SaltSmart	Canister lid, 1 foot from edge
387-007	Dry pad	Canister lid, center
387-008	SaltSmart	Canister lid, center
387-009	Dry pad	Canister side, 5 feet from base
387-010	SaltSmart	Canister side, 5 feet from base
387-011	Dry pad	FME cover, 1 foot from edge
387-012	SaltSmart	FME cover, 1 foot from edge
387-013	Dry pad	FME cover, center
387-014	SaltSmart	FME cover, center
389-015	Dry pad	FME cover, 1 foot from edge
389-016	SaltSmart	FME cover, 1 foot from edge
387-017	SaltSmart	FME cover, center

3. RESULTS

3.1. SEM/EDS Analysis

SEM/EDS analysis of the dry pad samples was carried out to determine dust and salt mineralogy, to identify organic materials present, and to determine dust particle size and morphology. Analyzed samples include pads from the Hope Creek unused canister and from the FME cover (Table 1). SEM images were taken of characteristic features and EDS element mapping was done to assess mineralogy. Results are summarized here with typical images from some samples; a complete suite of analyses is provided in Appendix A, and allows the reader to better assess the representativeness of the results provided here.

3.1.1. Pad blank

The Scotch-Brite™ pads used for this sampling project are similar to those used previously in dust sampling at the Calvert Cliffs facility, which are described in Enos et al. (2013). Figure 1 is a backscattered electron image of the Scotch-brite™ pad blank (Enos et al. 2013, Figure 9). The pads are made of nylon fibers 30-50µm in diameter, with aluminum oxide particles 200-400 µm in size as the abrasive, bound together with a cured resin (15-40 wt%). Titania is also present as white letters and numbers that are stenciled onto the pad. In at least some cases, the side of the pad used to sample the canister surface was the side with the letters. The coarse fibers and large abrasive grains provide good, broad substrates for dust particles, and are coarse enough to resist movement due to charging in the electron beam, providing a stable surface for imaging and analysis of dust particles.

It should be noted that although these pads were the same part number as those used in the Calvert Cliffs sampling, they were not purchased at the same time as the previous pads, and while the pads are grossly similar, slight differences were observed between these and the previous pads. For instance, within the pad matrix, these pads contained an organic compound that shrank in the SEM, leaving crevices on the pad surface. This was not observed on the pads used at Calvert Cliffs.

3.1.2. Samples from the Surface of Canister MPC-387

All of the Scotch-Brite™ pad samples that were collected from the canister were analyzed. These include three samples from the canister side at distances of 1 foot above the base (387-001), 5 feet above the base (387-009), and 1 foot below the top (387-003). Two additional samples were collected from the canister lid, 1 foot from the top edge (387-387-005), at the center (387-007).

The dry pad samples 387-001 and 387-003, from the side of the canister, were heavily coated with particulates (Figure 2). Sample 387-009, collected 5 feet above the base of the canister, is more lightly covered, but the mineralogy of the particles is the same. The great majority of the particles on the canister side are stainless steel, probably produced by grinding and finishing during the manufacturing of the canister. Note that in Figure 2 and all other SEM figures, the Ni map is not included to save space, however, as a component of stainless steel, Ni was co-located with Fe and Cr in all maps. A magnified image of the particles from 387-003, with EDS element maps, is shown in Figure 3. Rare aluminosilicate and salt particles are also present. These are

likely to have been deposited during storage at Hope Creek, although that is not certain. The aluminosilicates include quartz (Si-O) and a Ca-Mg aluminosilicate. Salt phases include Ca-SO_4, K-SO_4, and Na-K-SO_4 phases (sulfate or bisulfate) and Mg-Ca-carbonate; some examples are shown in Figure 4 and Figure 5. Additional images and element maps are provided in Appendix A.

Samples 387-005 and 387-007, from the top of the canister, are relatively lightly loaded (Figure 6). As with the samples from the side of the canister, the most abundant particles are stainless steel (Figure 7). Environmentally derived dust particles are rare, but include quartz and Mg-bearing aluminosilicates. Many salt phases are present, commonly as multi-mineralic clusters but also as individual phases. Ca-SO_4 is the most common phase, but also occurring are Na-SO_4 and K-SO_4 phases, Na-NO_3, NaCl, and Ca-Mg carbonate; these are often associated with aluminosilicates, probably clays (Figure 8 to Figure 12).

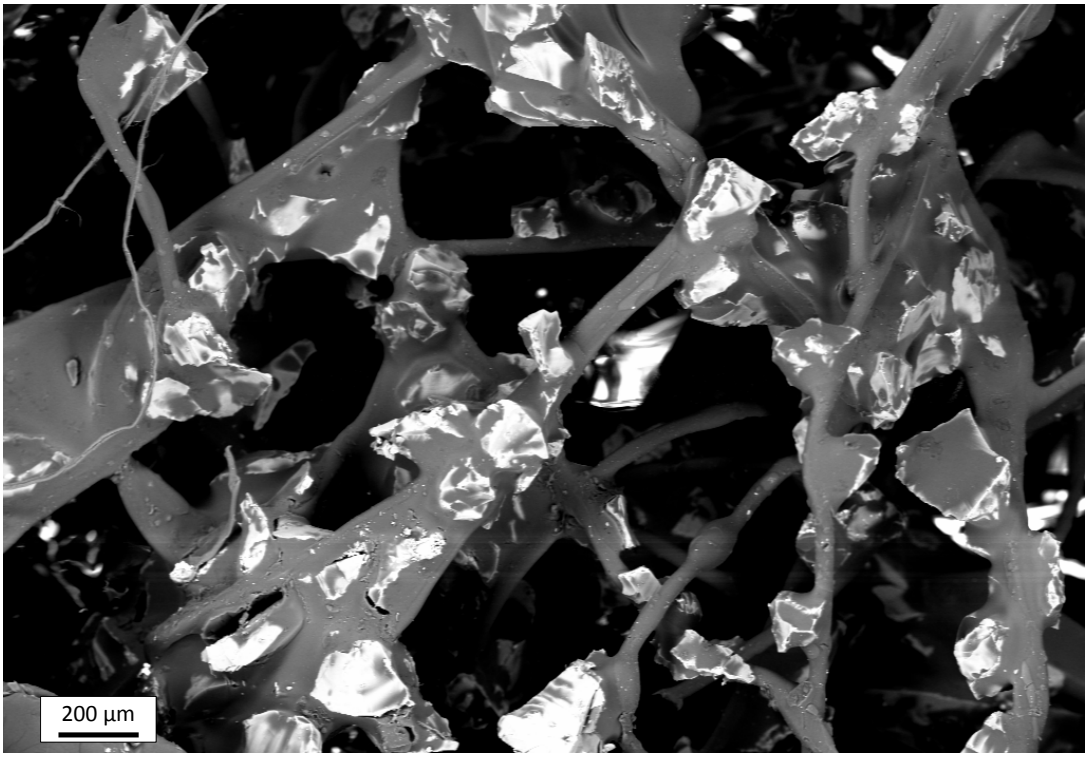

Figure 1. SEM backscattered electron image of the Scotch-Brite™ pad blank, showing the abrasive particles within the polymeric matrix.

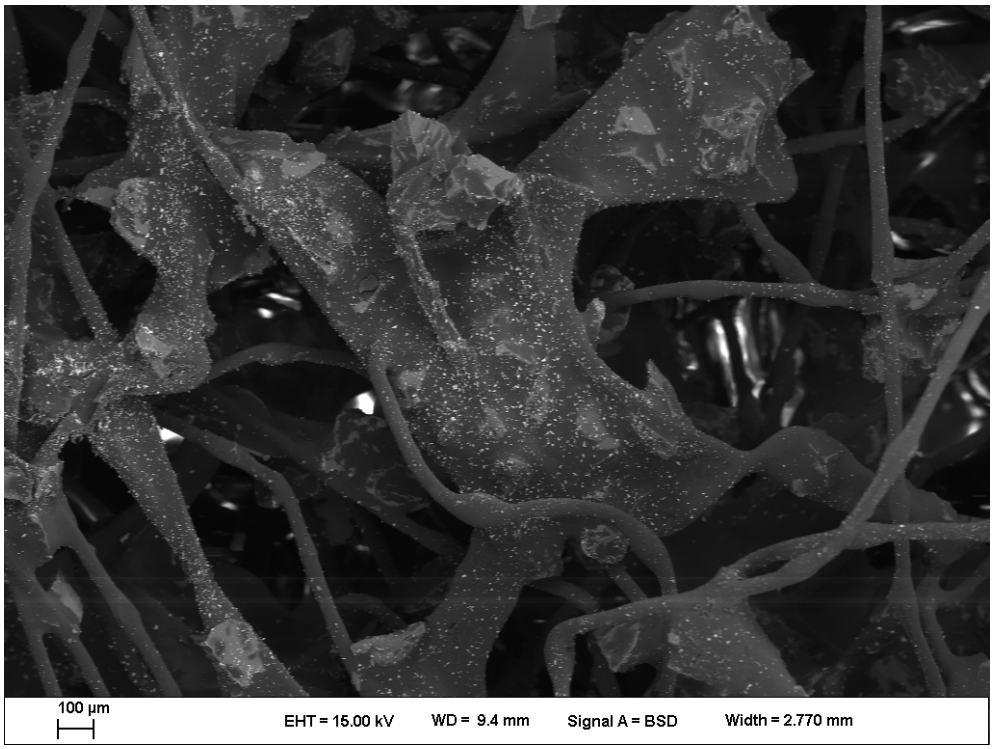

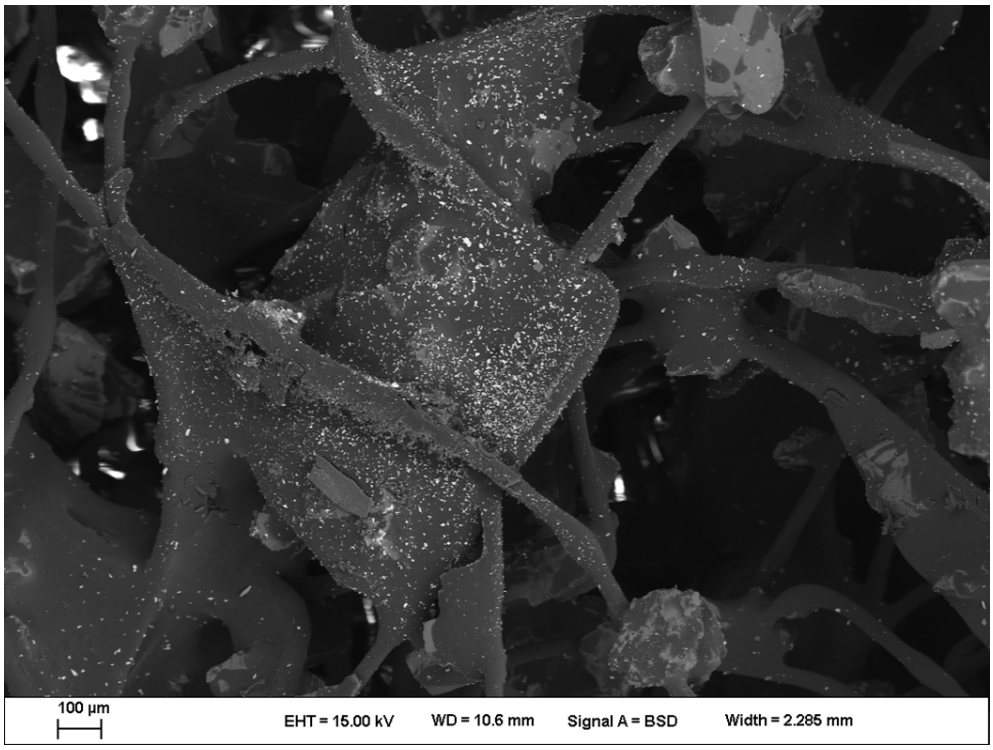

Figure 2. Upper: SEM image of pad sample 387-001, collected from the canister side, 1 foot above the bottom edge. Lower: SEM image of pad sample 387-003, collected from the canister side, 1 foot below the upper edge.

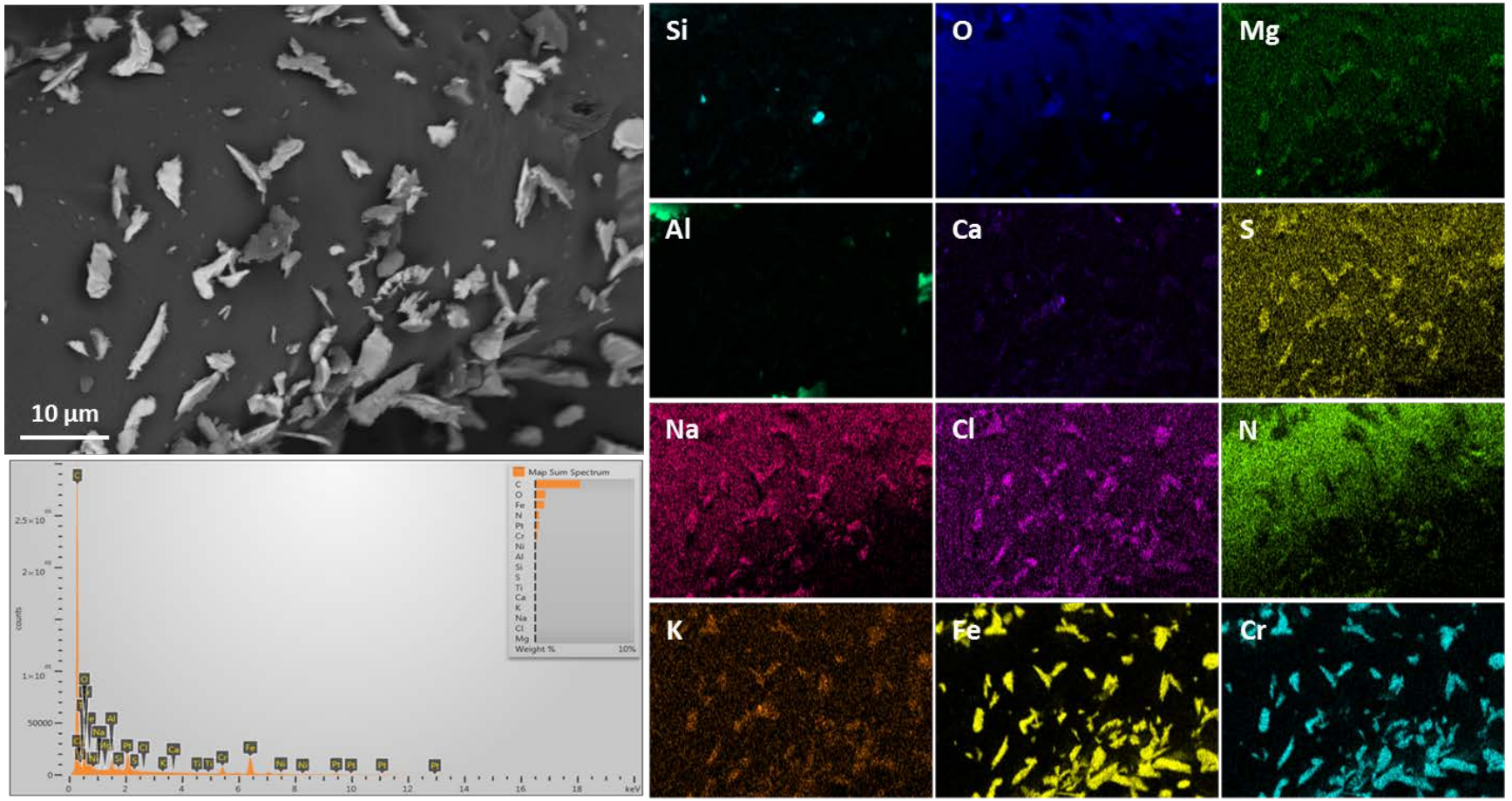

Figure 3. SEM image/EDS map of Sample 387-003, collected from the canister side, 1 foot above the bottom edge. Almost all particles are stainless steel.

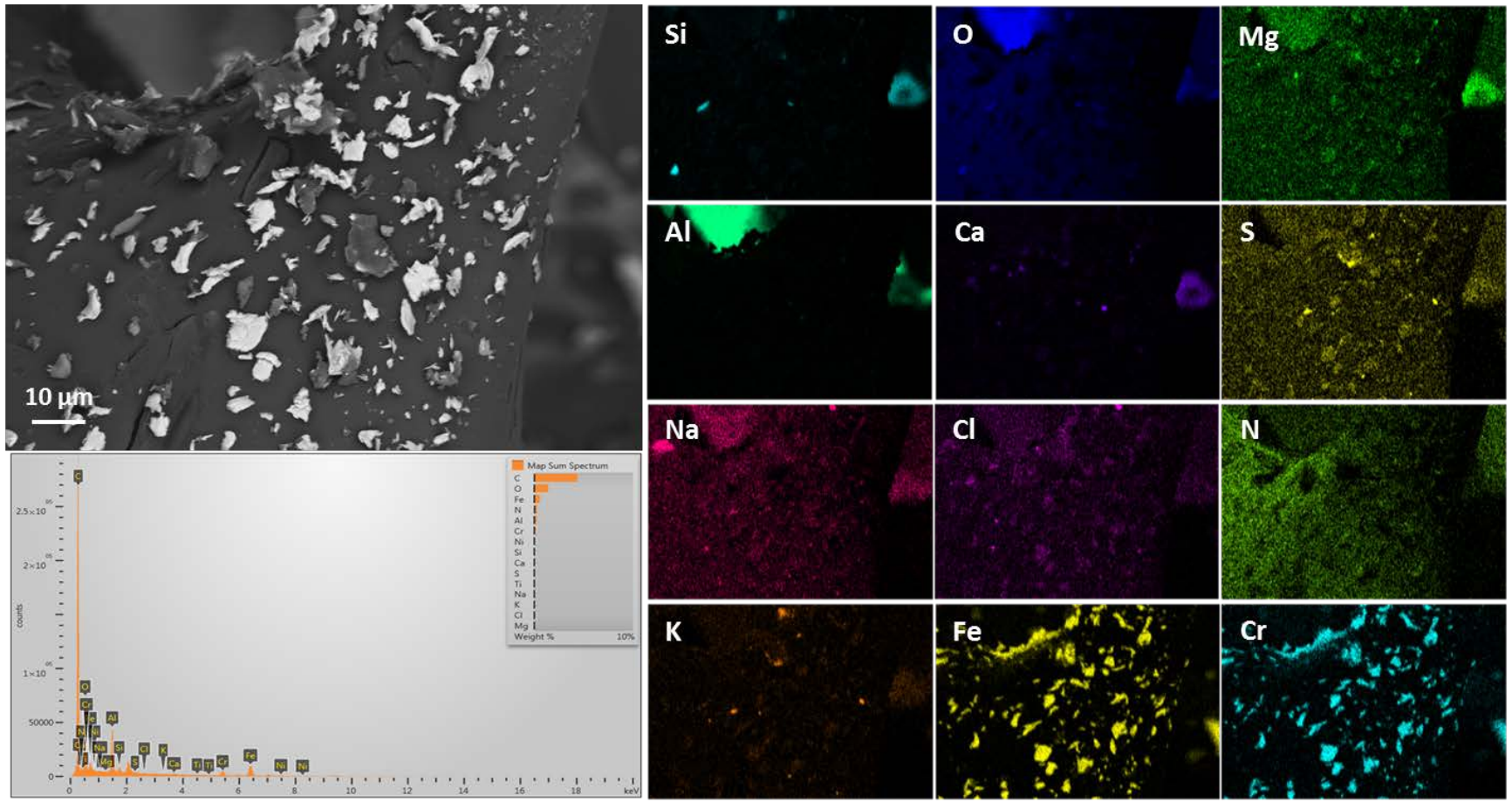

Figure 4. SEM image/EDS map of Sample 387-001, collected from the canister side, 1 foot above the bottom edge. Almost all particles are stainless steel. Note small grains of a Na-K-SO_4 phase.

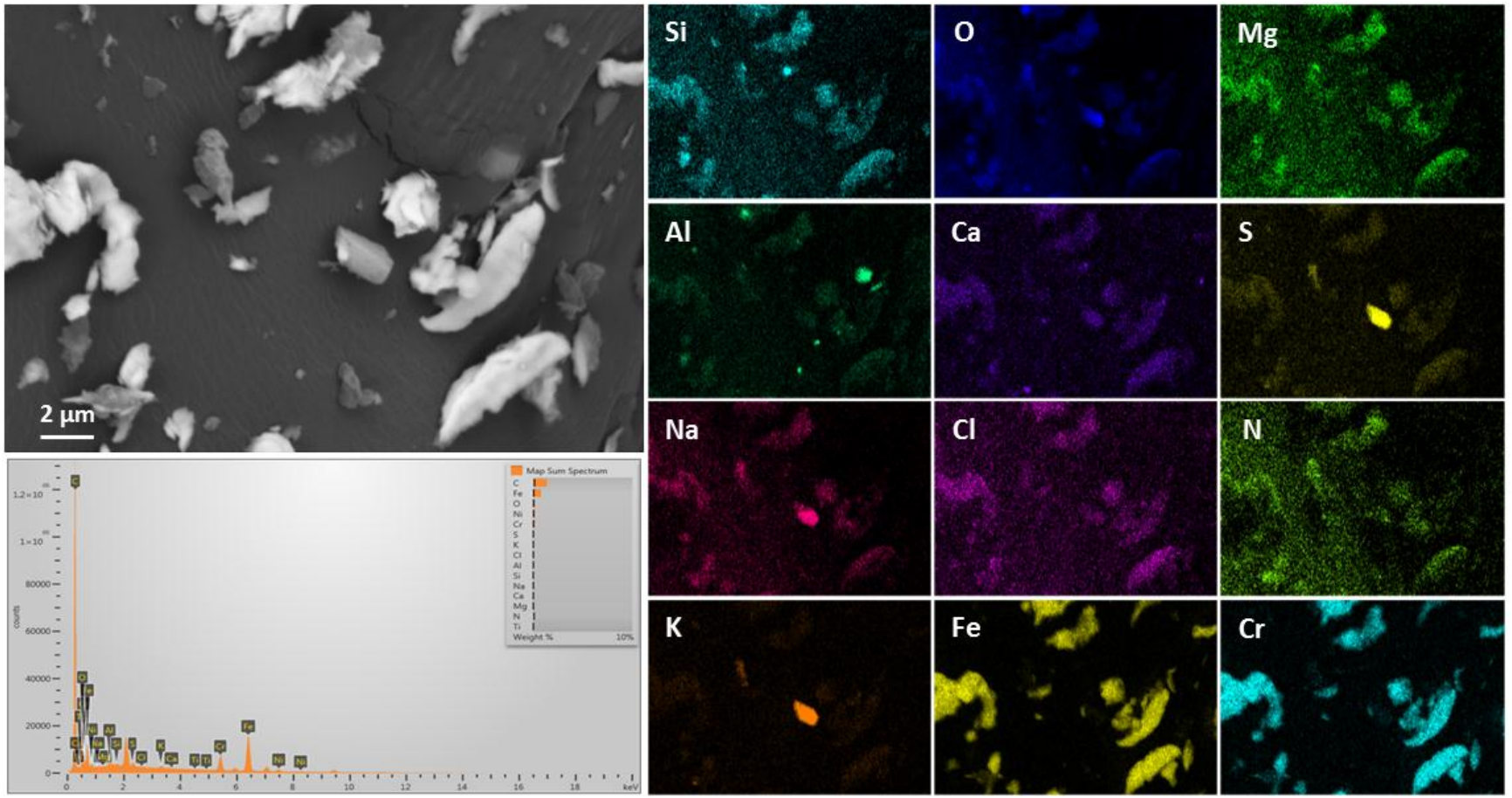

Figure 5. SEM image of sample 387-001, collected from the canister top, showing the heavy dust load. Magnified image of small Na-K-SO_4 grain shown in Figure 4, upper right.

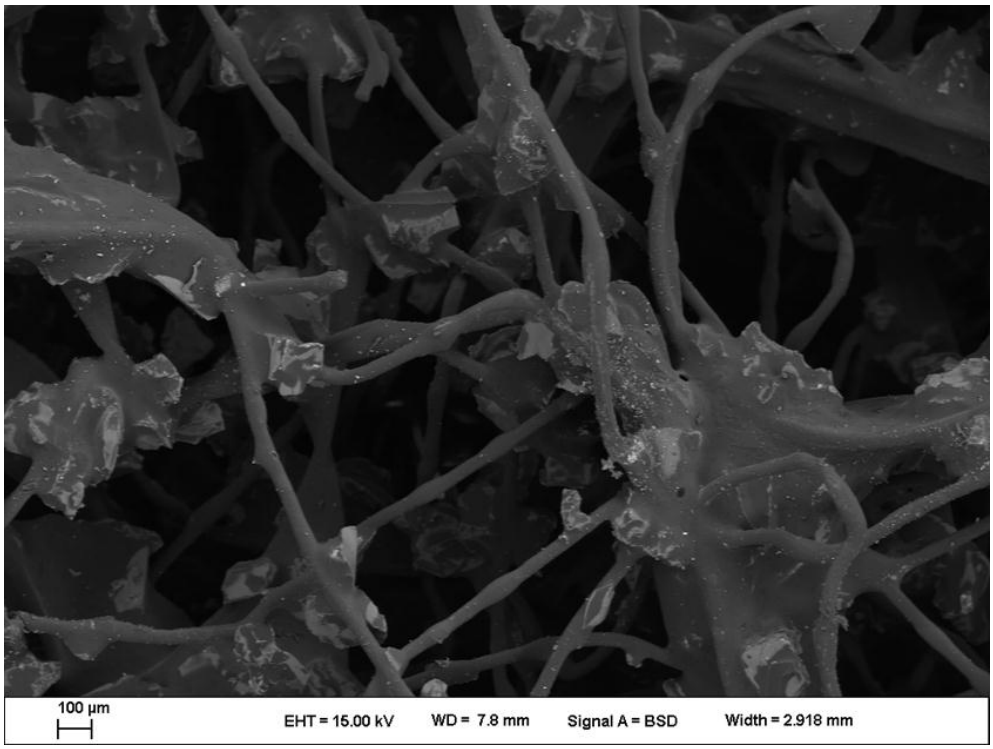

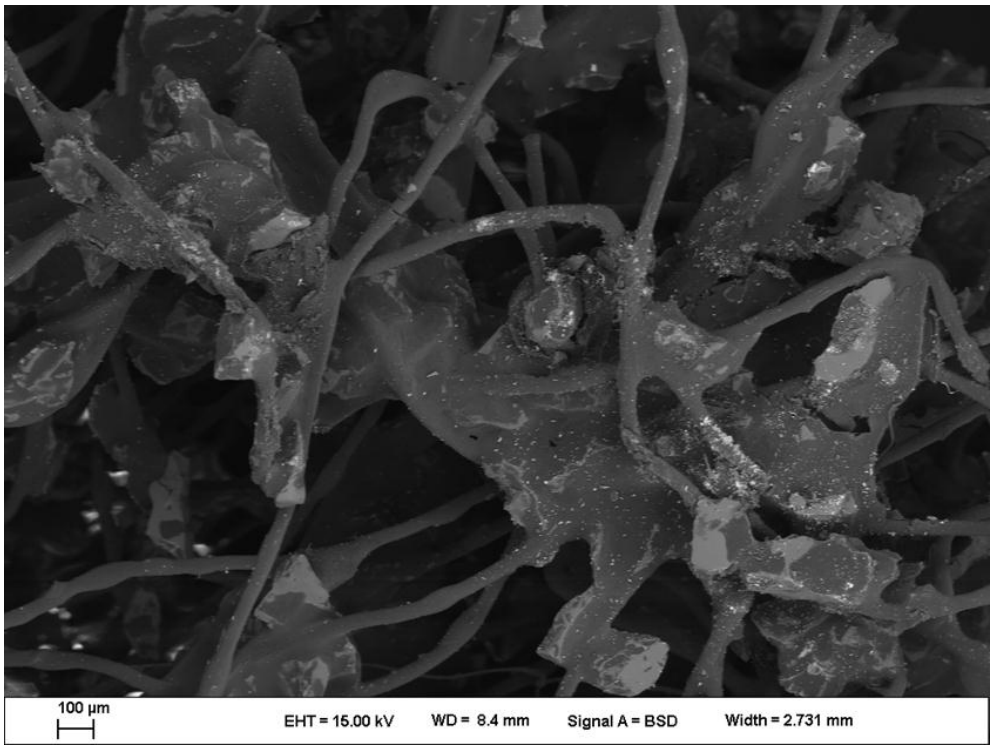

Figure 6. Upper: SEM image of pad sample 387-005, collected from the canister top, 1 foot from the edge. Lower: SEM image of pad sample 387-007, collected from the center of the canister top. Note light salt load (canister was stored with FME cover on top).

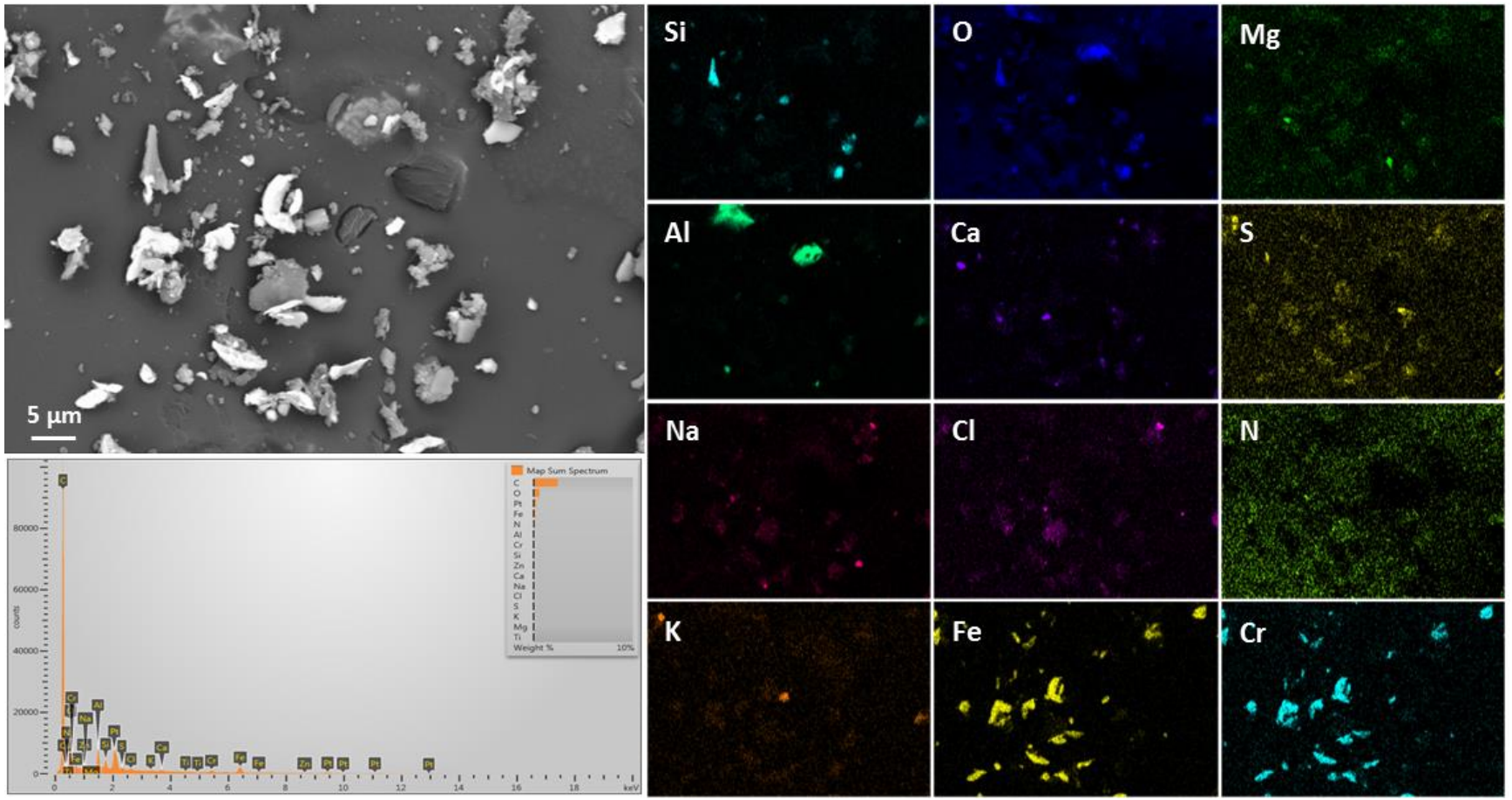

Figure 7. SEM image/EDS map #1 of Sample 387-005, collected from the canister top, 1 foot from the edge. Most particles are stainless steel. Note Na-Cl grain in upper left, K-SO_4 particle in upper right.

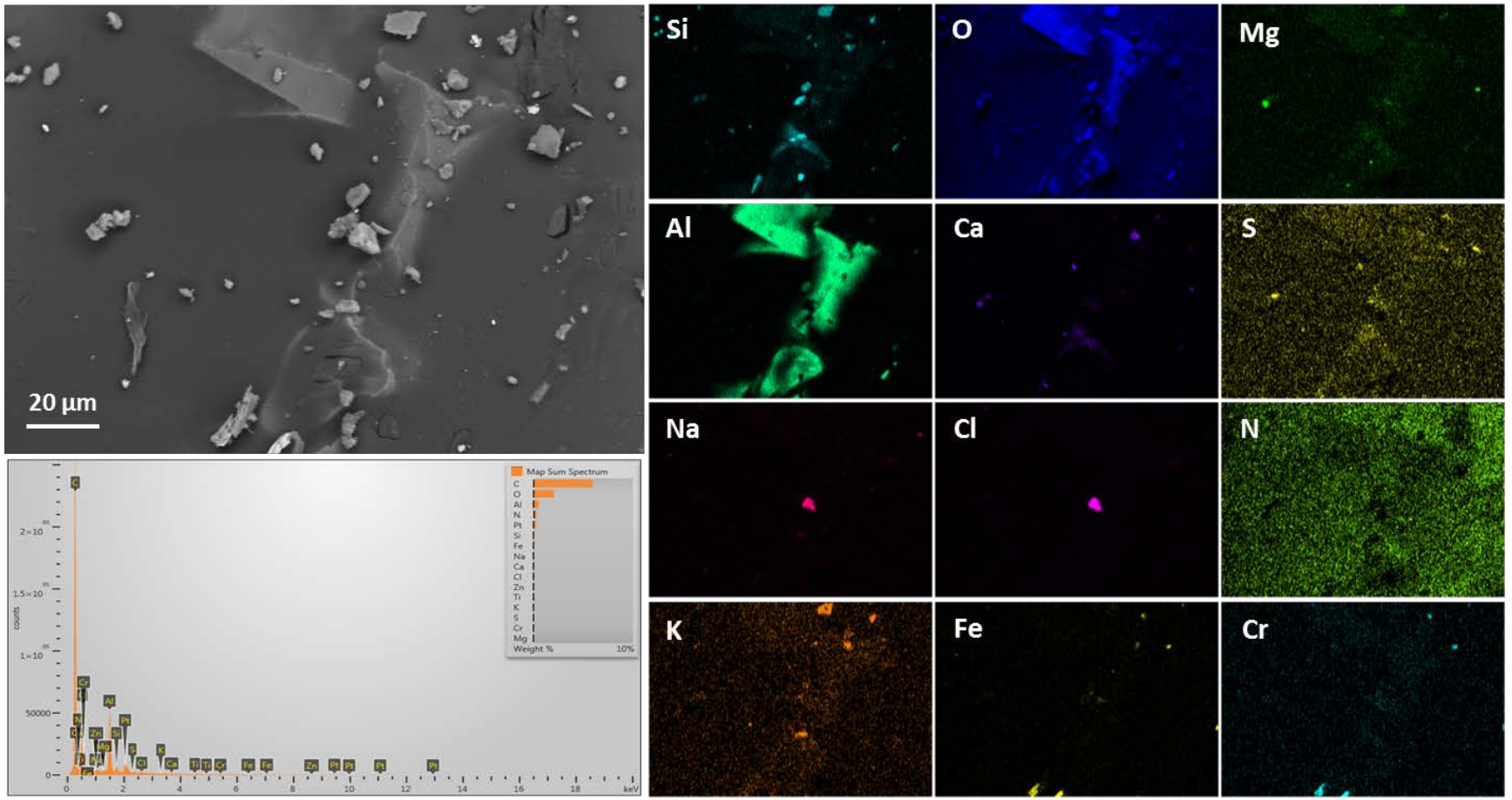

Figure 8. SEM image/EDS map #2 of Sample 387-005, collected from the canister top, 1 foot from the edge. Note Na-Cl grain in the center of the image.

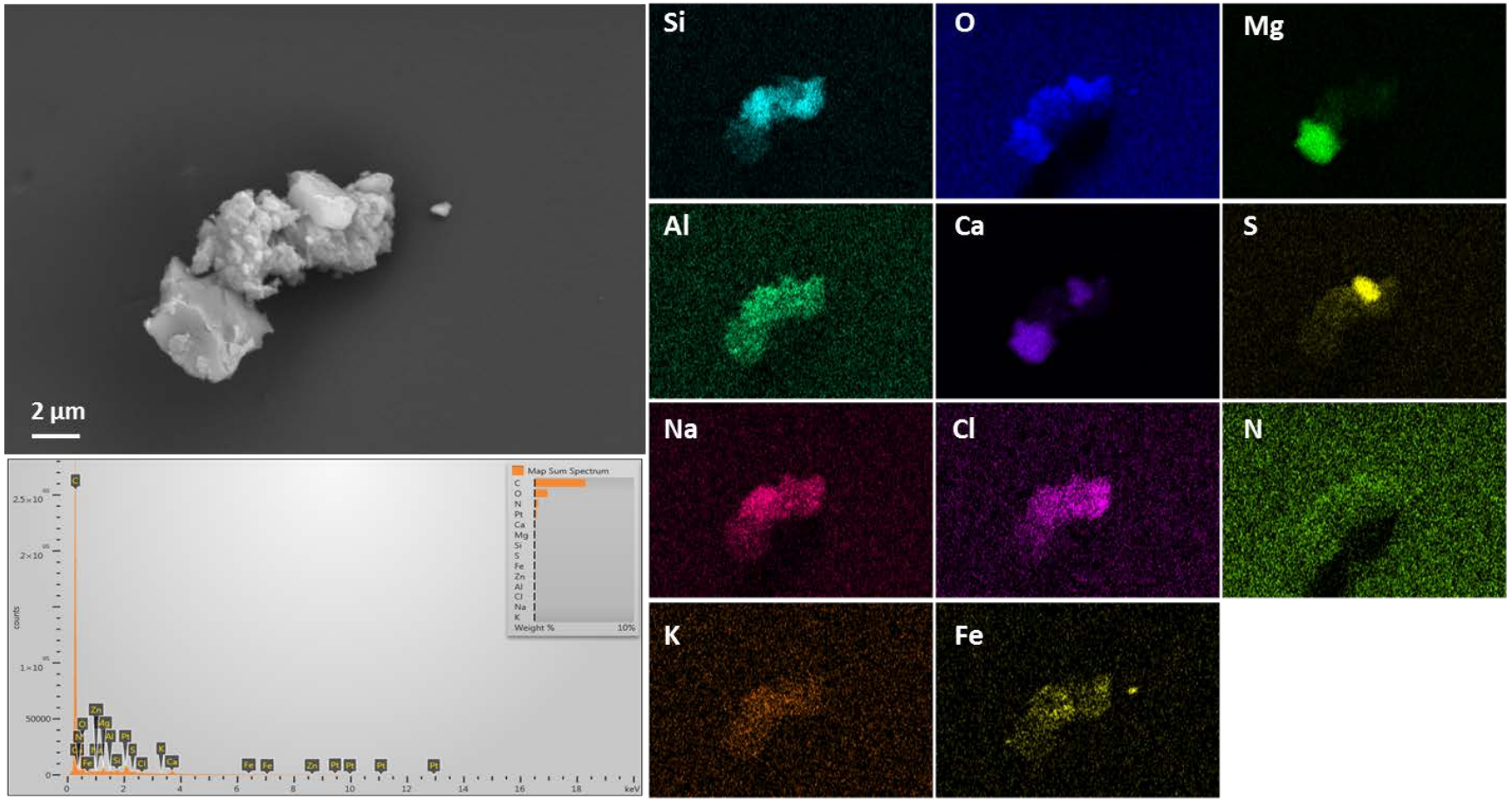

Figure 9. SEM image/EDS map #3 of Sample 387-005, collected from the canister top, 1 foot from the edge. Magnified image of composite grain in left center of Figure 8. Grain contains Ca-Mg-CO_3 and Ca-SO_4 phases.

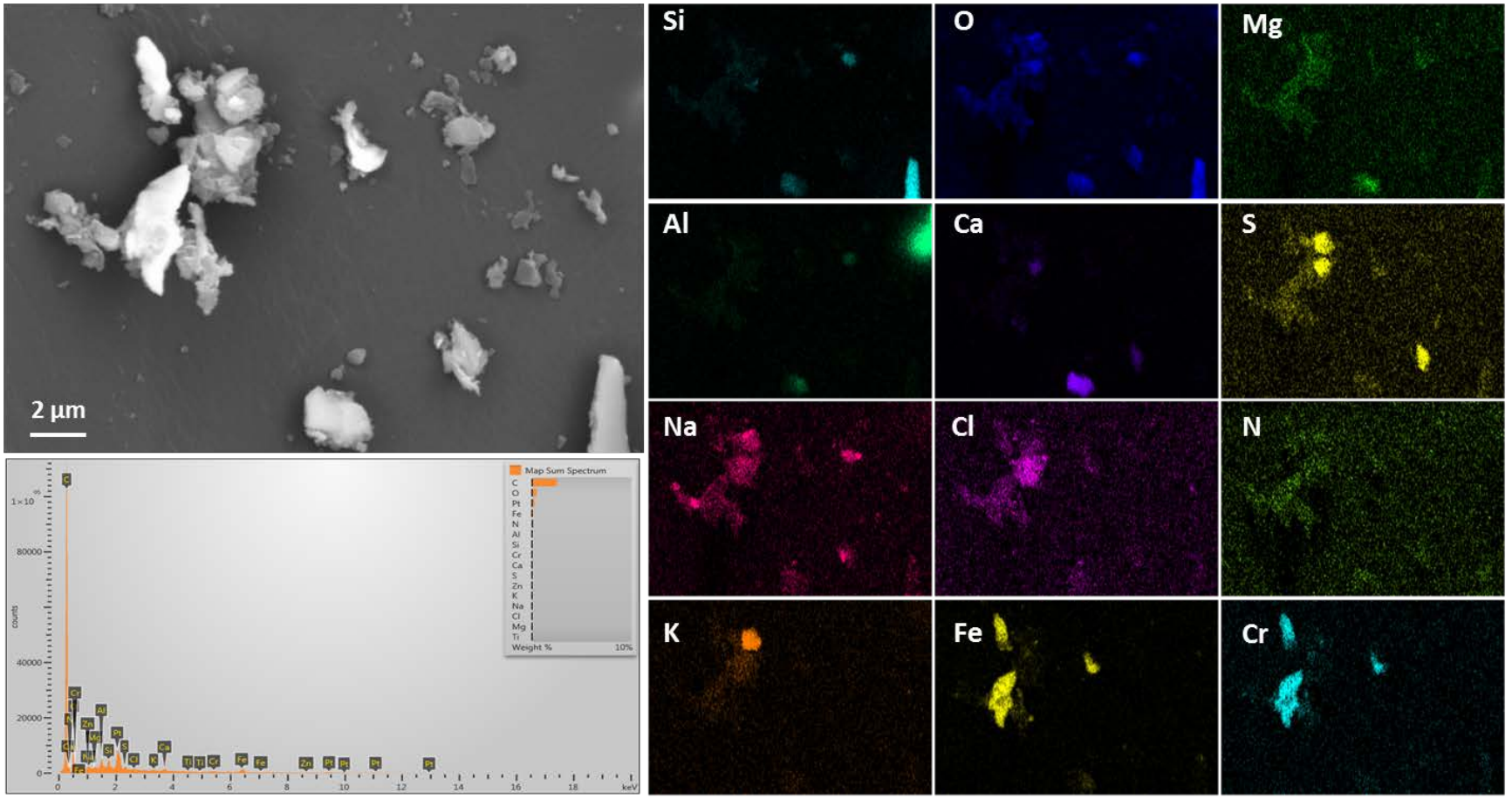

Figure 10. SEM image/EDS map #4 of Sample 387-005, collected from the canister top, 1 foot from the edge. Note stainless steel particles and SO_4 phases.

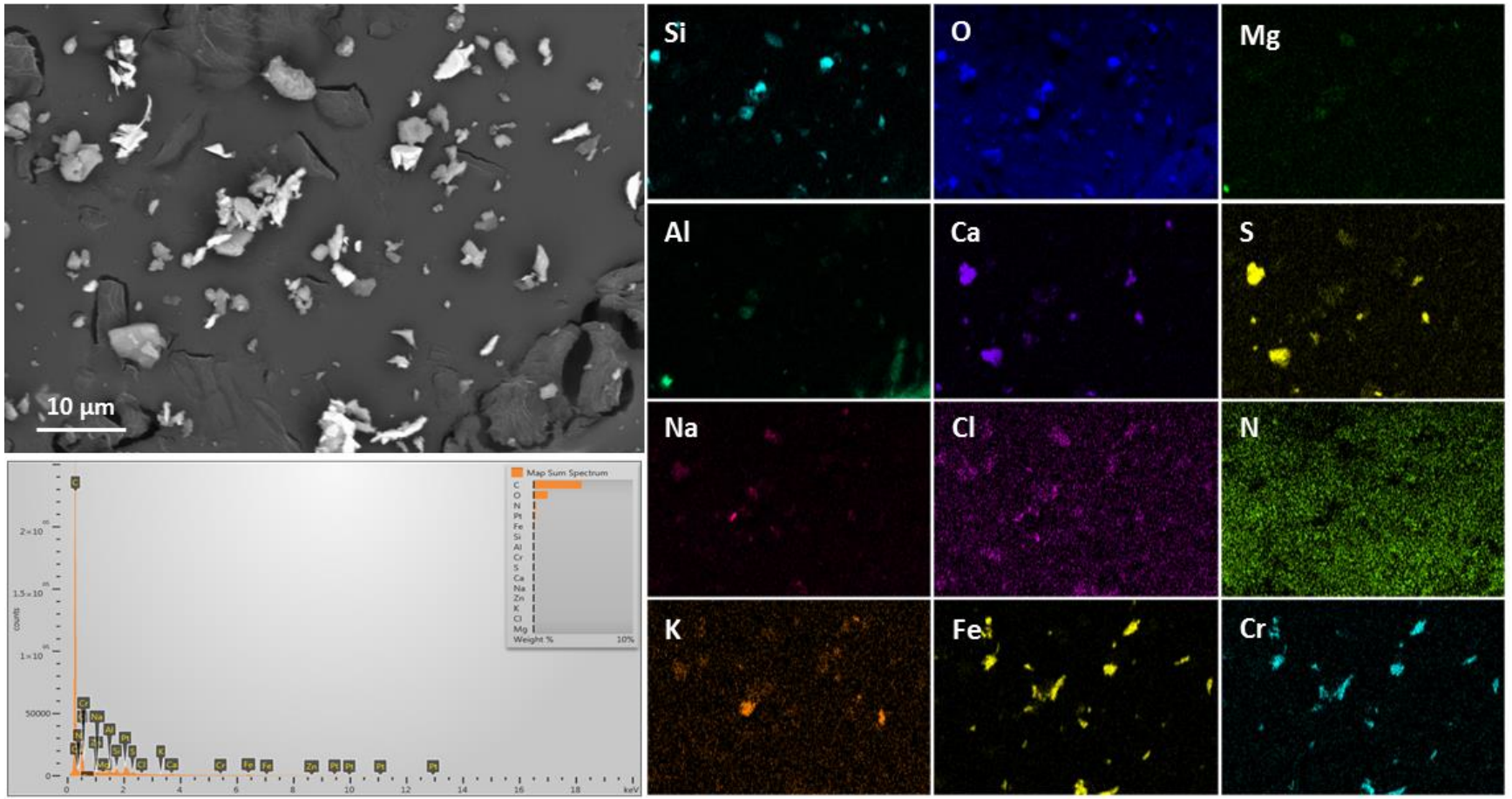

Figure 11. SEM image/EDS map #1 of Sample 387-007, collected from the center of the canister top. Note stainless steel and Ca-SO_4 grains.

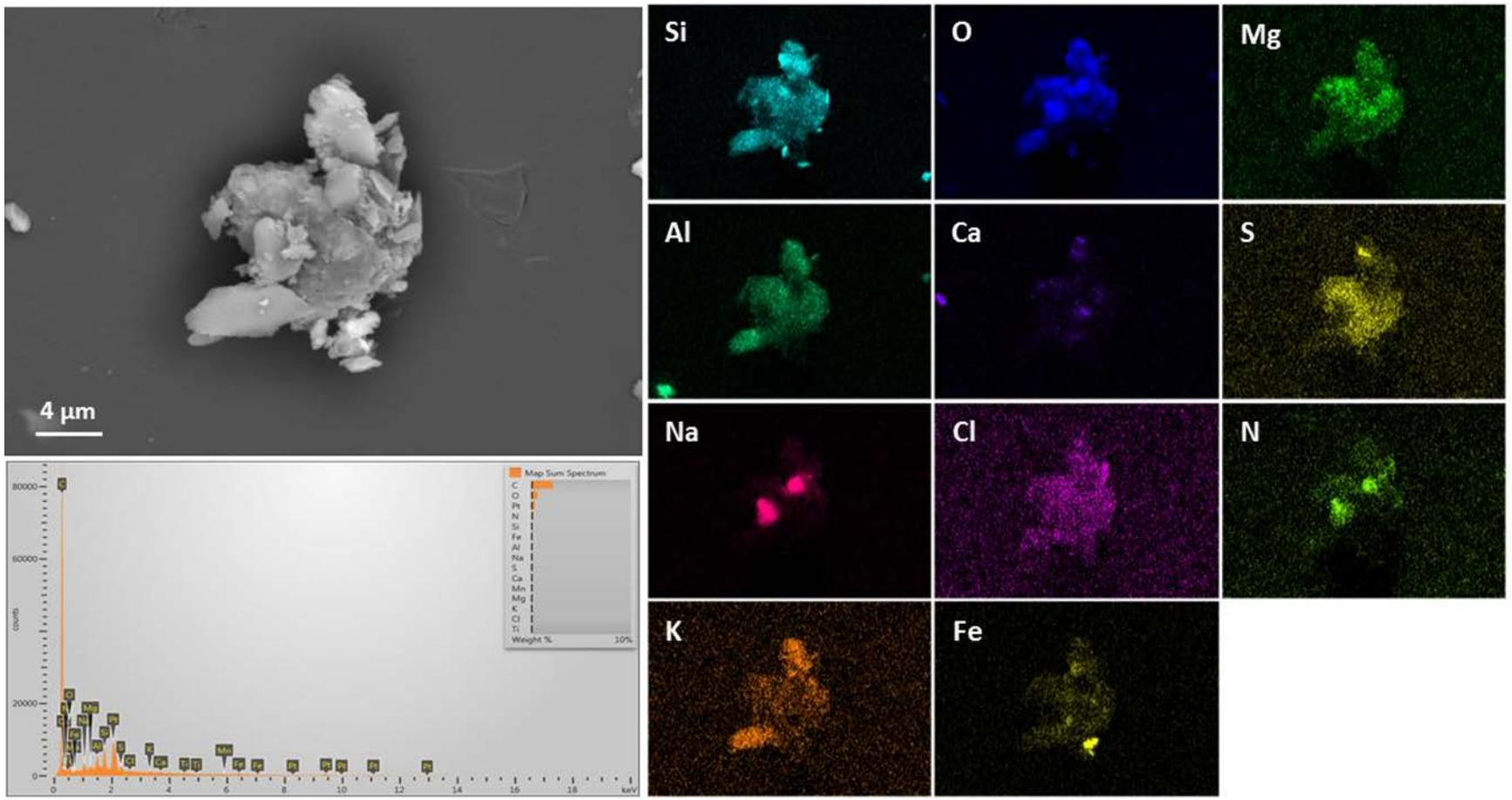

Figure 12. SEM image/EDS map #3 of Sample 387-007, collected from the center of the canister top. Aluminosilicate grain, with associated Na-NO_3.

3.1.2. Samples from the Foreign Material Exclusion Cover

Three Scotch-Brite™ dry pad samples from the FME cover were examined by SEM. These included 387-011, collected 1 foot from the edge of the cover; 387-013, collected from the center of the FME cover, and 389-15, also collected 1 foot from the edge of the cover.

The dust loads on the dry pad samples were variable. Sample 387-011 was lightly loaded, while the other two were more heavily coated. Typical pad regions for 387-011 and 387-013 are shown in Figure 13 (see Appendix A for an overview image of 389-015). In addition to having generally higher dust loads than the samples from the canister itself, the FME samples have significantly different compositions. While the canister dusts consisted almost entirely of stainless steel particles, the dust on the FME cover seems to be dominantly terrestrially-derived silicate and aluminosilicate particles, and stainless steel particles are rare. Salt phases are common, and consist almost entirely of sulfates, but a few specks of nitrate-rich material were observed. No unequivocal chloride mineral grain was observed.

Some representative SEM images and EDS maps are shown for the FME samples in Figure 14 to Figure 22. The silicate minerals include quartz and various Na, K, Ca, Mg, and Mg-Fe aluminosilicates that are probably a mixture of feldspars and clays. Calcium carbonate is present. Sulfates are the most abundant salts present, occurring as Ca-SO_4 but mostly as a Na-Al-SO_4 phase. While Na-Al-SO_4 minerals occur naturally, in areas of hydrothermal alteration, the natural minerals are unlikely to be present in aerosols at the Hope Creek site. The Na-Al-SO_4 phase probably formed, either prior to or after deposition, by a particle-gas conversion reaction between sodium-and-aluminum-bearing aerosol particles and sulfuric acid captured as SO_2 from the atmosphere. Naturally occurring Na-Al phases are also unlikely to be present as aerosols at the Hope Creek site. However, both a particulate (cryolite, Na_3AlF_6) and a gas-phase compound ($NaAlF_4$) are found in emissions from aluminum smelting operations that use the Hall-Heroult process for refining aluminum (Kvande and Drabløs, 2014). These could react with atmospheric sulfuric acid (also present in smelter emissions) to form the Na-Al-SO_4 phase observed by SEM. There is a large Al recycling and smelting company in Camden NJ, 40 miles NE of the Hope Creek site. This company, State Metal Industries Inc., uses the Hall-Heroult method (http://www.statemetalindustries.com/statemetalindustries/). It seems likely that the Na-Al-SO_4 phase observed in the dusts from the unused canister at Hope Creek can be sourced to reactions between Na-Al phases in the smelter emissions and atmospheric SO_2/sulfuric acid.

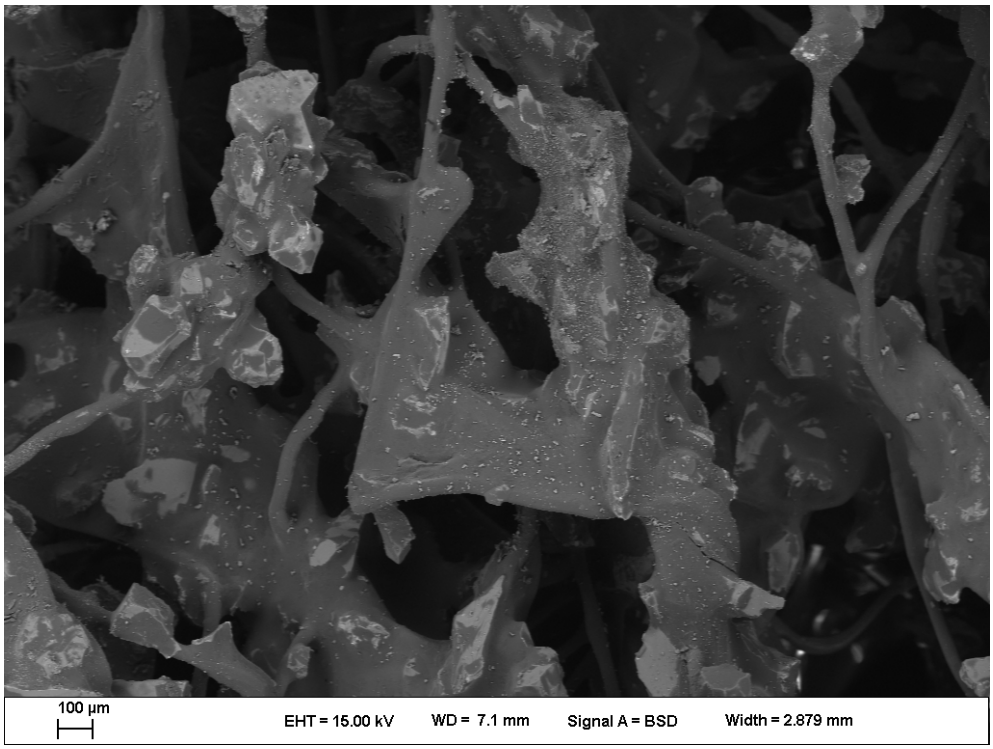

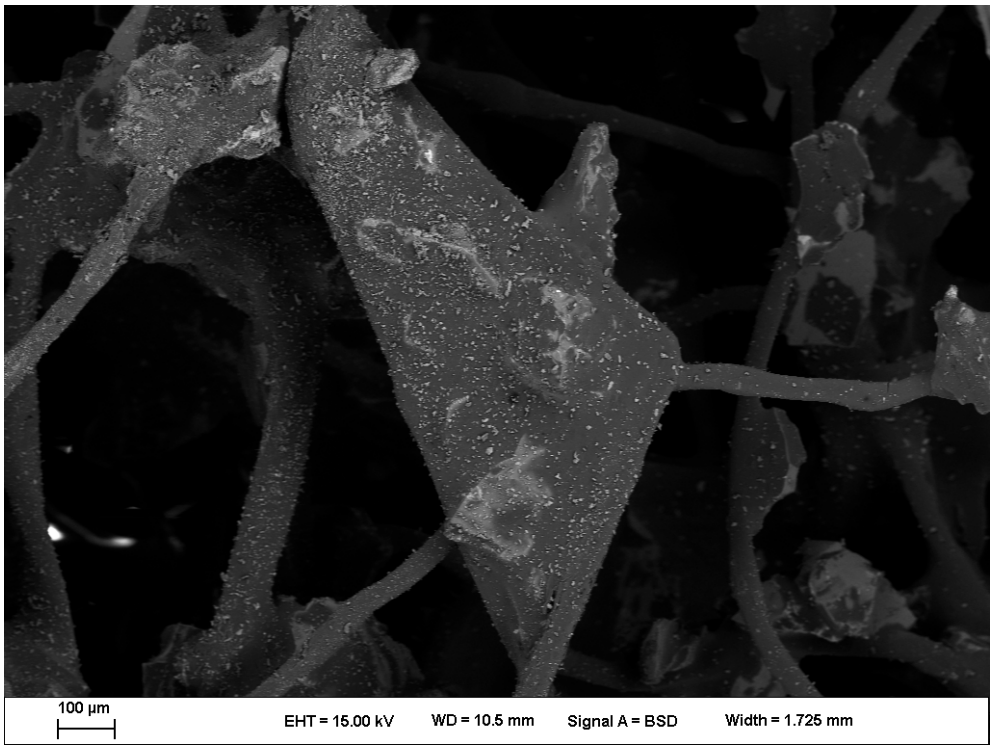

Figure 13. Upper: SEM image of pad sample 387-011, collected from the FME cover, 1 foot from the edge. Lower: SEM image of pad sample 387-013, collected from the center of the FME cover.

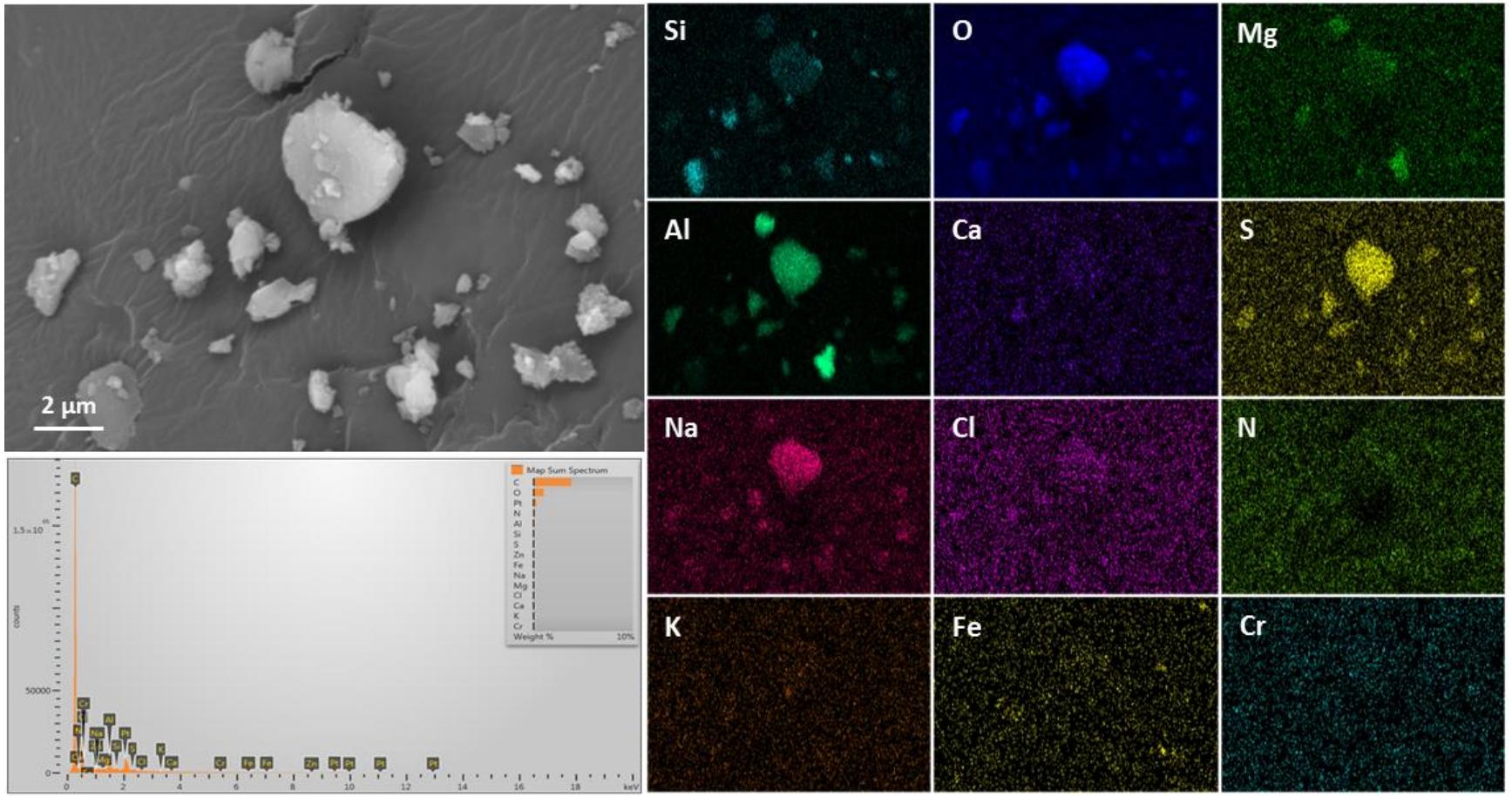

Figure 14. SEM image/EDS map #1 of Sample 387-011, collected 1 foot from the edge of the FME cover. Dust particles are quartz and aluminosilicates, with a large particle consisting of Na-Al-SO_4.

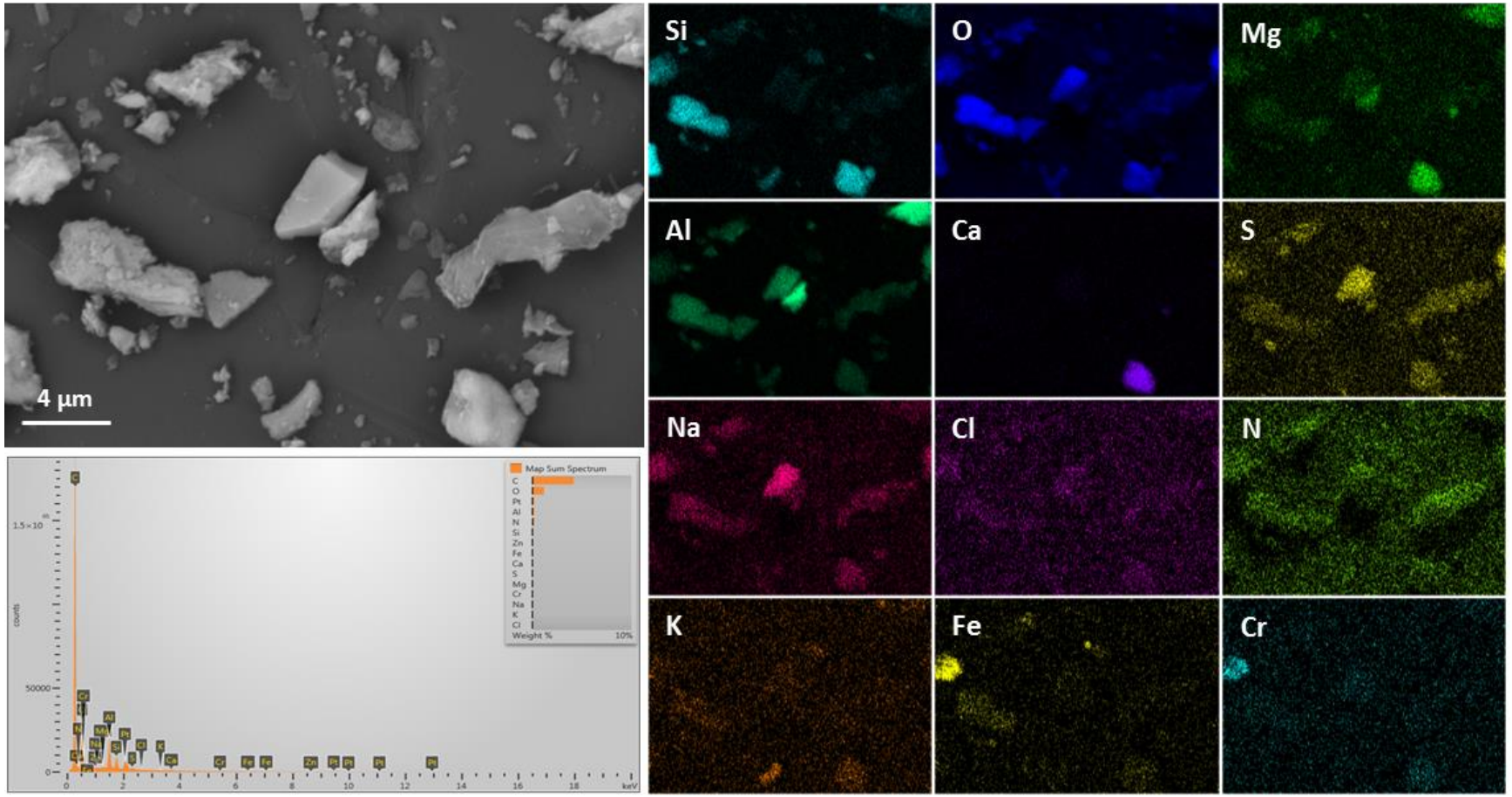

Figure 15. SEM image/EDS map #1 of Sample 387-011, collected 1 foot from the edge of the FME cover. Particles are mostly aluminosilicates, but note the Na-Al-SO_4 grain in the center of the image.

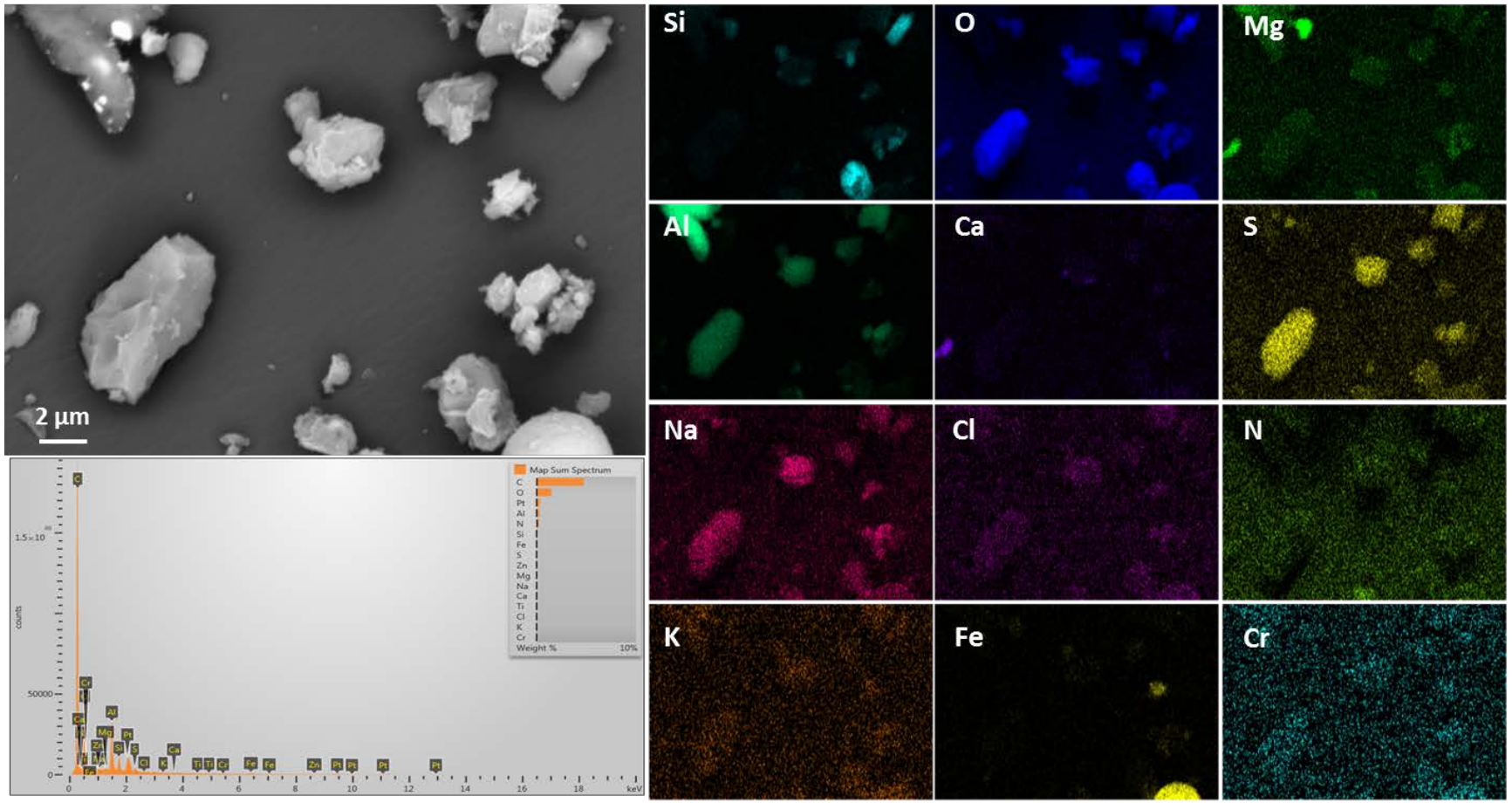

Figure 16. SEM image/EDS map #1 of Sample 387-011, collected 1 foot from the edge of the FME cover. Note multiple grains of Na-Al-SO_4.

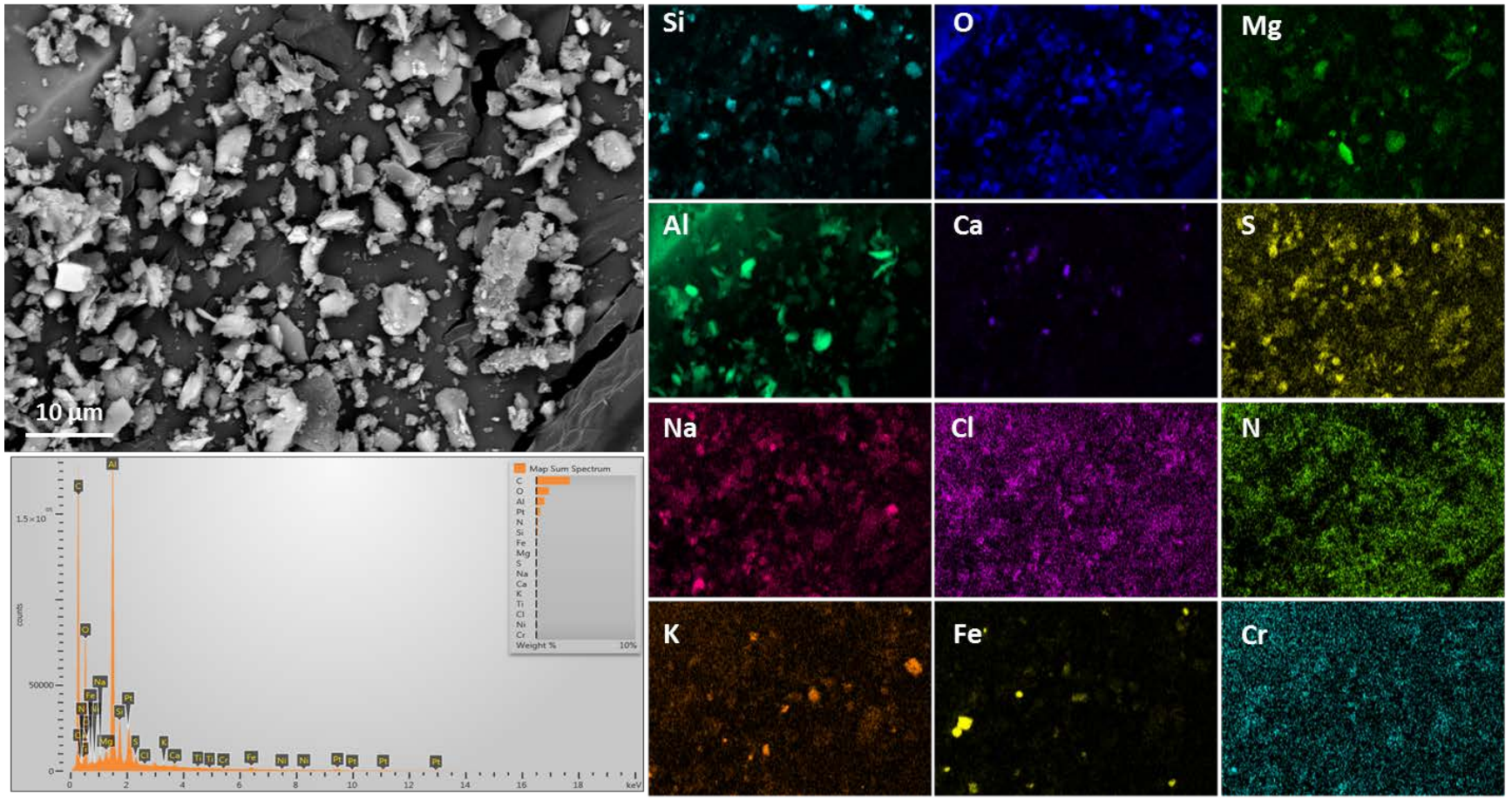

Figure 17. SEM image/EDS map #2 of sample 387-013, collected from the center of the FME cover. Grains are largely aluminosilicates, but note the abundance of SO_4 phases.

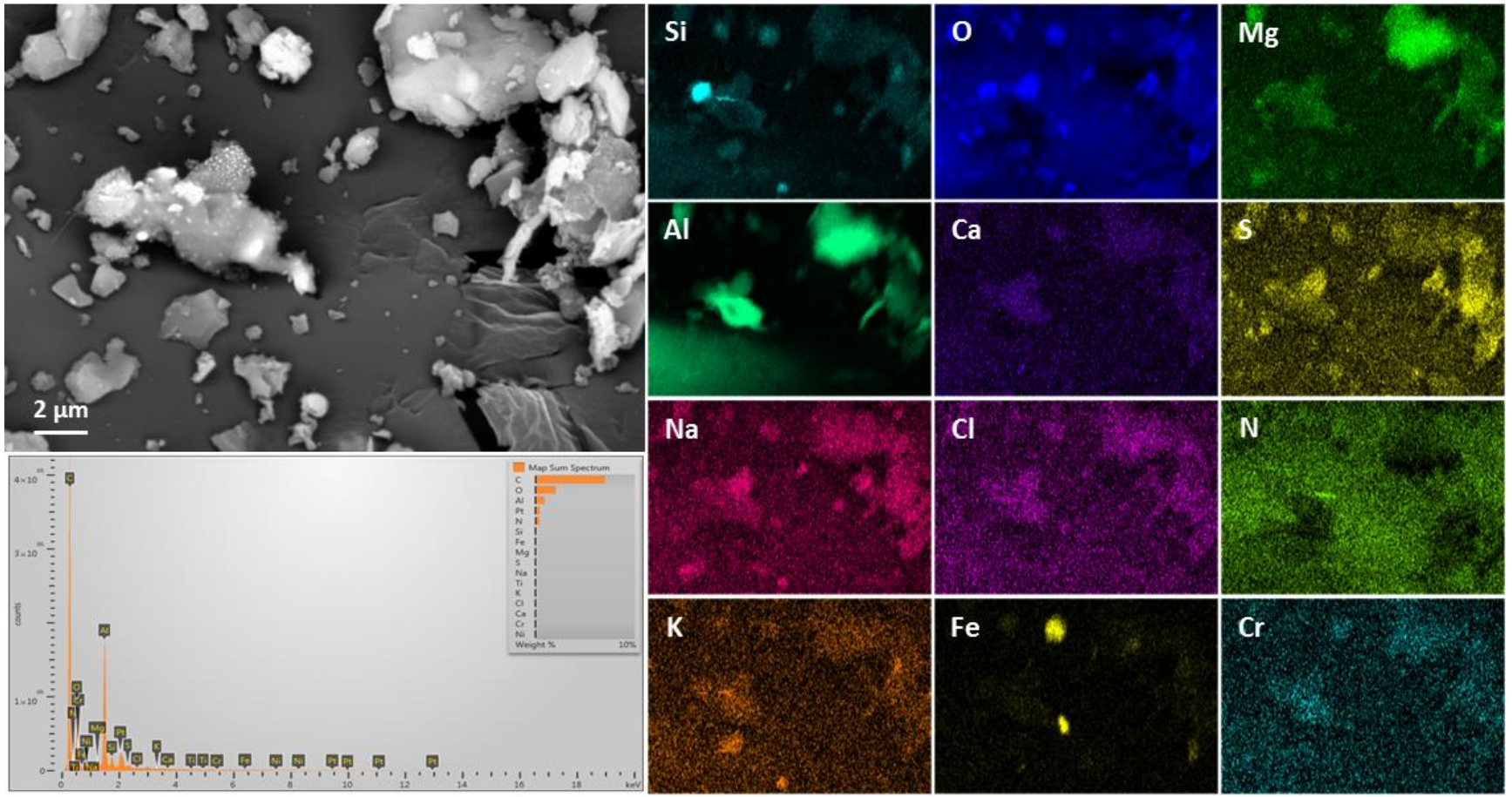

Figure 18. SEM image/EDS map #2 of sample 387-013, collected from the center of the FME cover. Grains are mostly aluminosilicates, but note the Na-SO_4 grain in left center that decomposed in the electron beam.

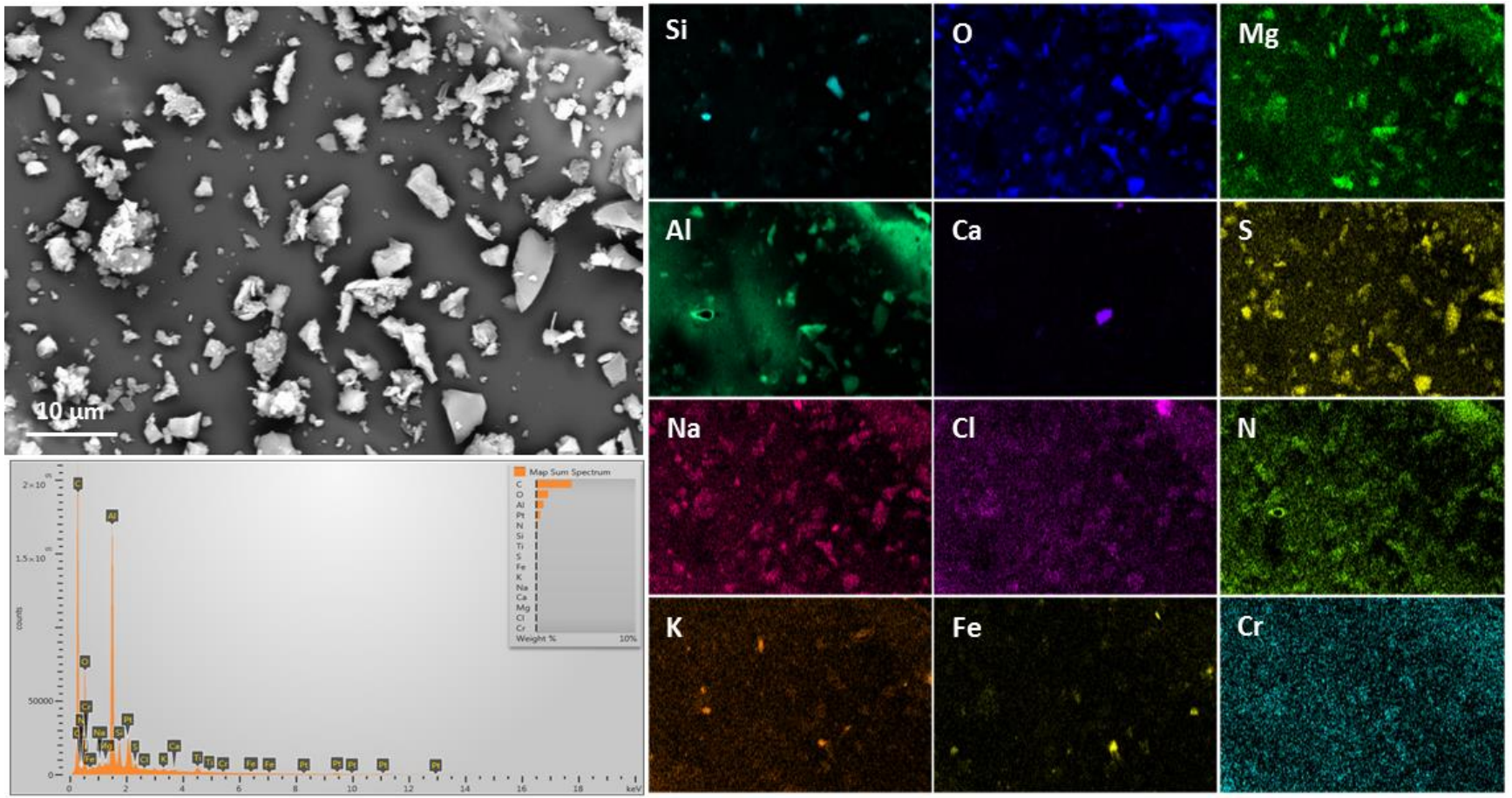

Figure 19. SEM image/EDS map #2 of sample 387-013, collected from the center of the FME cover. Note abundance of SO_4 phases.

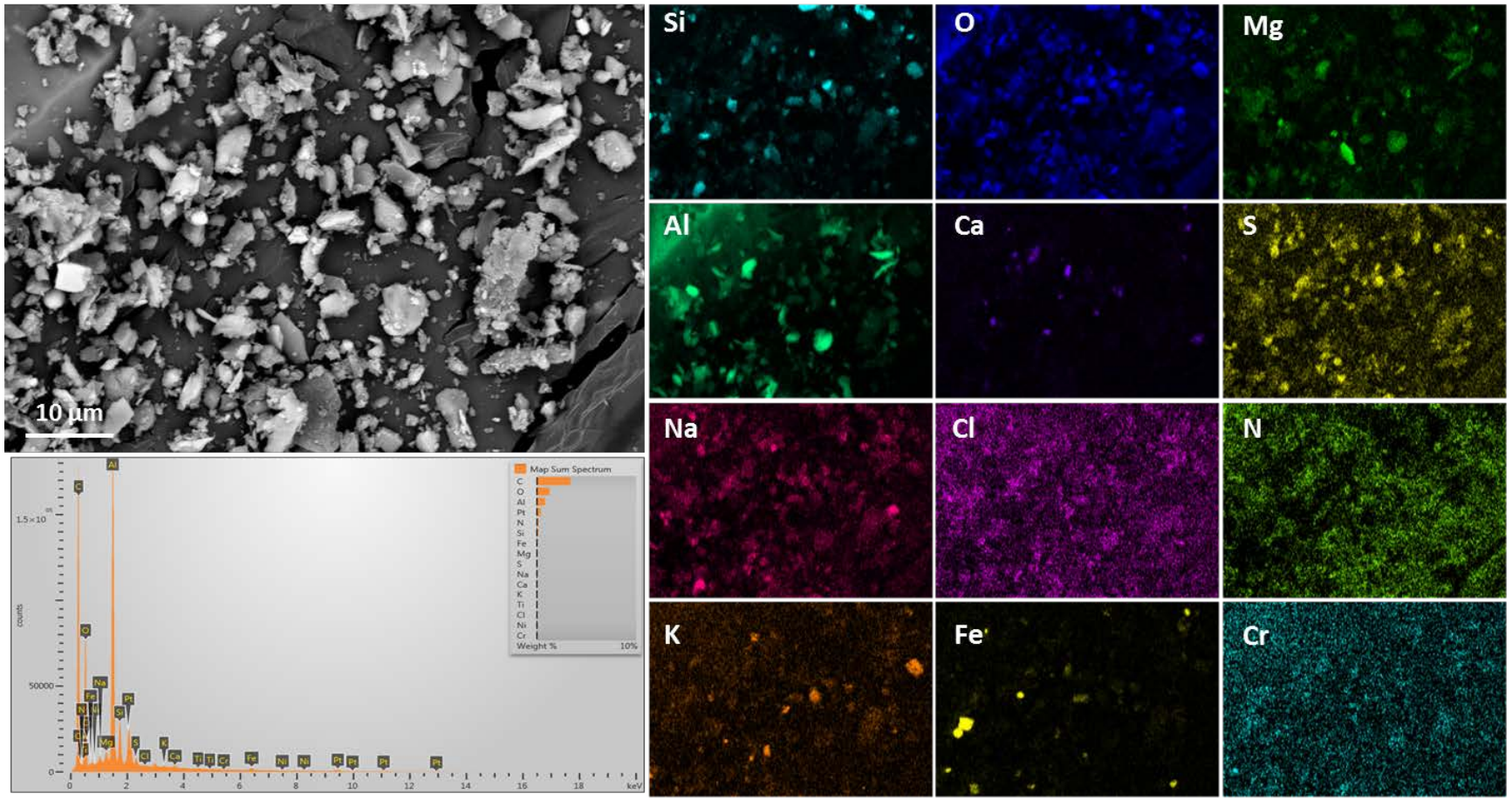

Figure 20. SEM image/EDS map #2 of sample 387-013, collected from the center of the FME cover. Most grains are aluminosilicates, but SO4 phases are abundant.

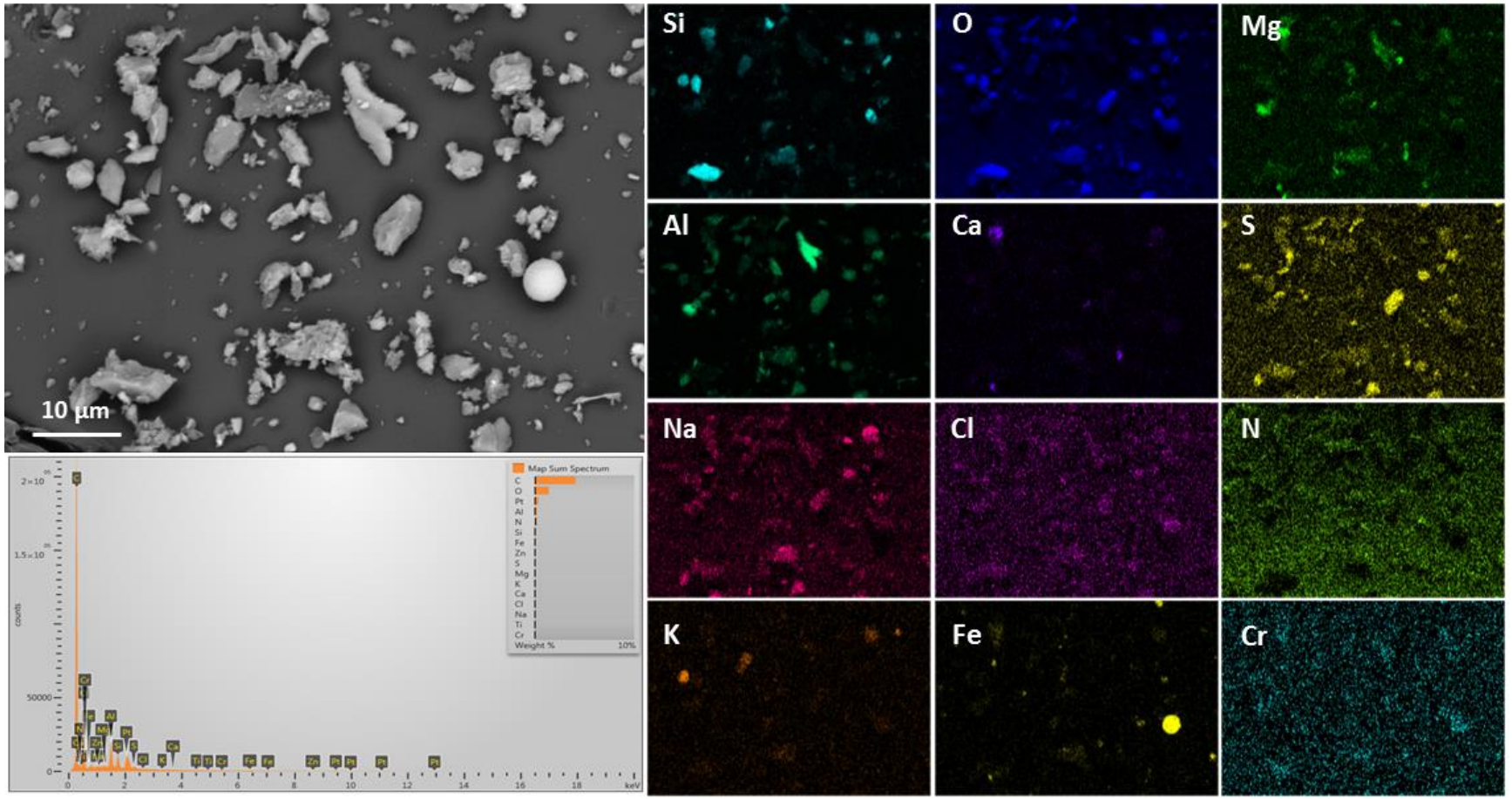

Figure 21. SEM image/EDS map #2 of sample 389-015, collected 1 foot from the edge of the FME cover. Most grains are silicates/aluminosilicates, but note abundance of Na-Al-SO_4 grains, and single sphere of iron oxide.

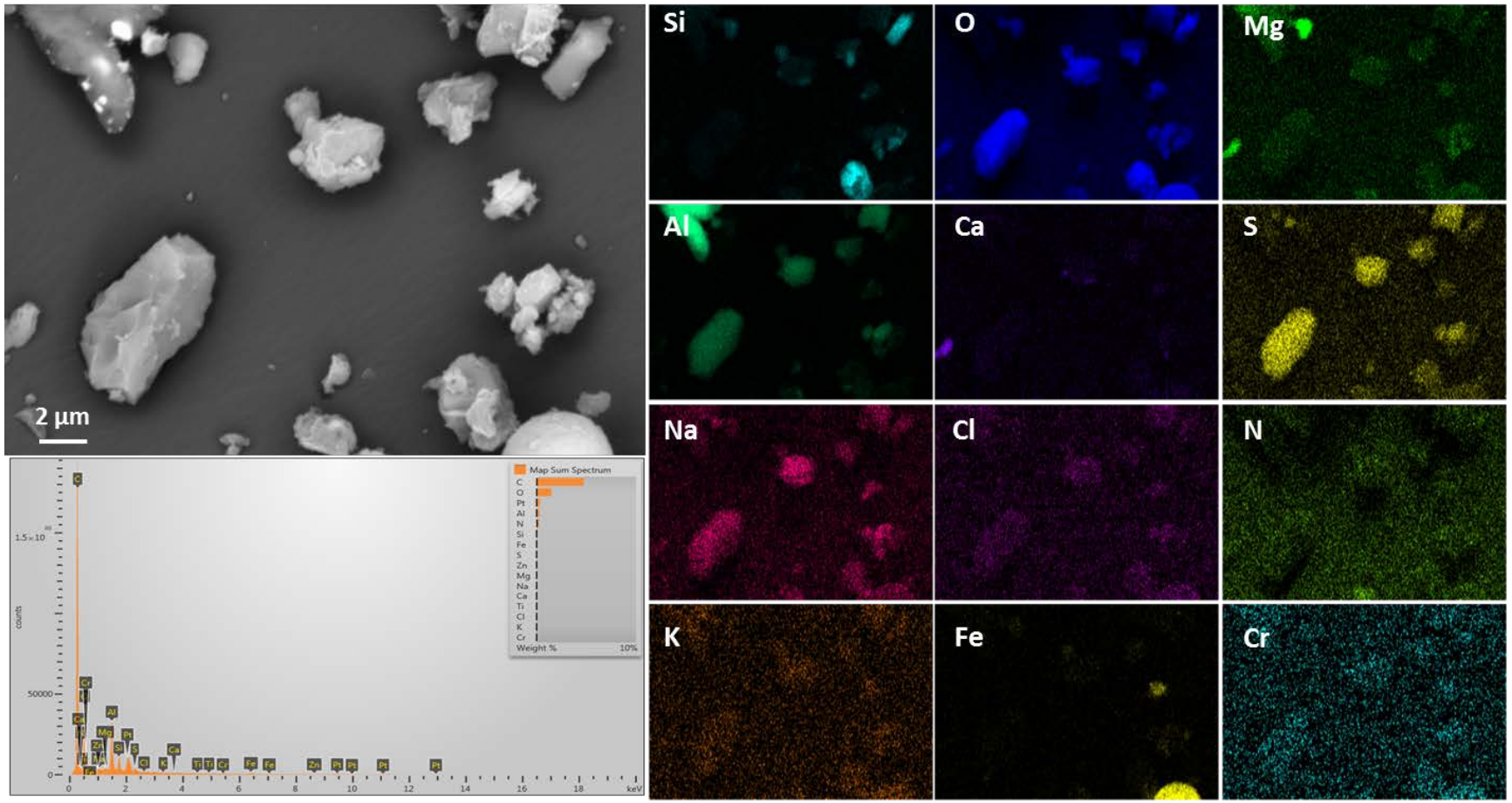

Figure 22. SEM image/EDS map #2 of sample 389-015, collected 1 foot from the edge of the FME cover. Magnified image of Na-Al-SO4 phases in the upper right hand corner of Figure 21.

3.1.2. Summary of SEM/EDS Analyses

Dust samples collected from the canister surfaces and from the FME covers differed greatly. Dusts from the canister surface were dominantly stainless steel particles generated during manufacturing of the canister. Environmentally derived particles—silicates/aluminosilicates and salts--were sparse. Dust loads on the canister surface were light, for both the side and the top. This is not unexpected, as the canister lid was covered by the FME cover during the one-year storage interval. Although the FME covers were washed by rain prior to sampling, it is clear that the dust loads were heavier, and that the particles were dominantly environmentally derived. Some salts were present despite the rain, although it is not clear if they are representative of what was present prior to the rainfall.

For both the canister and FME cover samples, chloride salts were rare, and consisted small isolated grains of NaCl. Nitrate phases were also rare. Ca-Mg carbonate, and more rarely, Ca-carbonate, were present in minor amounts. However, the most common salts were sulfates. Ca-SO_4 and Na-Al-SO_4 were the most common sulfates, but Na-SO_4 and K-SO_4 phases were also present. Most of these, while occurring naturally (generally in arid climates), are unlikely to be present as detrital grains at the Hope Creek site, and probably form by particle-gas conversion reactions involving chloride and nitrate salts, and atmospheric SO_2 or sulfuric acid. Reactions involving ammonium sulfate are also possible.

SO_2 reacts with water and oxygen to form H_2SO_4, via the following reaction:

$$2SO_2(g) + 2H_2O + O_2 \rightarrow 2H_2SO_4(aq)$$

If there is sufficient relative humidity that the surfaces of salt particles have a deliquesced or adsorbed water film, then sulfuric acid then reacts with the minerals, transforming carbonates, chlorides, and nitrates to sulfates via reactions such as:

$$2NaCl(s) + H_2SO_4(aq) \rightarrow Na_2SO_4(s) + 2HCl(g)$$

$$2NaNO_3(s) + H_2SO_4(aq) \rightarrow Na_2SO_4(s) + 2HNO_3(g)$$

$$CaCO_3(s) + H_2SO_4(aq) \rightarrow CaSO_4(s) + CO_2(g) + H_2O$$

These reactions are schematic in the sense that bisulfate phases or hydrated sulfates may form instead, and $H_2SO_4(aq)$ is fictive, representing dissociated H^+ and HSO_4^-/SO_4^{2-}. The reactions will proceed as written as long as the acid gas partial pressures generated by the solution are higher than the levels in the atmosphere. This is generally true because of the acidification of the brine by reaction with SO_2; the equilibrium acid gas partial pressures are higher at low pH. Elevated temperatures also elevate acid gas partial pressures.

To form the observed Na-Al-SO_4 phase, either cryolite (Na_3AlF_6) or $NaAlF_4$ gas in aluminum smelter emissions could react via:

$$Na_3AlF_6(s) + 3H_2SO_4(aq) \rightarrow NaAl(SO_4)_2(s) + Na_2(SO_4)(s) + 6HF(g)$$

$NaAlF_4(g) + 2H_2SO_4(aq) \rightarrow NaAl(SO_4)_2(s) + 4HF(g)$

These reaction probably occurred while the salts were aerosols, prior to deposition onto the canister surface.

If RH values are sufficiently high to allow a thin film of brine to form on the particle surfaces, then conversion reactions with ammonium sulfate are also possible. For example with a water layer as a medium for reaction, the following reaction could occur:

$2NaCl(s) + (NH_4)_2SO_4(s) \rightarrow Na_2SO_4(s) + 2HCl(g) + 2NH_3(g)$

Similar reactions can be written for all of the salts discussed above. All of these reactions convert atmospheric aerosols into sulfates, either prior to deposition or afterwards on the canister surface. Chloride and nitrate salts, if deposited, would eventually convert to sulfates. As ammonium (NH_4^+) converts to NH_3 and degases, it yields a proton that replaces the one lost with the acid gas. When acid degassing alone occurs, the pH of the remaining solution rises, and the generation rate of acid gases drops—the reaction is self-limiting. But coupled acid and ammonia degassing does not result in a rise in pH, and the degassing rate can be maintained. Hence. these reactions can result in the rapid loss of chloride and nitrate from deliquesced brines.

3.2. XRF Analysis

XRF analysis was used to quantify element concentrations on the Scotch-Brite™ pads. The XRF was capable of mapping the pads with a spot to spot resolution of 25 µm, providing spatial information on the scale of the pad areas. This information provides a link between the SEM data, which is confined to small areas on the sample surface, and the chemical analysis, which does not discriminate spatially, but rather provides an averaged composition for all the phases present. Moreover, the analysis provides element ratios which may be useful in estimating concentrations of some insoluble elements.

To address the relatively low signal from elements in the dust on the Scotch-Brite™ pads, the total spectra from each pad were subtracted from the spectrum obtained from a clean, unused blank pad. The residual spectrum provided peaks that could be assigned to the dust on the pads. This method works reasonably for qualitative assessment of material present on these pads. For each XRD pattern, a qualitative analysis is provided. It is important to note, when evaluating the XRF patterns provided in this report, that peak heights do not correspond to elemental abundances, but rather are a function of varying detection efficiencies as a function of wavelength.

The XRF results for a few representative samples are shown here; the complete suite of analyses is provided in Appendix B. In each case, the raw XRF pattern is shown, as well as a blank-subtracted XRF pattern, to emphasize the differences between the samples and the blank.

Because the FME covers had been exposed to a rainstorm, it was expected that all water-soluble salts had been washed off the surface, and the samples from the FME cover were not analyzed by XRF. Later SEM work showed that dust and salts were present, but by that time, the samples had been sectioned, and were no longer available for analysis.

Samples 387-001, 387-003, and 387-005 from the canister side had very similar patterns (Appendix B). The pattern for 387-001 is shown in Figure 23, and a blank-subtracted pattern in Figure 24. For each of these three samples, the pads are enriched in Fe, Cr, and Ni; this is consistent with the SEM observations that particles of stainless steel are the dominant contaminant on the side of the canister. Sample 387-009, also from the side of the canister, has a similar pattern, but with the addition of Ti and Zn (Appendix B). For this sample, white stenciled lettering was visible on Scotch-Brite™ pad surface; this paint has previously been shown to be TiO_2, and explains the elevated Ti in the X-ray spectrum. The paint on the canister overpacks contains Zn, and flakes of paint may be the source of the zinc on this sample. Zinc-rich particles were also observed on the pad samples from the in-service canisters from Hope Creek (Bryan and Enos, 2014).

Sample 387-007, from the canister lid, displays a slightly different pattern. The sample is enriched in stainless steel components, but is also somewhat enriched in Si, S, and K (Figure 25). This suggests that environmentally-derived dusts, silicates and sulfates, are slightly enriched on the top of the canister relative to the sides, even though the FME cover was in place.

micro-XRF for: **MPC-387-001** "XRF Spectrum"

Scan Area
23mm x 8mm (Width x Height)
31min scan (deviation depends on detector dead time)

Full Spectrum (5cps/eV)

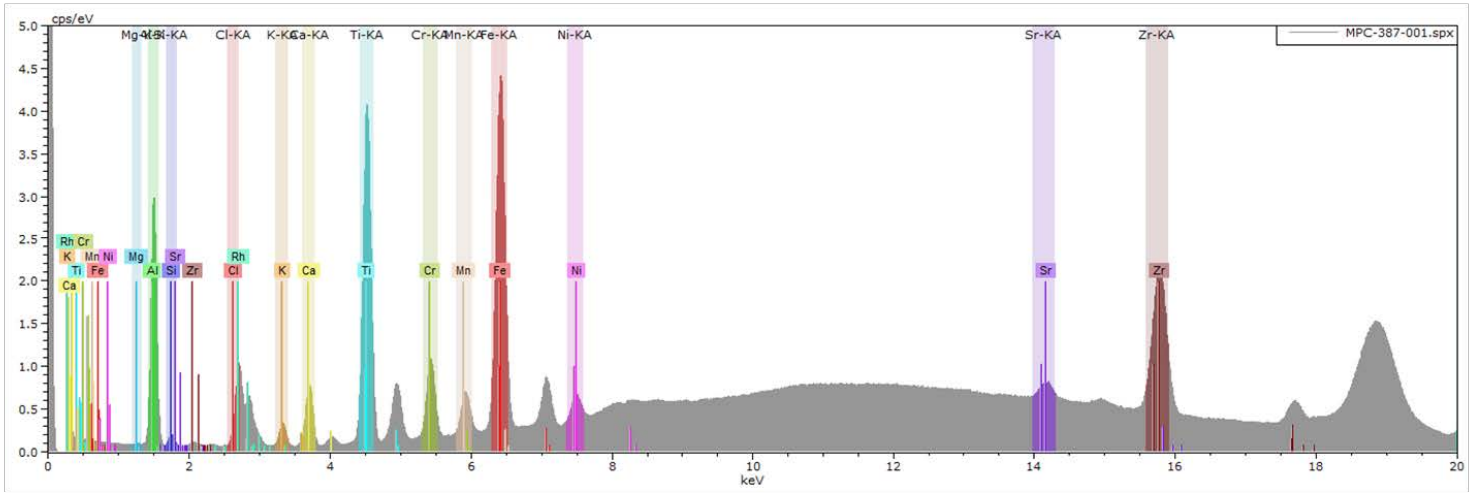

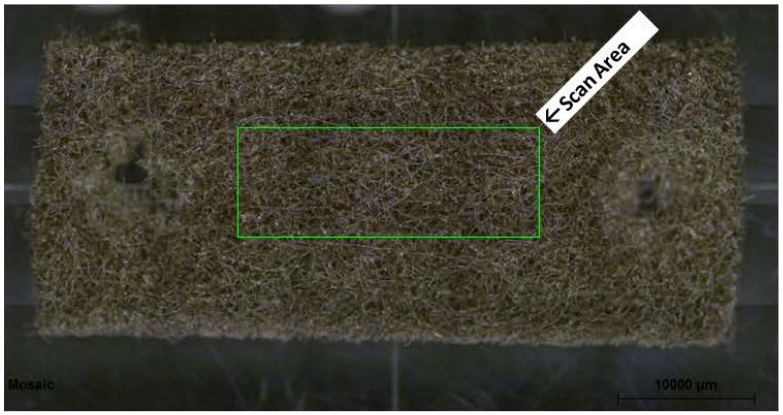

Semi-Quantitative Results

Element	AN	Net	norm. C. [wt.%]	Atom C. [at.%]	Error (1 Sigma) [wt.%]
Chlorine	17	0	0.00	0.00	
Aluminium	13	352582	66.69	78.48	0.12
Silicon	14	16348	2.97	3.36	0.00
Titanium	22	802368	10.53	6.98	0.00
Zirconium	40	628818	5.99	2.08	0.00
Calcium	20	130856	3.23	2.56	0.00
Potassium	19	37315	1.68	1.36	0.01
Rhodium	45	119339	0.00	0.00	
Strontium	38	82321	0.64	0.23	0.01
Manganese	25	86651	0.61	0.35	0.01
Chromium	24	194542	1.67	1.02	0.01
Magnesium	12	407	0.24	0.31	0.01
Iron	26	924817	5.37	3.05	0.00
Nickel	28	82757	0.39	0.21	0.01
		Total	**100.00**	**100.00**	

Figure 23. XRF pattern and XRF qualitative analysis results for pad 387-001.

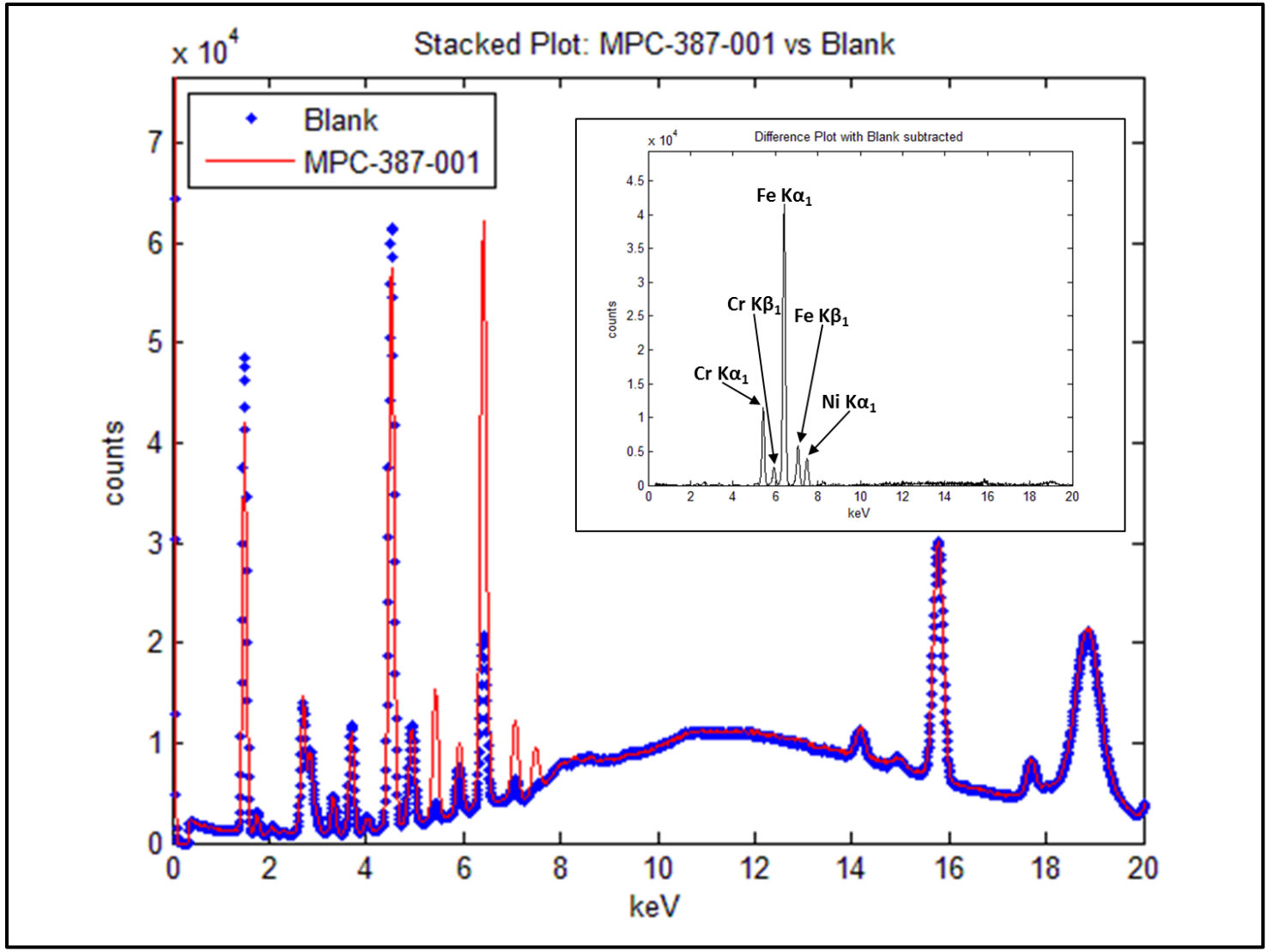

Figure 24. XRF pattern for 387-001 and the Blank pad. The inset shows the blank-subtracted pattern. Stainless steel components are enriched in the dust on the pad.

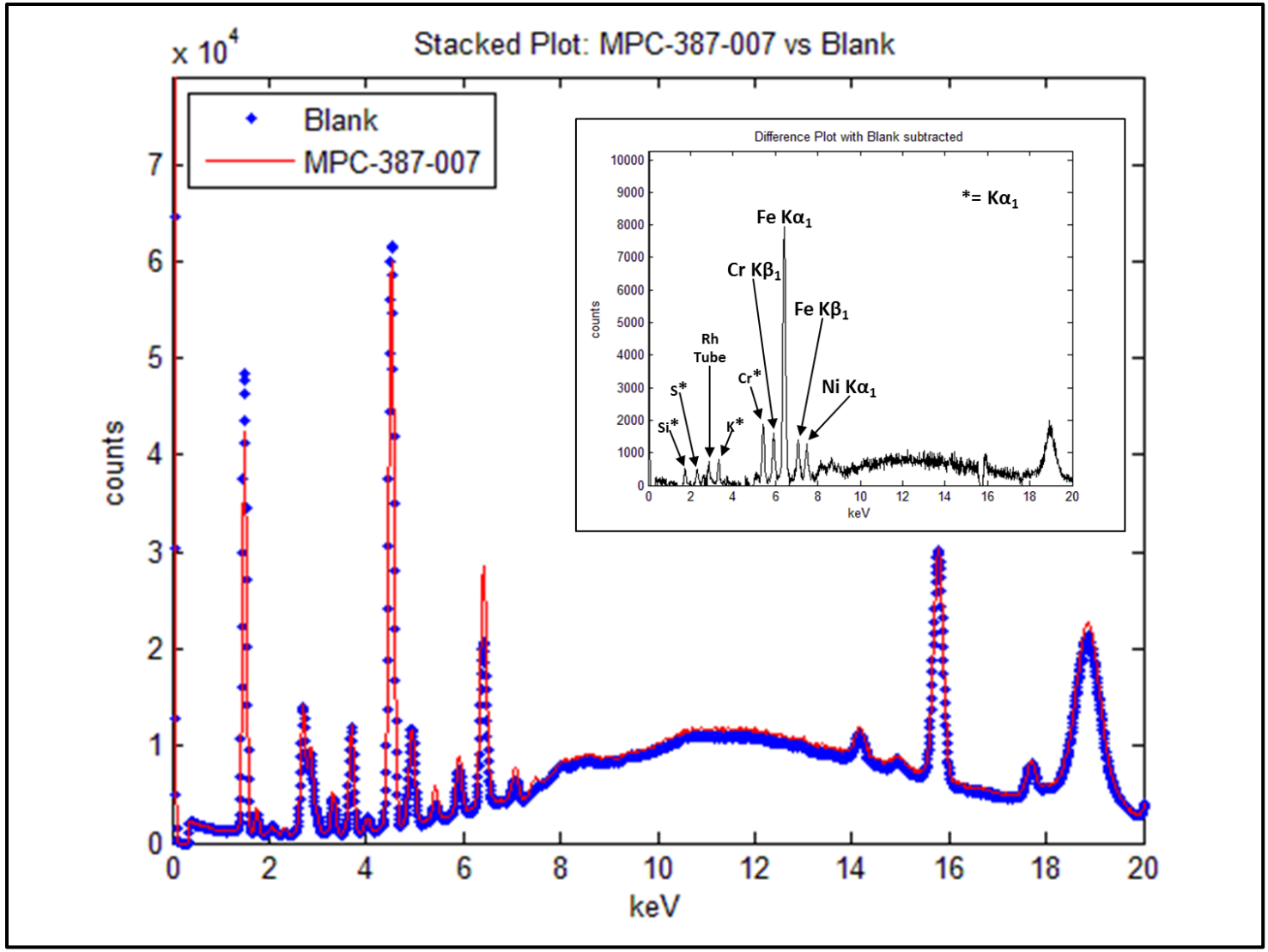

Figure 25. XRF pattern and XRF qualitative analysis results for Hope Creek sample 387-007, from the top of the canister. Relative to the blank, the pad is enriched in stainless steel components, with minor enrichments in S, K, and Si.

3.3. Chemical Analysis

The methods used for chemical analysis of the SaltSmart™ and dry pad samples from Hope Creek and Diablo Canyon are described in Bryan and Enos (2014). As discussed in that document, the soluble salts extracted from the SaltSmart™ sensors and from the dry pads were analyzed. The results of the soluble salt analyses are presented and discussed below.

3.3.1. SaltSmart™ Sensors

Nine SaltSmart™ sensors were analyzed from the Hope Creek unused canister (MPC-387). Although there was no discoloration on the wicks, concentrations of soluble salts were significant in the SaltSmart™ samples, as suggested by the conductivity measurements recorded on-site. Measured compositions for the soluble salts extracted from the SaltSmart™ sensors are provided in Table 2, in units of µg per sample. Values in micro-equivalents (µEq) are provided in Table 3, along with the calculated charge balance errors. Also shown in these tables are several SaltSmart® blanks run at Sandia; see Bryan and Enos (2014) for a description of these samples. The blanks are included here to allow better assessment of the significance of the measured values for the unknowns. Blank-subtracted concentrations for the samples are provided in Table 4 and Table 5. The results are relatively consistent with the samples collected from in-service canisters (MPC-143 and MPC 144) at Hope Creek; sulfate and nitrate are the most abundant anions, but some chloride is present, and the most abundant cations are Ca^{2+} and Na^{+}. The samples from the unused canister yield higher soluble salt loads, and also higher chloride surface loads, than the samples from sides of MPC-143 and MPC-144, but less than the samples from the tops of the in-service canisters. The estimated chloride surface loadings for the unused canister samples are given in Table 6; these were calculated assuming 100% extraction efficiency by the SaltSmart™ sensors, and a surface contact area of 3 cm^2.

The element concentrations in the blanks and samples are plotted against Ca, the most abundant element in the blanks, in Figure 26. Anion and cation concentrations in the samples are much higher than that in the blanks for all species except for phosphate, indicating that there is a large component for each that came from the dust. For phosphate, the sample and blank ranges overlap completely, suggesting that the phosphate was largely, if not entirely, leached from components in the SaltSmart™ sensors, and does not represent a component in the soluble salts.

It is clear that the ion concentrations measured for the samples, while low, are much greater than the values measured for the Sandia blanks. This is true even for the samples collected from the FME, which was presumably rinsed by rain. In fact, the FME samples are very similar in concentration to those from the package. This is difficult to reconcile with the low on-site SaltSmart conductivity readings for these samples. The samples were stored for about 2 weeks prior to analysis, much longer than the blanks, and there was a possibility that the higher values for the samples were due to greater degrees of leaching from SaltSmart™ components, as opposed to representing soluble salts collected from the FME covers. However, the lack of any consistent trend between the samples and blanks indicates that the higher concentrations in the samples are not due to leaching during the longer storage time.

Data for samples collected from MPC-143 and MPC-144, the Hope Creek in-service canisters (see Table 9, Bryan and Enos, 2014) are plotted with the blanks and unused canister samples in Figure 27 and Figure 28. Samples from the sides of the in-service canisters MPC-143 and MPC-144 plot on a trend between the blanks and the samples from the unused canister and the FMEs (MPC-387 and MPC-389), while samples from the tops of the in-service canisters are enriched in many elements relative to samples from the unused canisters. The data do not support a great deal of interpretation, but it is perhaps notable that the canister-top samples fall on a similar trend as the other samples for most species, but not for those that are most likely to be affected by degassing — NH_4, Cl^-, and possibly NO_3^-.

As with the previous SaltSmart™ analyses of soluble salts from canister surfaces, the soluble salts are deficient in anions, and, as previously, it seems likely that this is due to a significant fraction of the soluble species being present as carbonates; carbonate was not analyzed.

Table 2. Ion Concentrations in the Hope Creek SaltSmart™ Samples (µg/sample).

Sample #	Location	Na^+	K^+	Ca^{2+}	Mg^{2+}	NH_4^+	F^-	Cl^-	NO_3^-	PO_4^{3-}	SO_4^{2-}	SUM
387-002	Side, 1' from base	7.0	2.2	7.5	0.67	4.1	nd	2.8	9.2	*0.19*	7.2	40.8
387-004	Side, 1' from top	13.6	2.0	7.6	0.62	5.2	*0.19*	3.0	8.4	0.57	12.0	53.1
387-006	Lid, 1' from edge	9.2	2.3	10.6	0.82	2.7	nd	2.0	11.6	0.41	9.5	49.2
387-008*	Lid, center	na	na	na	na	na	nd	4.2	14.9	1.79	10.0	30.9
387-010	Side, 5' from base	6.0	1.7	9.0	0.86	3.3	nd	1.7	6.2	1.6	7.5	37.7
387-012	FME cover, 1' from edge	10.4	2.3	8.9	0.62	4.3	nd	2.4	6.2	0.52	8.7	44.3
387-014	FME cover, center	9.5	3.4	6.9	0.67	4.3	nd	1.9	9.5	0.96	9.4	46.5
389-016	FME cover, 1' from edge	6.4	1.3	6.4	0.75	4.4	nd	2.1	4.4	1.1	8.2	35.2
387-017	FME cover, center	6.7	1.4	7.8	1.0	3.7	nd	2.2	5.9	0.85	9.3	38.8
B1-6	—	0.88	1.2	2.2	0.23	1.4	*0.10*	1.3	3.9	0.87	0.45	12.5
B1-8(1)	—	nd	0.23	1.2	0.15	1.4	0.53	0.42	*0.29*	*0.34*	*0.26*	4.8
B1-10	—	*0.01*	0.35	1.5	0.21	1.1	0.38	0.68	2.3	0.97	0.35	7.8
B1-12	—	0.33	1.0	1.3	0.19	1.2	*0.26*	1.2	2.2	0.91	0.33	8.9
B1-14	—	nd	*0.14*	1.1	0.16	1.2	0.32	0.44	0.92	1.29	*0.23*	5.8
B1-8(2)	—	nd	0.26	1.4	0.27	1.0	0.38	0.39	1.3	nd	0.52	5.5
SS-Bl-8 min-1	—	nd	nd	1.3	0.20	1.1	nd	0.36	1.6	nd	0.58	5.1
SS-Bl-8 min-2	—	nd	nd	1.2	0.18	1.5	nd	0.69	0.9	0.5	0.25	5.2
SS-Bl-15 min	—	nd	nd	1.5	0.49	5.7	0.24	0.67	1.1	1.6	1.68	12.9

* Sample spilled. Too little sample remained to analyze both cations and anions, so only anions were analyzed.
Values in italics were above the detection limit, but too low for accurate quantification.

Table 3. Ion Concentrations in the Hope Creek SaltSmart™ Samples (µEq/sample).

Sample #	Location	Na^+	K^+	Ca^{2+}	Mg^{2+}	NH_4^+	F^-	Cl^-	NO_3^-	PO_4^{3-}	SO_4^{2-}	Cat. Sum	An. Sum	Chg. Bal. Error
387-002	Side, 1' from base	3.0E-01	5.5E-02	3.8E-01	5.5E-02	2.3E-01	nd	7.8E-02	1.5E-01	6.1E-03	1.5E-01	1.02	0.38	45.2
387-004	Side, 1' from top	5.9E-01	5.1E-02	3.8E-01	5.1E-02	2.9E-01	1.0E-02	8.5E-02	1.4E-01	1.8E-02	2.5E-01	1.36	0.50	46.3
387-006	Lid, 1' from edge	4.0E-01	6.0E-02	5.3E-01	6.7E-02	1.5E-01	nd	5.7E-02	1.9E-01	1.3E-02	2.0E-01	1.21	0.45	45.3
387-008*	Lid, center	na	na	na	na	na	nd	1.2E-01	2.4E-01	5.7E-02	2.1E-01	—	0.62	—
387-010	Side, 5' from base	2.6E-01	4.5E-02	4.5E-01	7.1E-02	1.8E-01	nd	4.7E-02	1.0E-01	5.0E-02	1.6E-01	1.01	0.35	48.1
387-012	FME cover, 1' from edge	4.5E-01	5.8E-02	4.4E-01	5.1E-02	2.4E-01	nd	6.6E-02	1.0E-01	1.6E-02	1.8E-01	1.24	0.37	54.6
387-014	FME cover, center	4.1E-01	8.6E-02	3.4E-01	5.5E-02	2.4E-01	nd	5.5E-02	1.5E-01	3.0E-02	2.0E-01	1.13	0.43	44.6
389-016	FME cover, 1' from edge	2.8E-01	3.4E-02	3.2E-01	6.2E-02	2.5E-01	nd	6.0E-02	7.1E-02	3.5E-02	1.7E-01	0.94	0.34	47.2
387-017	FME cover, center	2.9E-01	3.5E-02	3.9E-01	8.5E-02	2.1E-01	nd	6.2E-02	9.5E-02	2.7E-02	1.9E-01	1.00	0.38	45.4
B1-6	—	3.8E-02	3.0E-02	1.1E-01	1.9E-02	7.8E-02	*5.2E-03*	3.5E-02	6.3E-02	2.8E-02	9.3E-03	—	—	—
B1-8(1)	—	nd	5.9E-03	5.8E-02	1.2E-02	7.8E-02	2.8E-02	1.2E-02	*4.7E-03*	*1.1E-02*	*5.4E-03*	—	—	—
B1-10	—	*5.6E-04*	8.9E-03	7.6E-02	1.7E-02	6.1E-02	2.0E-02	1.9E-02	3.6E-02	3.1E-02	7.3E-03	—	—	—
B1-12	—	1.4E-02	2.6E-02	6.6E-02	1.6E-02	6.9E-02	*1.4E-02*	3.3E-02	3.5E-02	2.9E-02	6.8E-03	—	—	—
B1-14	—	nd	*3.6E-03*	5.5E-02	1.3E-02	6.6E-02	1.7E-02	1.3E-02	1.5E-02	4.1E-02	*4.8E-03*	—	—	—
B1-8(2)	—	nd	6.6E-03	7.2E-02	2.2E-02	5.7E-02	2.0E-02	1.1E-02	2.0E-02	nd	1.1E-02	—	—	—
SS-Bl-8 min-1	—	nd	nd	6.3E-02	1.6E-02	6.2E-02	nd	1.0E-02	2.6E-02	nd	1.2E-02	—	—	—
SS-Bl-8 min-2	—	nd	nd	5.9E-02	1.5E-02	8.3E-02	nd	2.0E-02	1.5E-02	1.5E-02	5.1E-03	—	—	—
SS-Bl-15 min	—	nd	nd	7.4E-02	4.0E-02	3.2E-01	1.2E-02	1.9E-02	1.8E-02	4.9E-02	3.5E-02	—	—	—

* Sample spilled. Too little sample remained to analyze both cations and anions, so only anions were analyzed.
Values in italics were above blank values, but too low to accurately quantify.
na - not analyzed
nd – not detected.

Table 4. Ion Concentrations in the Hope Creek SaltSmart™ Samples (µg/sample), After Subtracting Average Blank Values.

Sample #	Location	Na^+	K^+	Ca^{2+}	Mg^{2+}	NH_4^+	F^-	Cl^-	NO_3^-	PO_4^{3-}	SO_4^{2-}	SUM
387-002	Side, 1' from base	6.9	1.8	6.1	0.4	2.3	nd	2.1	7.6	nd	6.7	34.0
387-004	Side, 1' from top	13.4	1.6	6.2	0.4	3.4	nd	2.4	6.8	nd	11.4	45.6
387-006	Lid, 1' from edge	9.1	2.0	9.2	0.6	1.0	nd	1.4	10.0	nd	9.0	42.1
387-008*	Lid, center	na	na	na	na	na	nd	3.6	13.3	nd	9.5	26.3
387-010	Side, 5' from base	5.8	1.4	7.5	0.6	1.6	nd	1.0	4.6	0.8	7.0	30.3
387-012	FME cover, 1' from edge	10.3	1.9	7.5	0.4	2.6	nd	1.7	4.6	nd	8.2	37.1
387-014	FME cover, center	9.3	3.0	5.5	0.4	2.5	nd	1.3	7.9	0.2	8.9	39.0
389-016	FME cover, 1' from edge	6.3	1.0	5.0	0.5	2.7	nd	1.4	2.8	0.3	7.7	27.7
387-017	FME cover, center	6.5	1.0	6.4	0.8	2.0	nd	1.5	4.3	0.0	8.8	31.3

Table 5. Ion Concentrations in the Hope Creek SaltSmart™ Samples (µEq/sample) After Subtracting Average Blank Values.

Sample #	Location	Na^+	K^+	Ca^+	Mg^+	NH_4^+	F^-	Cl^-	NO_3^-	PO_4^{3-}	SO_4^{2-}	Cat. Sum	An. Sum	Chg. Bal. Error
387-002	Side, 1' from base	3.0E-01	4.6E-02	3.1E-01	3.6E-02	1.3E-01	nd	5.9E-02	1.2E-01	nd	1.4E-01	0.81	0.32	43.4
387-004	Side, 1' from top	5.8E-01	4.2E-02	3.1E-01	3.2E-02	1.9E-01	nd	6.6E-02	1.1E-01	nd	2.4E-01	1.16	0.41	47.3
387-006	Lid, 1' from edge	3.9E-01	5.1E-02	4.6E-01	4.8E-02	5.4E-02	nd	3.8E-02	1.6E-01	nd	1.9E-01	1.01	0.39	44.5
387-008*	Lid, center	na	na	na	na	na	nd	1.0E-01	2.1E-01	nd	2.0E-01	—	0.51	—
387-010	Side, 5' from base	2.5E-01	3.6E-02	3.8E-01	5.2E-02	8.6E-02	nd	2.8E-02	7.4E-02	2.4E-02	1.4E-01	0.80	0.27	49.6
387-012	FME cover, 1' from edge	4.5E-01	4.9E-02	3.7E-01	3.2E-02	1.4E-01	nd	4.7E-02	7.5E-02	nd	1.7E-01	1.04	0.29	56.1
387-014	FME cover, center	4.1E-01	7.8E-02	2.7E-01	3.6E-02	1.4E-01	nd	3.6E-02	1.3E-01	5.1E-03	1.9E-01	0.93	0.35	45.0
389-016	FME cover, 1' from edge	2.7E-01	2.5E-02	2.5E-01	4.3E-02	1.5E-01	nd	4.1E-02	4.5E-02	1.0E-02	1.6E-01	0.74	0.26	48.5
387-017	FME cover, center	2.8E-01	2.6E-02	3.2E-01	6.6E-02	1.1E-01	nd	4.3E-02	6.9E-02	1.5E-03	1.8E-01	0.80	0.30	46.1

* Sample spilled. Too little sample remained to analyze both cations and anions, so only anions were analyzed.

Table 6. Measured Chloride concentrations, in mg/m^2, on the Hope Creek Unused Canister Surfaces.

Sample #	Location	Cl^-, mg/m^2
387-002	Side, 1' from base	9.2
387-004	Side, 1' from top	10.1
387-006	Lid, 1' from edge	6.8
387-008	Lid, center	14
387-010	Side, 5' from base	6
387-012	FME cover, 1' from edge	7.8
387-014	FME cover, center	6.5
389-016	FME cover, 1' from edge	7.1
387-017	FME cover, center	7.3

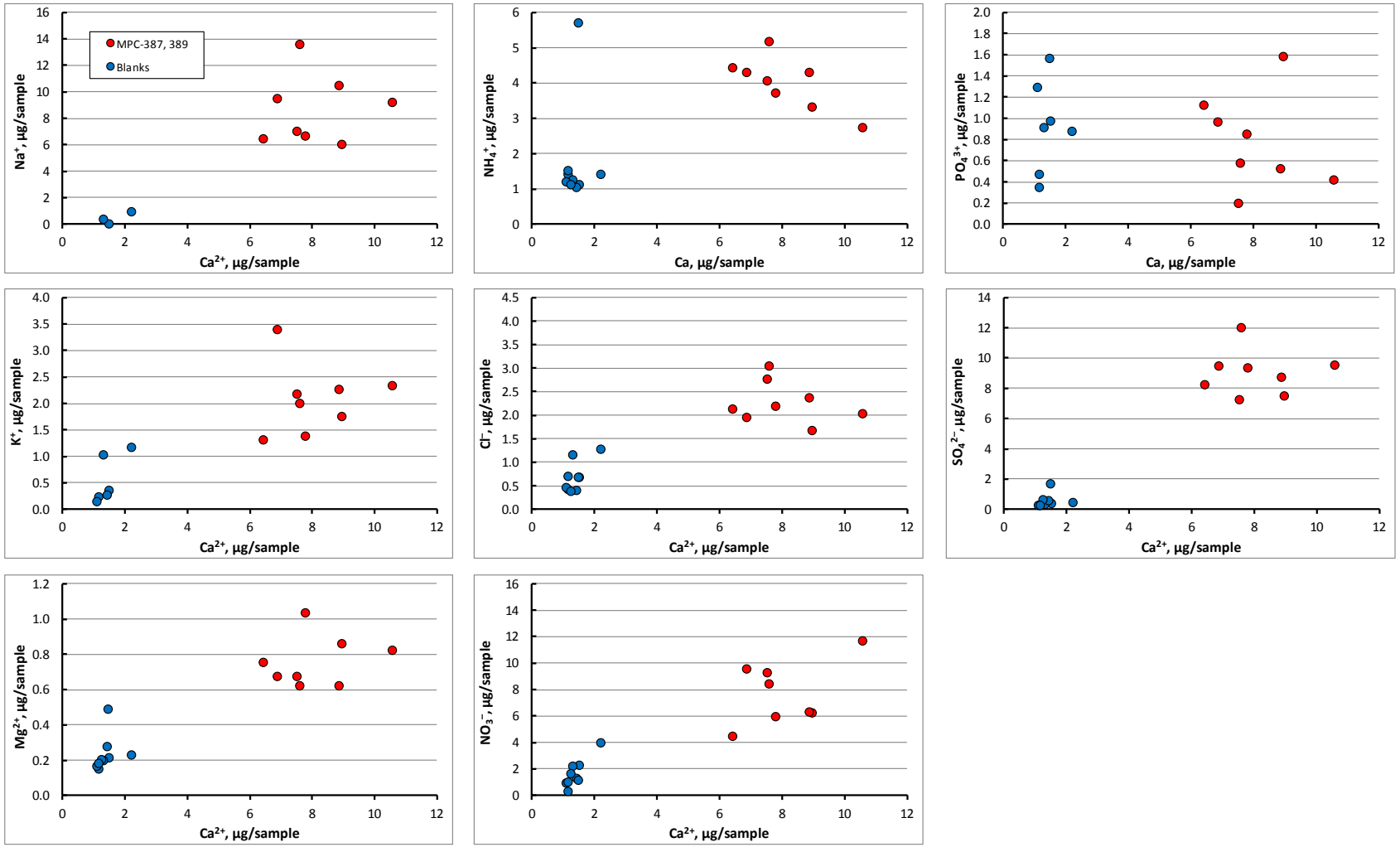

Figure 26. Plots of Ca^{2+} vs. other species in the unused canister and FME cover samples (MPC-387 and MPC-389) and the blanks.

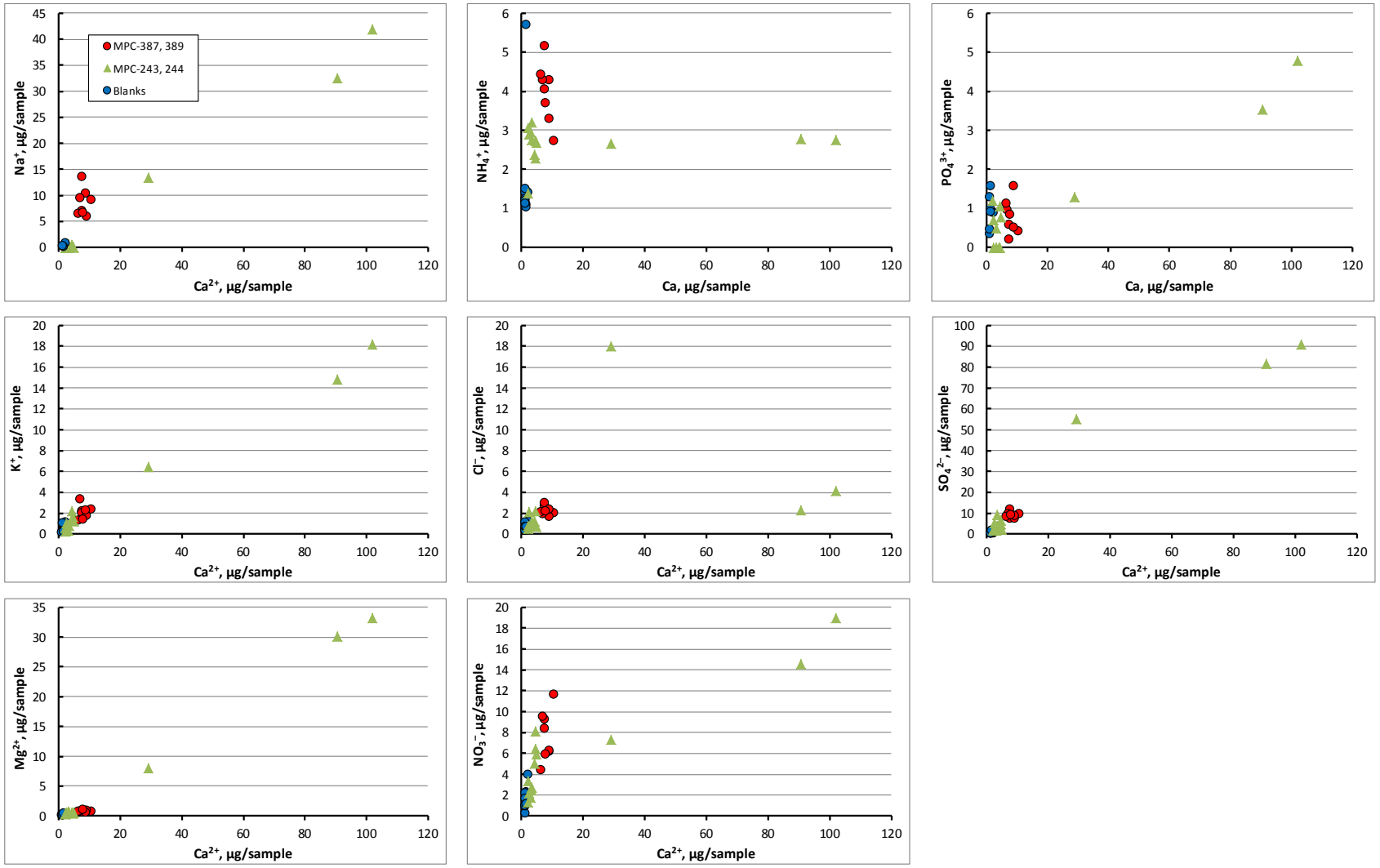

Figure 27. Plots of Ca^{2+} vs. other species in the unused canister and FME samples (MPC-387 and MPC-389), in-service canister samples (MPC-143 and MPC-144), and blanks. See Figure 30 for a blow-up of the lower range of the graphs.

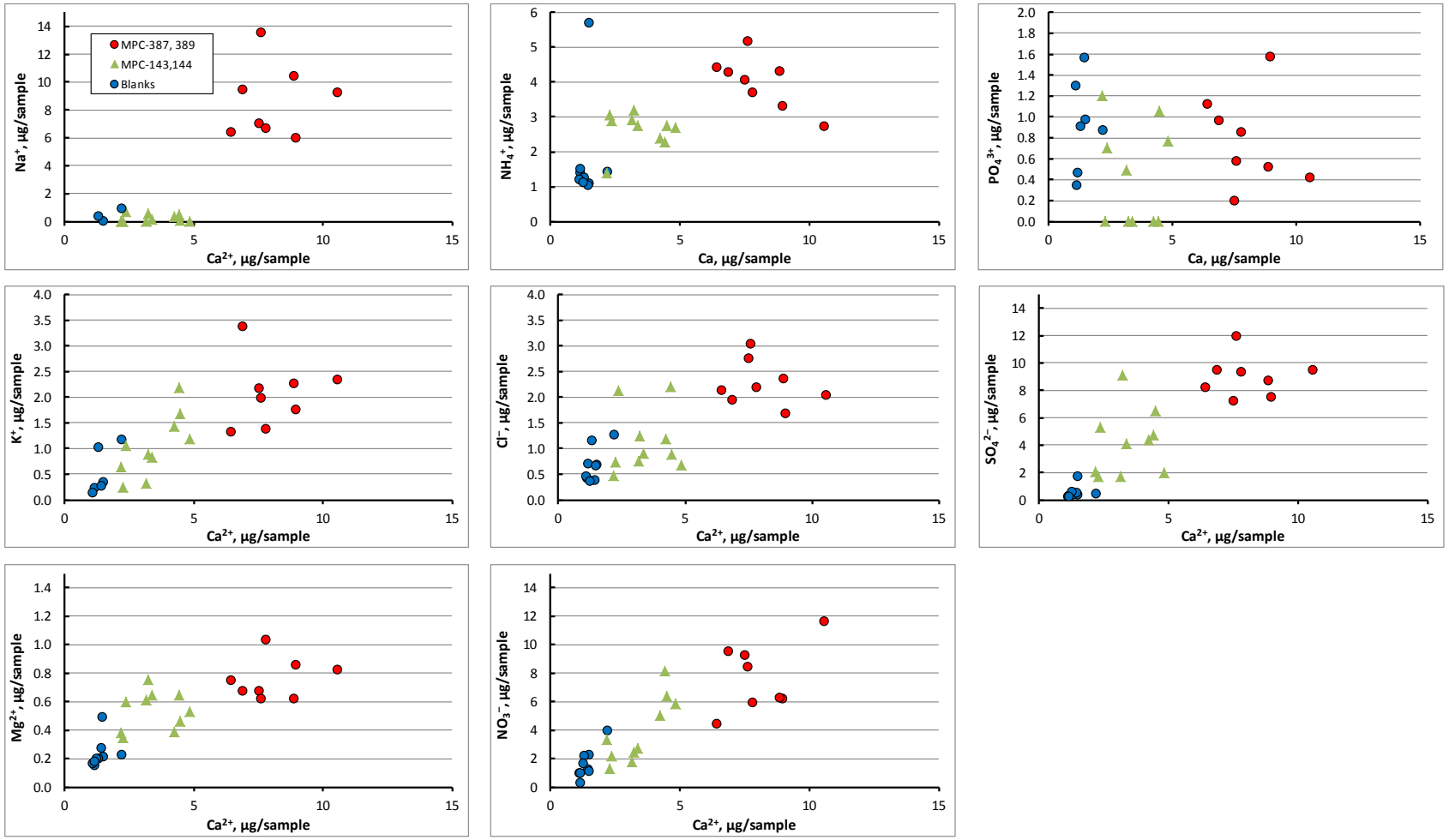

Figure 28. Plots of Ca^{2+} vs. other species in the unused canister and FME samples (MPC-387 and MPC-389), in-service canister samples (MPC-143 and MPC-144), and blanks. Graphs are expanded plots of the lower corners of graphs shown in Figure 27.

3.3.2 Dry Pad Samples

Seven dry pad samples were analyzed from Hope Creek unused canister MPC-387 and from the MPC-387 and MPC-389 FME covers. As was done previously (Bryan and Enos, 2014), the soluble salts were leached from the pads using deionized water, and then the leachate was analyzed to determine the composition of the leached materials. Measured compositions for the soluble salts extracted from the Scotch-Brite™ pads are provided in Table 7 in units of µg per sample. Also shown in these tables are two pad blanks. The blanks are included here to allow better assessment of the significance of the measured values for the unknowns. Note that one of the blanks was significantly smaller than the actual samples. The sample weights are also provided; they vary from pad to pad because a small piece of each was removed for SEM imaging and EDS analysis, and the remainders varied in weight. Measured element concentrations are provided as a function of sample weight in Figure 29. Values in micro-equivalents (µEq) are provided in Table 8, along with the calculated charge balance errors.

It is important to recognize that the dry pad data do not yield amounts of salts per unit area. The area on the canister surface that was contacted by the abrasive pads as they were brushed across the surface is unknown. More importantly, the collection efficiency of the pads is unknown, and is likely to be much less than 100%.

There are several notable features to the dry pad leachate data.

- The same elements were detected in the samples and the blanks, and the same elements were absent. The dominant cation in the dry pad leachates is Na^+. The cations Ca^{2+} and Mg^{2+} were not detected on any samples. The dominant anion in the dry pad leachates is Cl^-; SO_4^{2-} is subordinate, and NO_3^- values are similar to blank values. These results are inconsistent with the Saltsmart™ chemistry data, which showed that Ca^{2+} and SO_4^{2-} were major components in the soluble salts, and also with the SEM results, which showed that chlorides were rare on the canister surface, and sulfates were abundant.

- There is no significant difference in composition between the dry pad leachates taken from the FME covers and those from the canister surfaces. Furthermore, there is no consistent difference in soluble salt loading between the samples taken from horizontal surfaces (e.g. the canister lids and FME covers) and those from vertical surfaces (the canister sides). This seems especially odd in light of the fact that a thunderstorm rinsed the FME covers the night before sampling occurred.

  This is not necessarily inconsistent with the SEM results, which show higher dust loads on the flat surfaces, because the vast majority of the particles, regardless of location, are insoluble materials, either stainless steel particles or silicates/aluminosilicates. Note that the SaltSmart™ samples also showed no significant difference in soluble salt loading for samples from vertical and horizontal surfaces.

- For all species except for NO_3^-, concentrations in the samples from the canister and FME surfaces are higher than the blanks (Figure 29). The NO_3^- concentrations are similar in both the samples and the blanks.

The facts that the same components are enriched in the blanks as the samples, and that the components with the highest concentrations are inconsistent with the SaltSmart™ data, suggest most of the components leached from the dry pad samples may be coming from the pad matrix itself. However, cation and anion concentrations are uniformly higher in the samples relative to the blanks suggesting that much of the leachate may be coming from the sampled surfaces.

Given the discrepancies between the Scotch-Brite™ pad leachate data and the SaltSmart™ data, it is difficult to interpret the pad leachate data. The Scotch-Brite™ pad blanks were prepared at Sandia using the same techniques as the pad samples, and the blank values were very low, indicating that sample contamination during analysis at Sandia did not occur. However, sample pad contamination prior to, or during, sample collection at Hope Creek cannot be ruled out. Alternatively, it is possible that abrasion of the sample pads due to being rubbed across the metal surfaces damaged the pads (this is observed in SEM images), resulting in greater leaching from the sample pads than from the blanks, which were not abraded. The possibility that the majority of the observed soluble components on the pads were leached from the pad matrices cannot be ruled out.

Table 7. Ion Concentrations in the Hope Creek Dry Pad Samples (µg/sample).

Sample #	Location	Sample wt, g	Na^+	K^+	Ca^{2+}	Mg^{2+}	NH_4^+	Cl^-	NO_3^-	PO_4^{3-}	SO_4^{2-}	Sum
387-001	Side, 1' from base	1.3492	8.3	7.7	nd	nd	0.29	6.6	6.8	nd	3.6	33.2
387-003	Side, 1' from top	1.2581	9.5	3.8	nd	nd	0.29	13.8	5.9	nd	1.9	35.1
387-005	Lid, 1' from edge	1.3956	7.2	4.5	nd	nd	0.24	5.2	6.1	nd	3.4	26.6
387-007	Lid, center	1.3378	13.8	6.6	nd	nd	0.33	8.6	9.7	nd	8.5	47.6
387-009	Side, 5' from base	1.2250	21.7	5.5	nd	nd	0.28	26.1	9.4	nd	2.2	65.2
387-011	FME cover, 1' from edge	1.2301	17.2	4.8	nd	nd	0.43	20.5	3.0	nd	3.2	49.1
387-013	FME cover, center	1.2841	6.2	4.2	nd	nd	0.48	4.4	3.0	nd	5.6	23.8
389-015	FME cover, 1' from edge	1.3354	9.3	3.9	nd	nd	0.53	9.9	3.3	nd	4.0	30.8
Blank 1	—	0.5990	3.3	1.9	nd	nd	0.12	1.4	4.0	nd	0.8	11.5
Blank 2	—	1.2127	5.0	2.2	nd	nd	0.15	3.8	6.8	nd	1.2	19.2

Table 8. Ion Concentrations in the Hope Creek Dry Pad Samples (µEq/sample).

Sample #	Location	Na+	K^+	Ca^{2+}	Mg^{2+}	NH_4^+	Cl^-	NO_3^-	PO_4^{3-}	SO_4^{2-}	Cat. Sum	An. Sum	Chg. Bal. Error, %*
387-001	Side, 1' from base	3.6E-01	2.0E-01	nd	nd	1.6E-02	1.9E-01	1.1E-01	nd	3.8E-02	0.57	0.37	21.4
387-003	Side, 1' from top	4.1E-01	9.7E-02	nd	nd	1.6E-02	3.9E-01	9.6E-02	nd	1.9E-02	0.53	0.52	0.3
387-005	Lid, 1' from edge	3.1E-01	1.1E-01	nd	nd	1.3E-02	1.5E-01	9.9E-02	nd	3.5E-02	0.44	0.32	16.3
387-007	Lid, center	6.0E-01	1.7E-01	nd	nd	1.8E-02	2.4E-01	1.6E-01	nd	8.8E-02	0.79	0.58	15.5
387-009	Side, 5' from base	9.5E-01	1.4E-01	nd	nd	1.6E-02	7.4E-01	1.5E-01	nd	2.3E-02	1.10	0.93	8.2
387-011	FME cover, 1' from edge	7.5E-01	1.2E-01	nd	nd	2.4E-02	5.8E-01	4.8E-02	nd	3.3E-02	0.89	0.69	12.6
387-013	FME cover, center	2.7E-01	1.1E-01	nd	nd	2.7E-02	1.2E-01	4.9E-02	nd	5.8E-02	0.40	0.29	16.5
389-015	FME cover, 1' from edge	4.0E-01	1.0E-01	nd	nd	2.9E-02	2.8E-01	5.3E-02	nd	4.1E-02	0.53	0.41	12.6
Blank 1	—	1.4E-01	4.9E-02	nd	nd	6.9E-03	3.8E-02	6.5E-02	nd	8.6E-03	0.20	0.12	24.5
Blank 2	—	2.2E-01	5.7E-02	nd	nd	8.1E-03	1.1E-01	1.1E-01	nd	1.3E-02	0.28	0.24	7.8

* Charge balance error, % = ((Cations – Anions)/(Cations + Anions)) *100

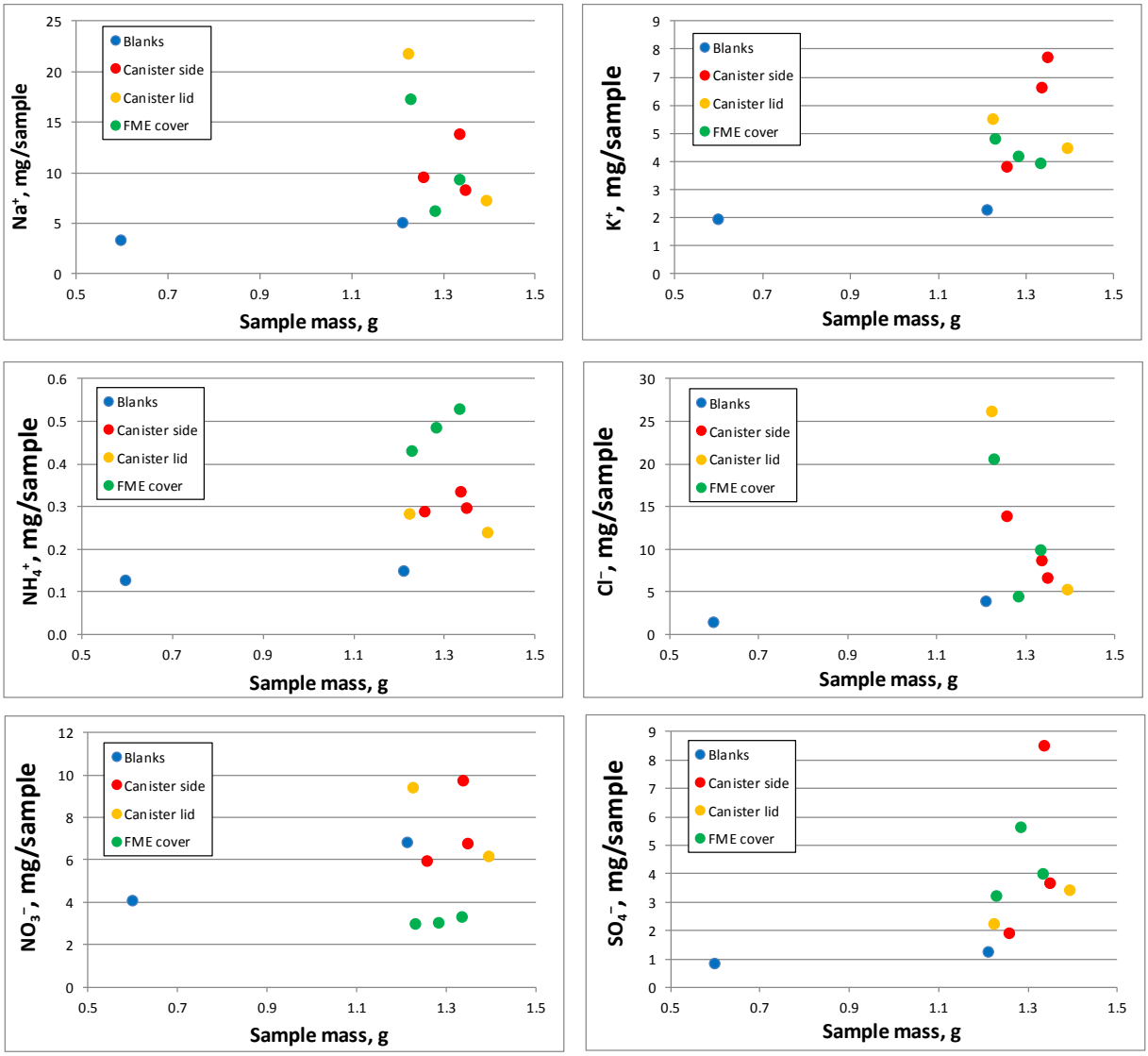

Figure 29. Plots of element concentrations vs sample weight, for leachate from dry sampling pads.

4. CONCLUSIONS

In November, 2013, EPRI directed the sampling of dusts on the surface of in-service SNF storage canisters at the Hope Creek ISFSI, from canisters in service for 7 years. The samples from the Hope Creek were characterized by Sandia National Labs (Bryan and Enos, 2014). In July, 2014, EPRI went back to the Hope Creek facility and sampled dust on the surface of an unused canister that had been stored in an overpack at the site for approximately one year. Since the canister was empty, and had no heat load, convective airflow through the overpack was very limited, and it was anticipated that dust loads on the canister surface would be very light. The dust compositional data for a cold, unused canister complements that from dust on the hot in-service canisters, potentially allowing evaluation of the effects of temperature on the salt compositions. The Foreign Material Exclusion (FME) cover that had been on the top of the canister during storage, and a second recently-removed FME cover, were also sampled. This report summarizes the results of analyses of dust samples collected from the unused Hope Creek canister and the FME covers.

The sample types collected were similar to those described previously for the Hope Creek and Diablo Canyon sampling episodes (Bryan and Enos, 2014). Both wet and dry samples of the dust/salts were collected, using SaltSmart™ sensors and Scotch-Brite™ abrasive pads, respectively. At SNL, the wet samples were analyzed by chemical analysis to determine the composition and abundance of soluble salts present. The pads containing the dry dust were removed from the stainless steel backing plates and analyzed by X-ray fluorescence to obtain bulk chemical compositions. Then, a small portion of the sponge was removed and retained for SEM analysis. The remaining sponge was washed thoroughly with deionized water and the leachate collected, filtered, and analyzed for soluble salts. The pads were washed, and a tiny amount of insoluble residue was collected; however, the sample size was too small for bulk analysis of the residue.

As discussed in the following sections, the dust samples from the surface of the unused canister at Hope Creek were dominantly particles of stainless steel. Terrestrially-derived silicate/aluminosilicate dust particles and salts were also present, but at much lower abundances. The salts were dominantly sulfates, with rare chlorides and nitrates. The FME covers had been stored in the open for a few days prior to sampling, and a rainstorm had washed them. Sampling showed that despite the rain, dust and salts remained on the surface; however, the degree to which these salts represent what was there prior to the rain is unknown. The FME dusts were almost entirely silicates/aluminosilicates, but sulfate salts were also abundant; nitrate and chloride salts were rare, as were stainless steel particles. The abundance of stainless steel particles on the canister surface, and the relative paucity of stainless steel particles relative to environmentally-derived particles on the FME cover, strongly suggest that the stainless steel particles were created during the canister manufacturing process and were not deposited after relocation of the canister to the Hope Creek Site.

Sulfate salts dominated the assemblages on the canister and FME surfaces, and included Ca-SO_4, but also Na-SO_4, K-SO_4, and Na-Al-SO_4. It is likely that these salts were formed by particle-gas conversion reactions, either prior to, or after, deposition. These involve reaction of carbonate, chloride, or nitrate salts with atmospheric SO_2, sulfuric acid, or ammonium sulfate to form

sulfate minerals. The Na-Al-SO_4 phase is unusual, and may have formed by reaction of Na-Al containing phases in aluminum smelter emissions with SO_2, also present in smelter emissions. An aluminum smelter is located in Camden, NJ, 40 miles NE of the Hope Creek Site.

While SaltSmart™ chemical analyses, SEM/EDS analyses, and XRF analysis are consistent in indicating that sulfates are the dominant salts present, the leachates from the dry pad samples differed and were rich in chloride. It is likely that the high chloride concentrations are artifacts due to leaching from the Scotch-Brite™ pad matrices; however, no definitive conclusion can be reached.

5. REFERENCES

Bryan C. and Enos D., 2014. *Analysis of Dust Samples Collected from Spent Nuclear Fuel Interim Storage Containers at Hope Creek, Delaware, and Diablo Canyon, California,* SAND2014-16383, Sandia National Laboratories, Albuquerque, NM (2014)

Calvert Cliffs Nuclear Power Plant, 2012. *Response to Request for Additional Information, RE: Calvert Cliffs Independent Spent Fuel Storage Installation License Renewal Application (TAC No. L24475),* ADAMS ML12212A216.

Calvert Cliffs Nuclear Power Plant, 2013. *Response to Request for Additional Information, RE: Calvert Cliffs Independent Spent Fuel Storage Installation License Renewal Application (TAC No. L24475),* ADAMS ML13170A574.

Enos D., Bryan C., and Norman K., 2013. *Data Report on Corrosion Testing of Stainless Steel SNF Storage Canisters,* FCRD-UFD-2013-000324, Sandia National Laboratories, Albuquerque, NM.

Kvande, H., and Drabløs, P. A., 2014. The Aluminum Smelting Process and Innovative Alternative Technologies: *Journal of Occupational and Environmental Medicine,* 56(5), S23-S32.

APPENDIX A: SEM/EDS DATA

SEM and EDS analysis of the Hope Creek and Diablo Canyon dust samples are discussed in Section 3.1, and a subset of the results was presented. This appendix contains the complete suite of analyses collected for these samples, allowing the reader to better evaluate the representativeness of the results provided in Section 3.1.

387-001
Overview Image

Notes: Pad sample 387-001, collected from the canister side, 1 foot above the bottom edge. Low magnification SEM image showing moderate to heavy particle load adhering to the sample fibers.

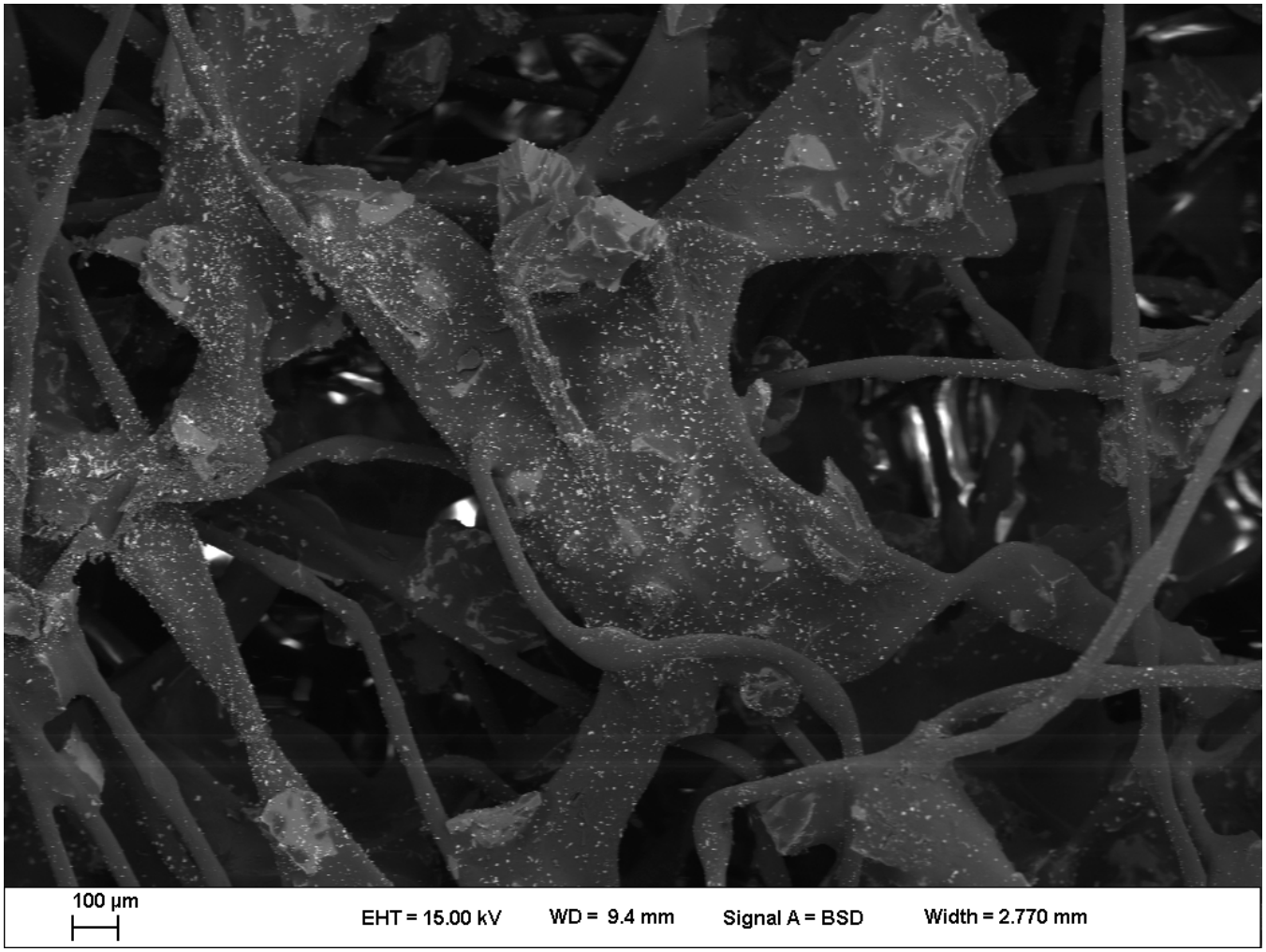

Sample 387-001, collected from the canister side, 1 foot above the bottom edge
Map A

Notes: Almost all particles are stainless steel. The large Al-O phase along the right hand edge is an aluminum oxide grain in the pad matrix (*these are common in the pad matrix, and will not be discussed again*).

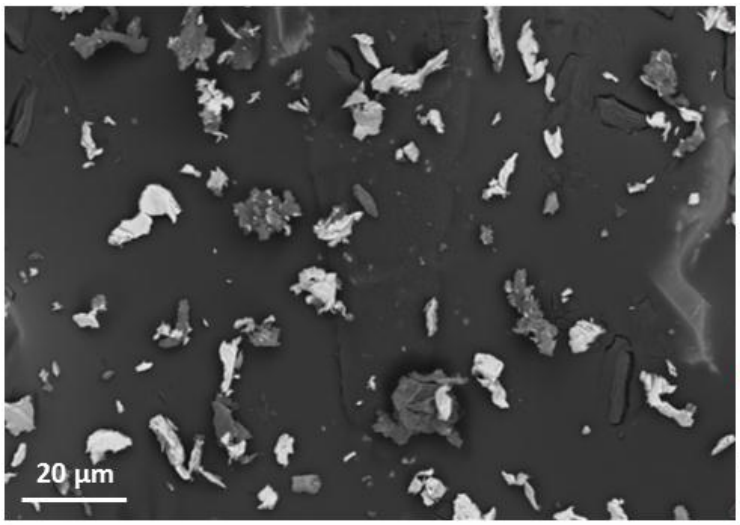

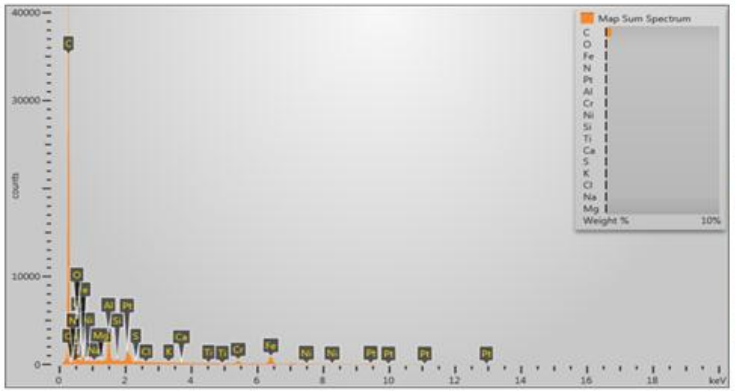

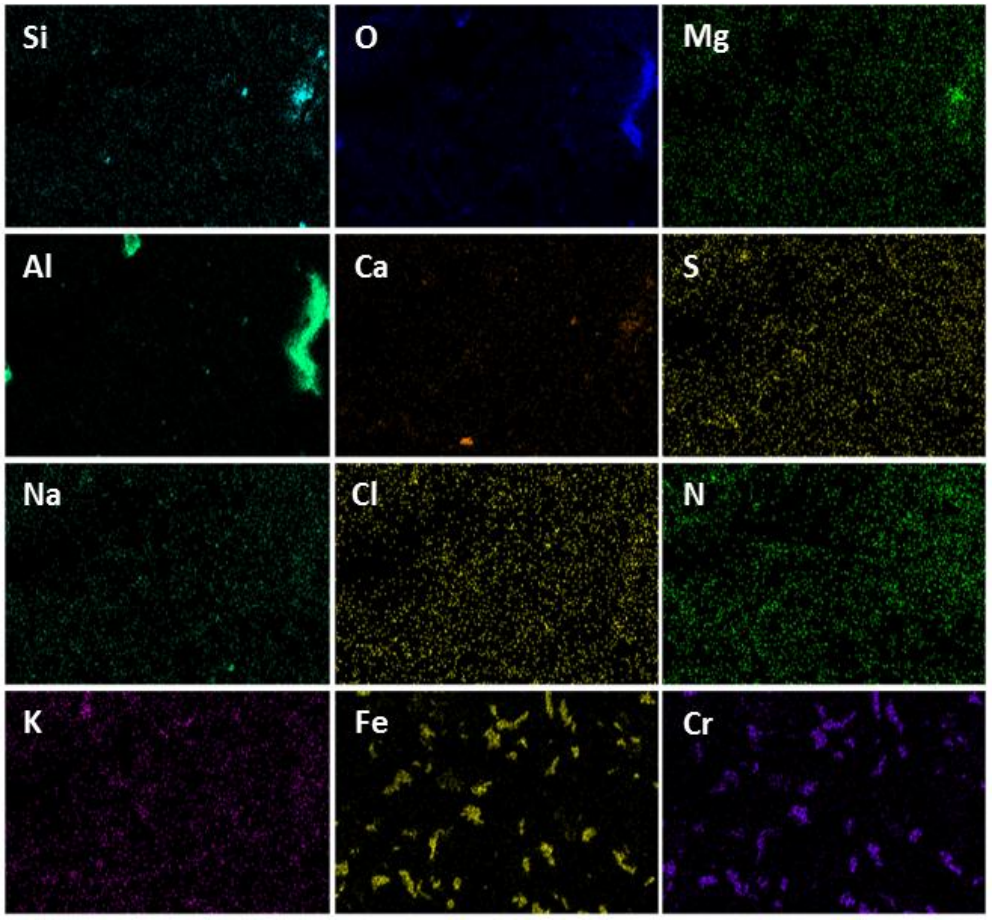

Sample 387-001, collected from the canister side, 1 foot above the bottom edge
Map B

Notes: Almost all particles are stainless steel; a Ca-Mg-aluminosilicate grain is in the center of the image.

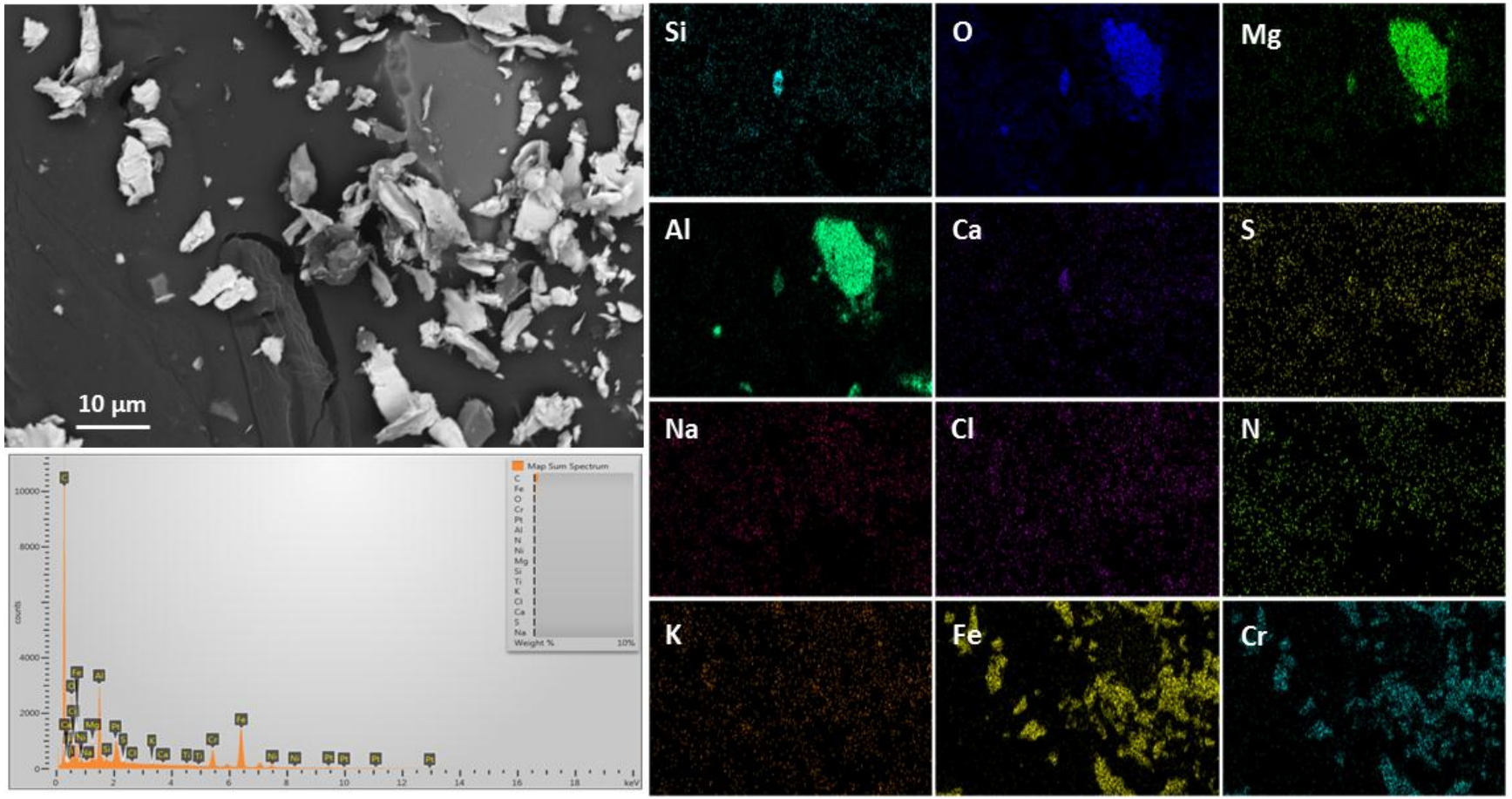

Sample 387-001, collected from the canister side, 1 foot above the bottom edge
Map C

Notes: Most grains are stainless steel.

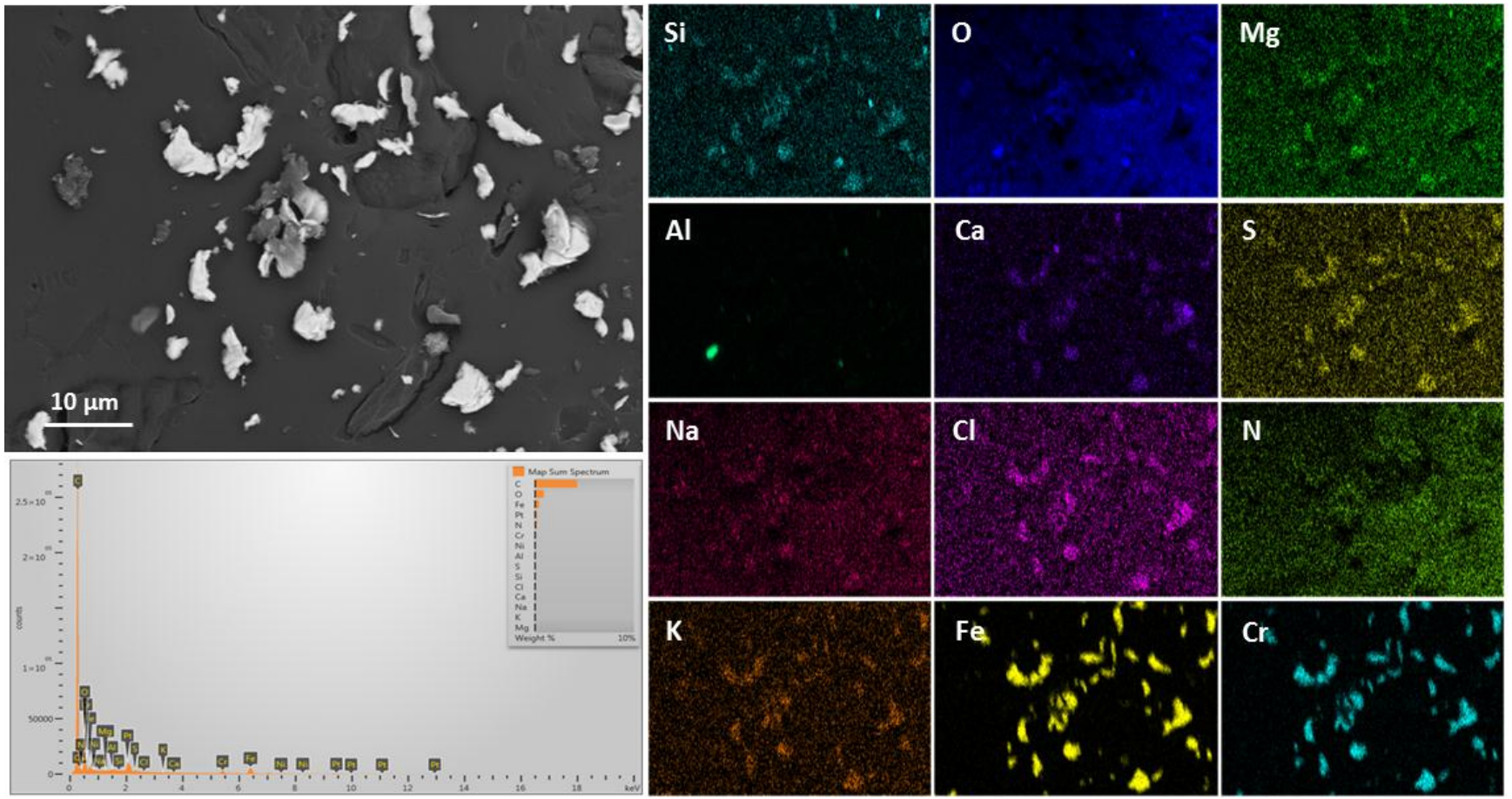

Sample 387-001, collected from the canister side, 1 foot above the bottom edge
Map D

Notes: Most grains are stainless steel; a few small grains of K-Na-SO_4 are present.

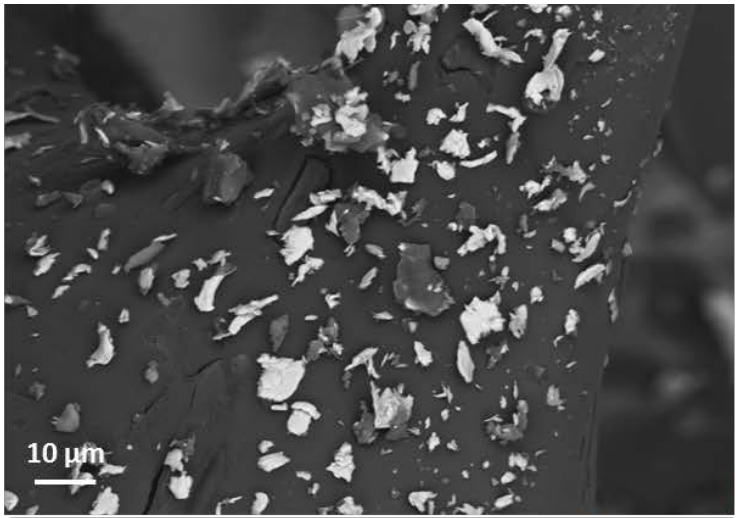

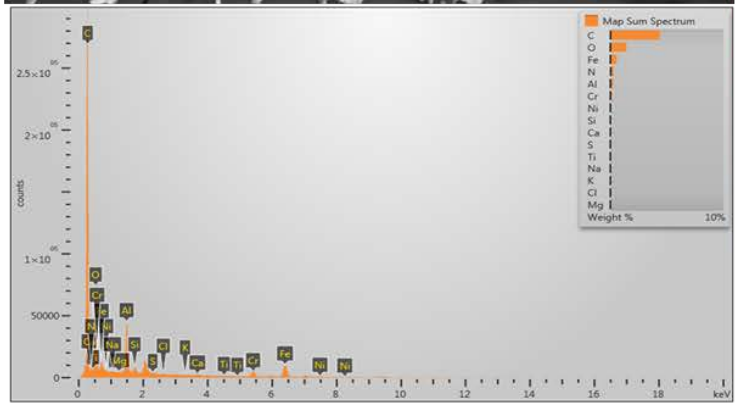

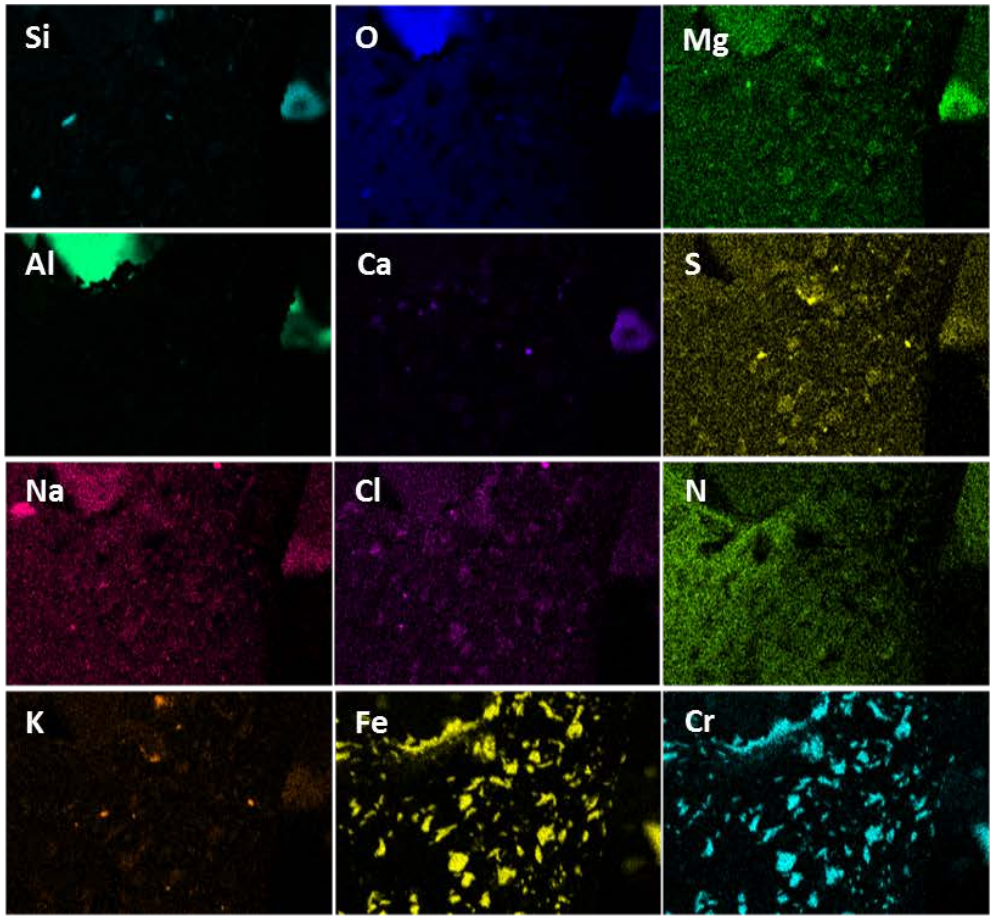

Sample 387-001, collected from the canister side, 1 foot above the bottom edge
Map E

Notes: Magnified image of K-Na-SO_4 grain in the left center of map D.

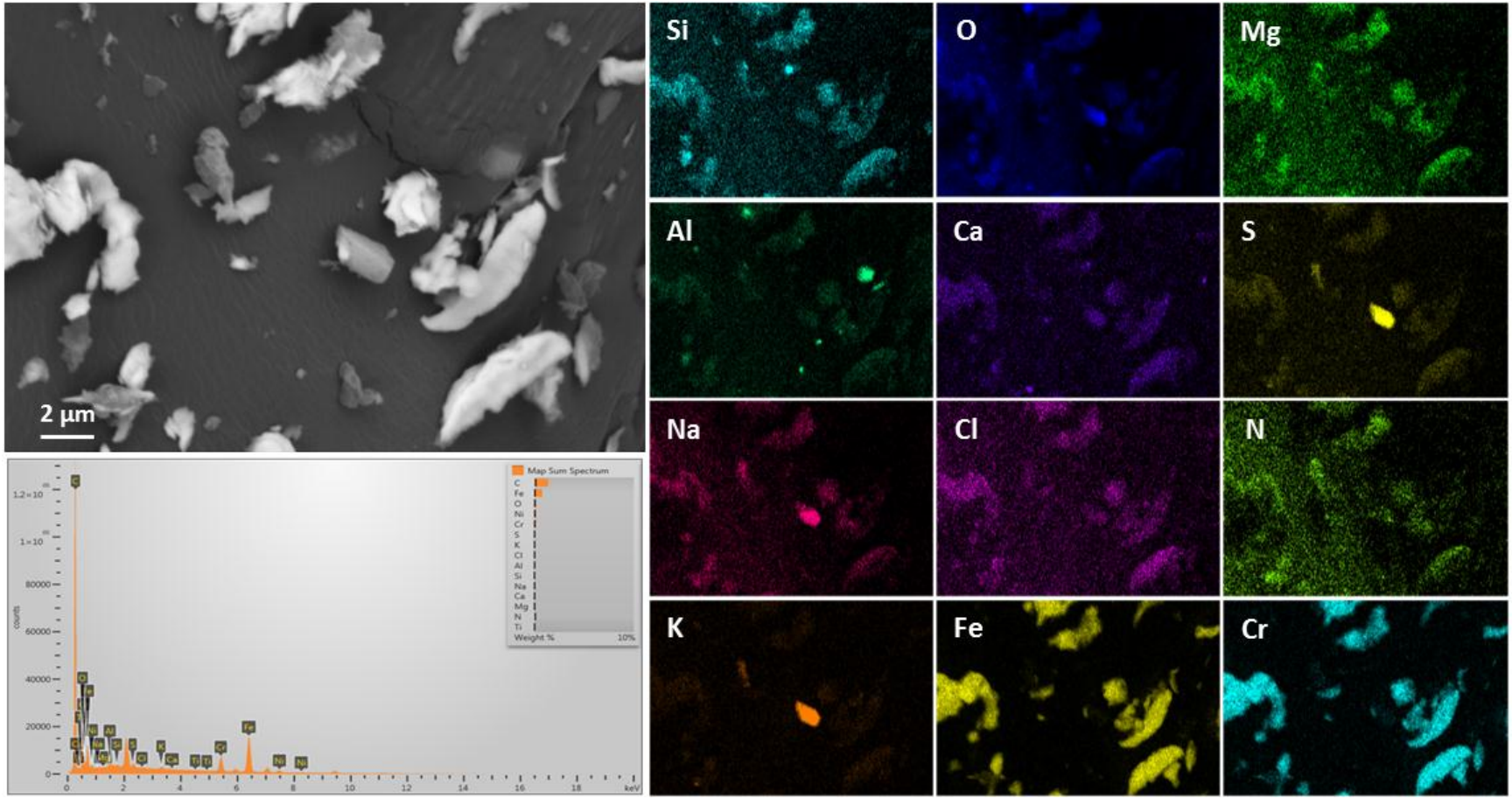

Sample 387-003, collected from the canister side, 1 foot below the upper edge
Overview Image

Notes: Low magnification SEM image showing moderate to heavy particle load adhering to the sample fibers.

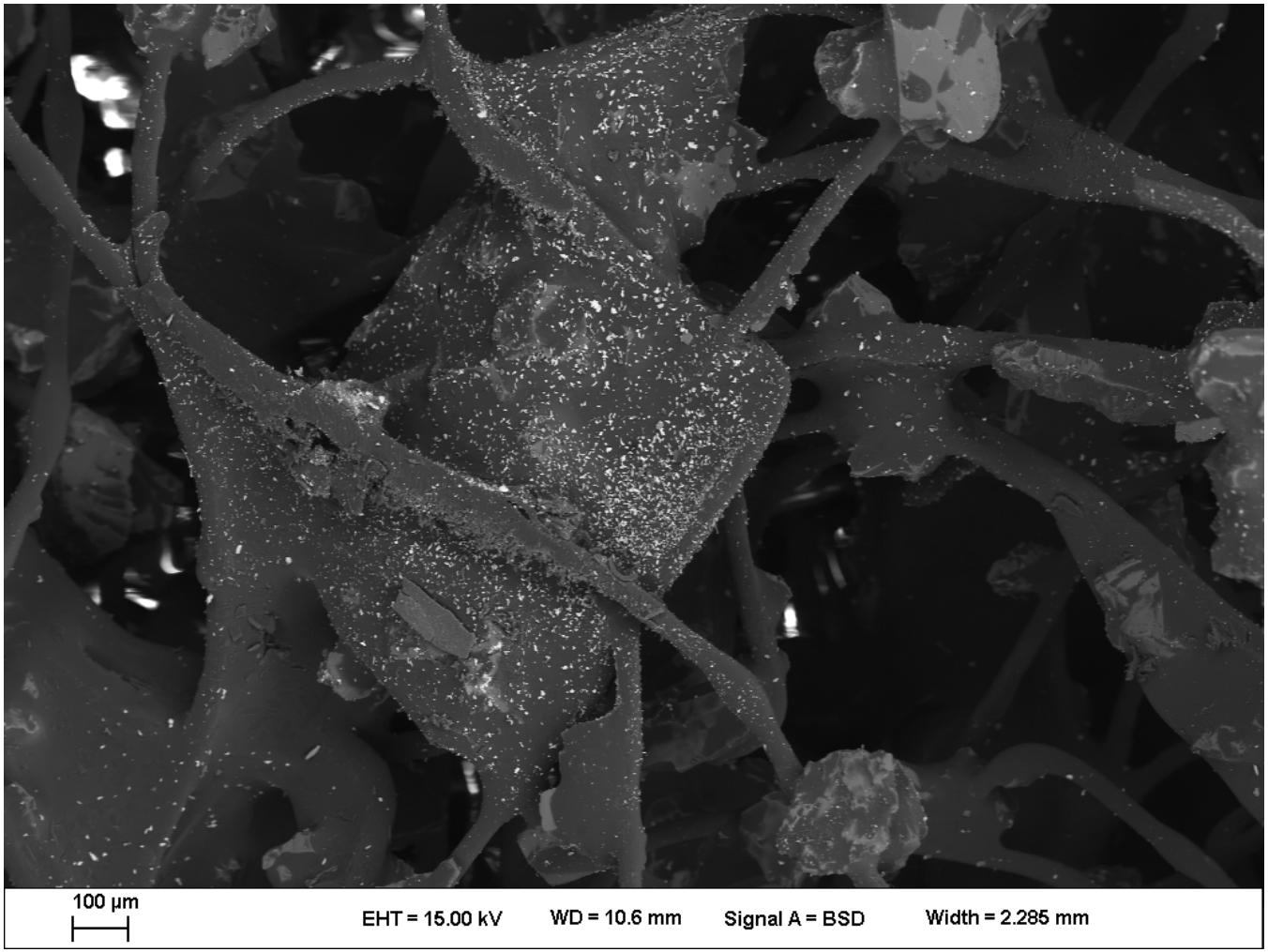

Sample 387-003, collected from the canister side, 1 foot below the upper edge
Map A

Notes: Most particles are stainless steel. Note large Ca-Mg-CO_3 grain in the center of the image.

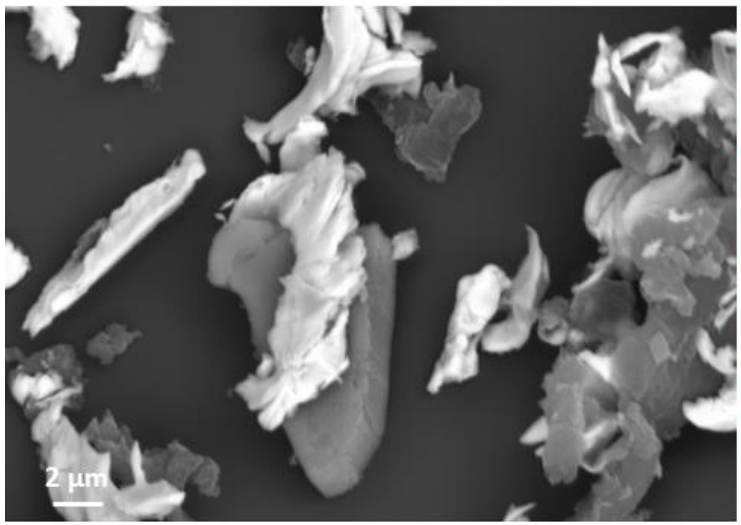

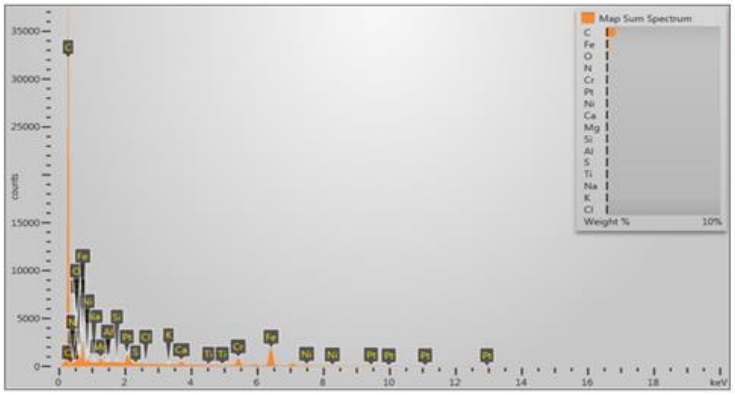

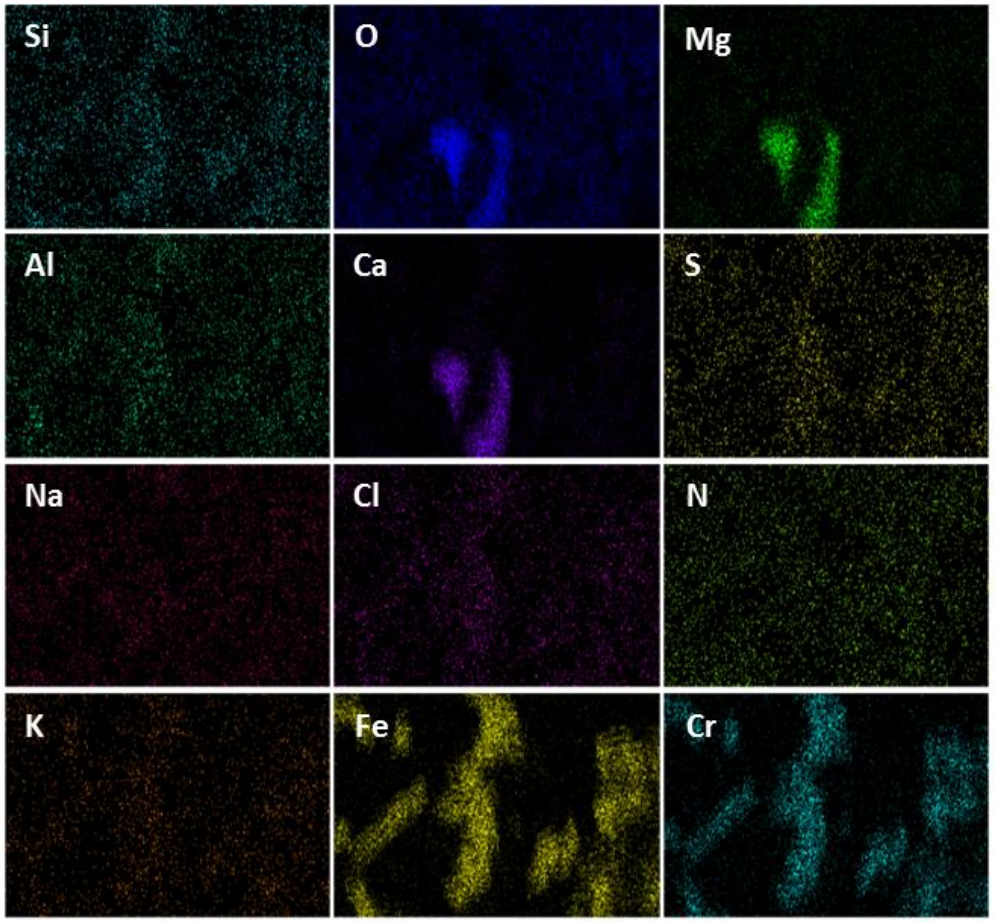

Sample 387-003, collected from the canister side, 1 foot below the upper edge
Map B

Notes: Almost all grains are stainless steel.

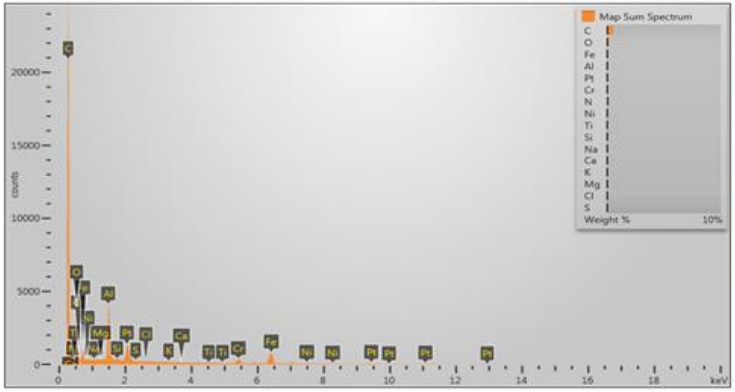

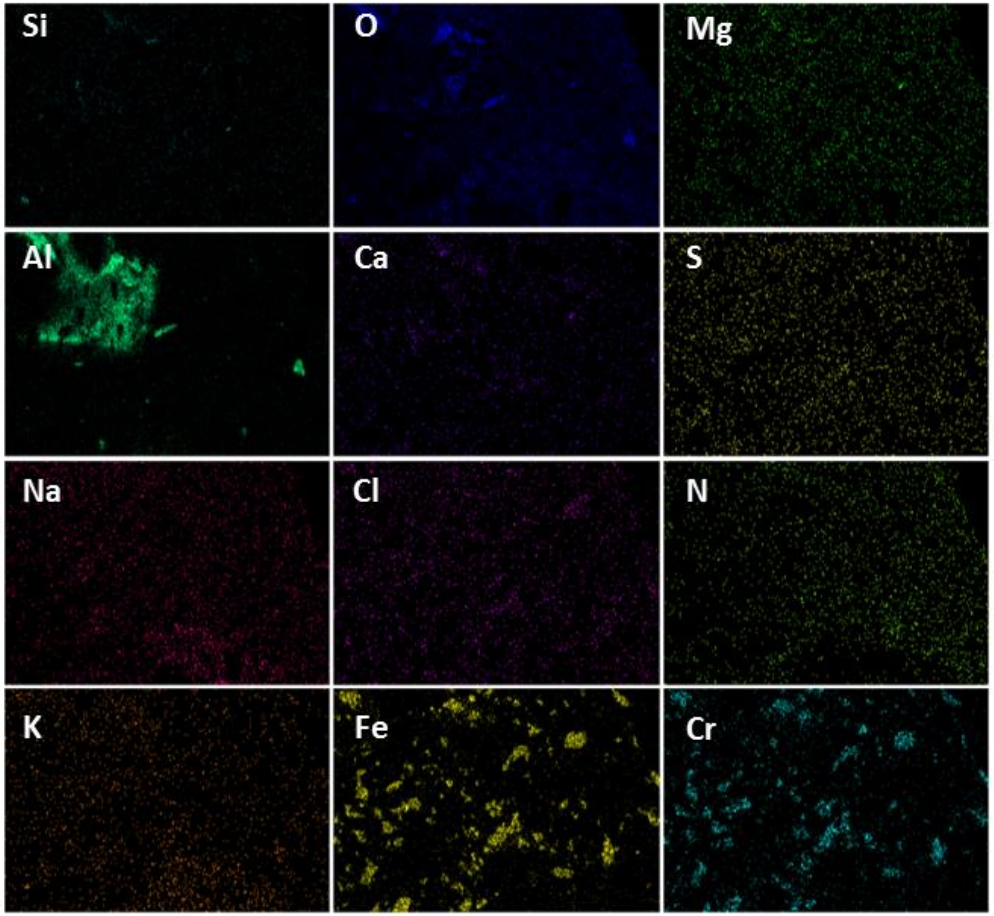

Sample 387-003, collected from the canister side, 1 foot below the upper edge
Map C

Notes: Almost all grains are stainless steel. Note grain of silica (quartz) in the center of the image.

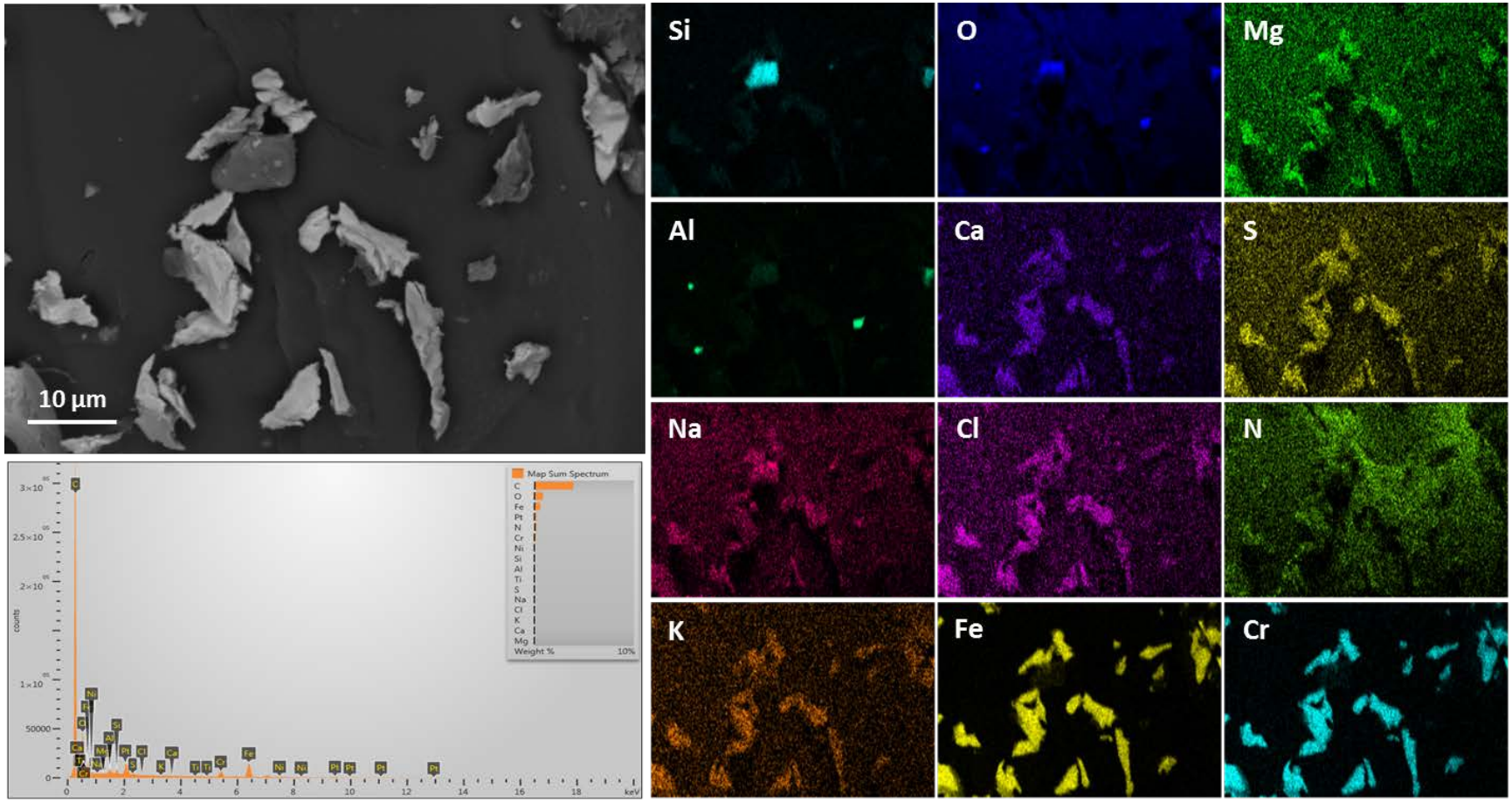

Sample 387-003, collected from the canister side, 1 foot below the upper edge
Map D

Notes: Almost all grains are stainless steel. Note grain of silica (quartz) in the center of the image.

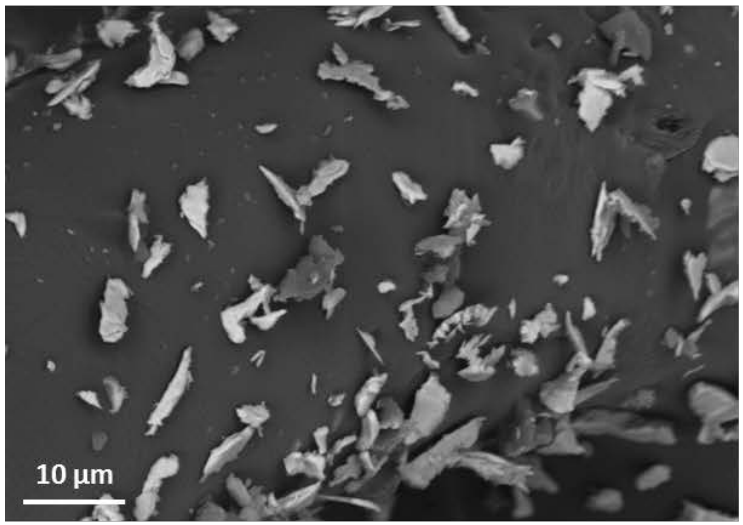

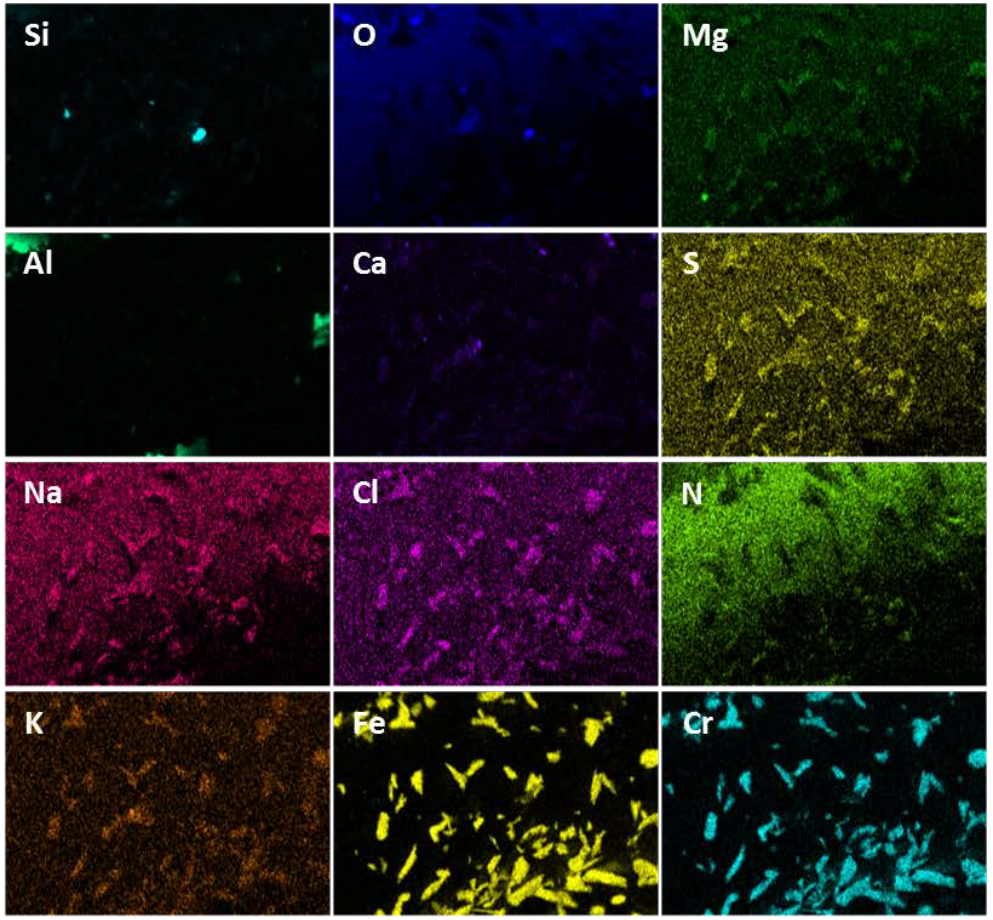

Sample 387-003, collected from the canister side, 1 foot below the upper edge
Map E

Notes: Almost all grains are stainless steel. A few grains of Si-O (quartz) are present, and a single grain of Ca-Mg-CO_3.

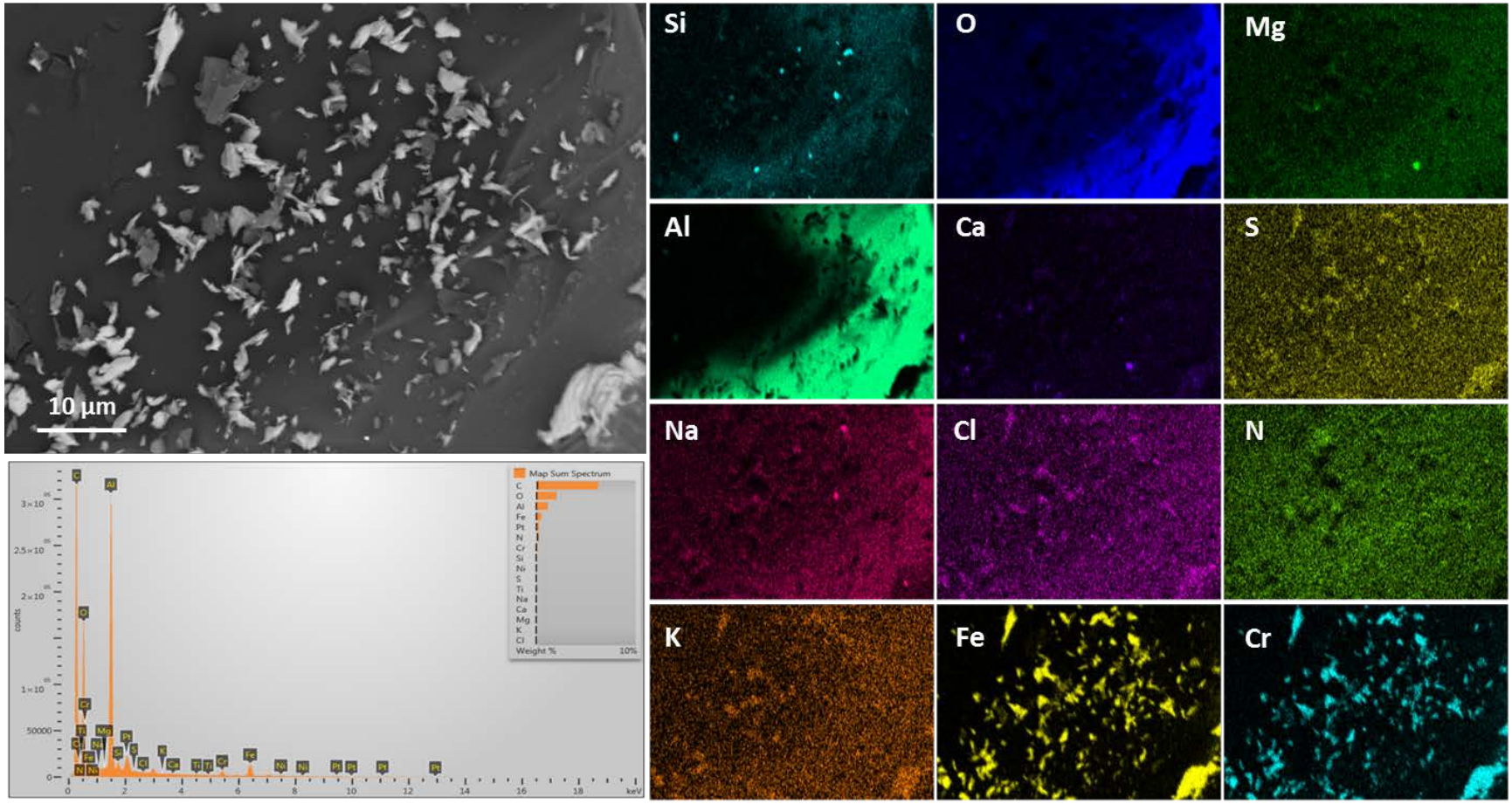

Sample 387-003, collected from the canister side, 1 foot below the upper edge
Map F

Notes: Magnified view of Ca-Mg-CO_3 grain and stainless steel grains in Map E.

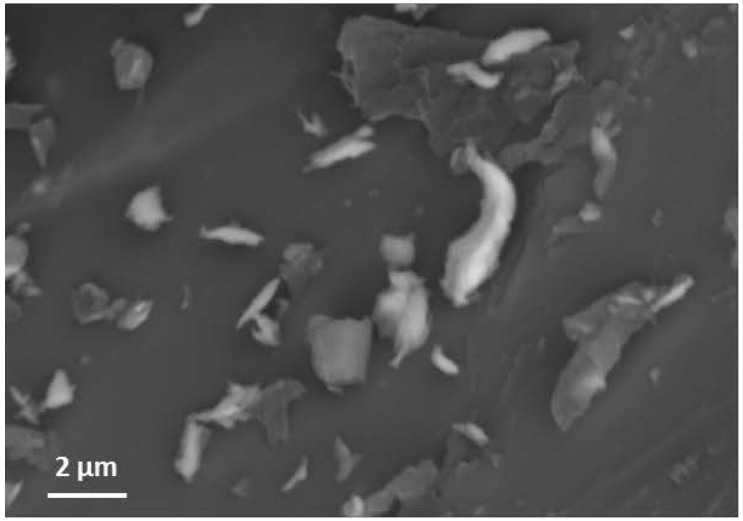

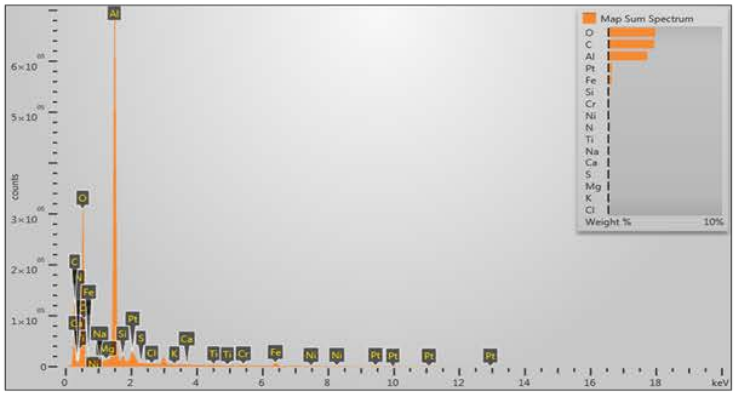

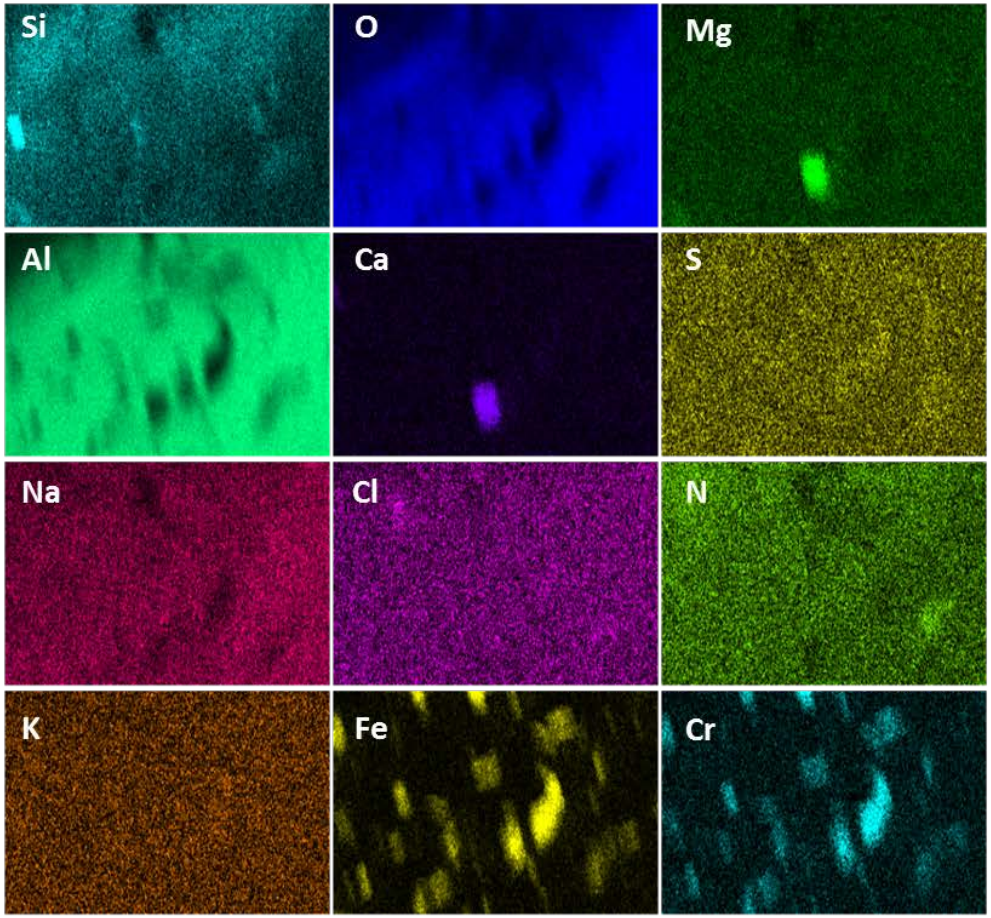

Sample 387-005, collected from the canister top, 1 foot from the edge
Overview Image

Notes: Low magnification SEM image of the dry pad sample 387-005, showing the light to moderate particle load adhering to the sample fibers.

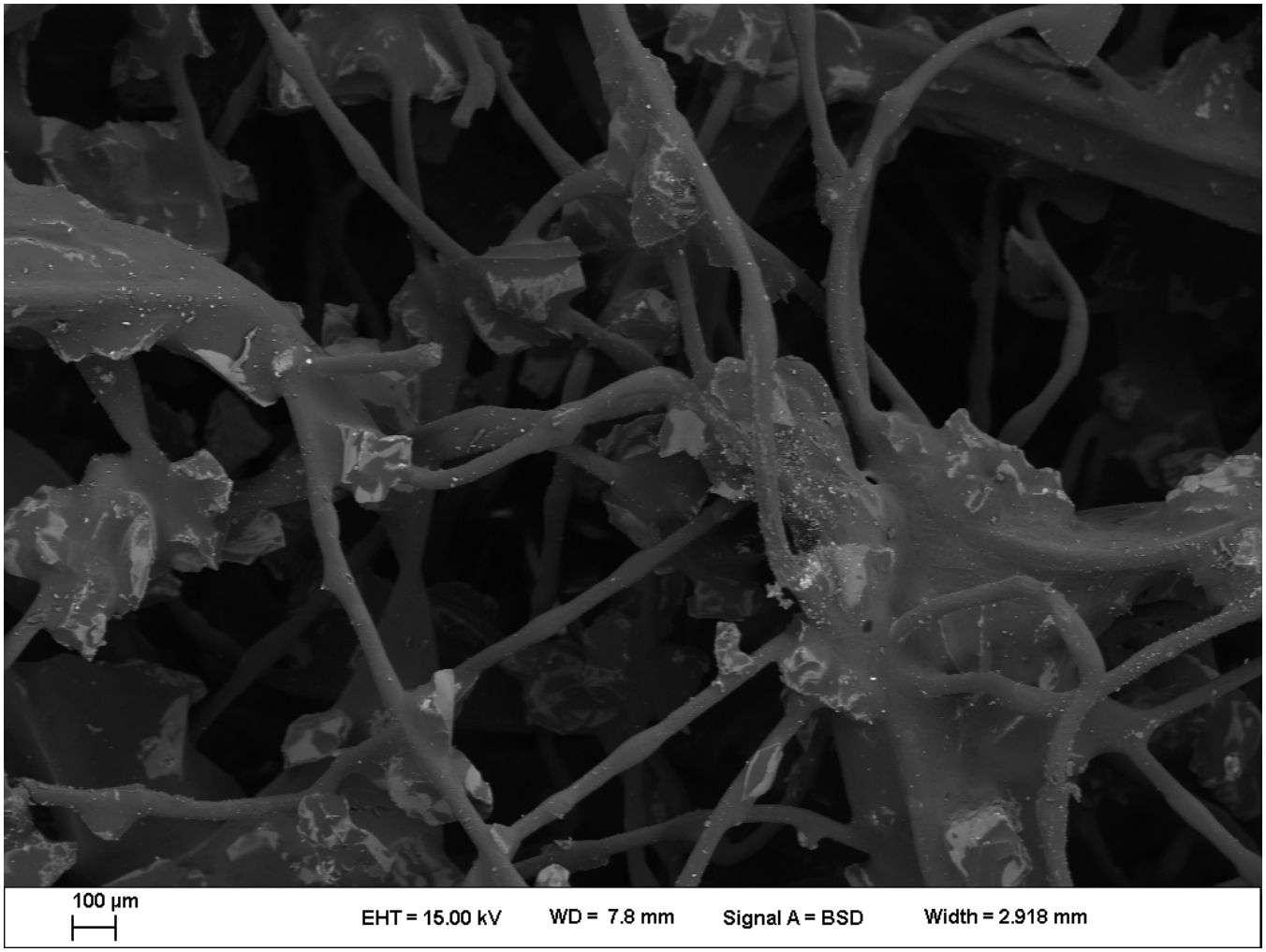

Sample 387-005, collected from the canister top, 1 foot from the edge
Map A

Notes: Magnified view of NaCl grain in the dust.

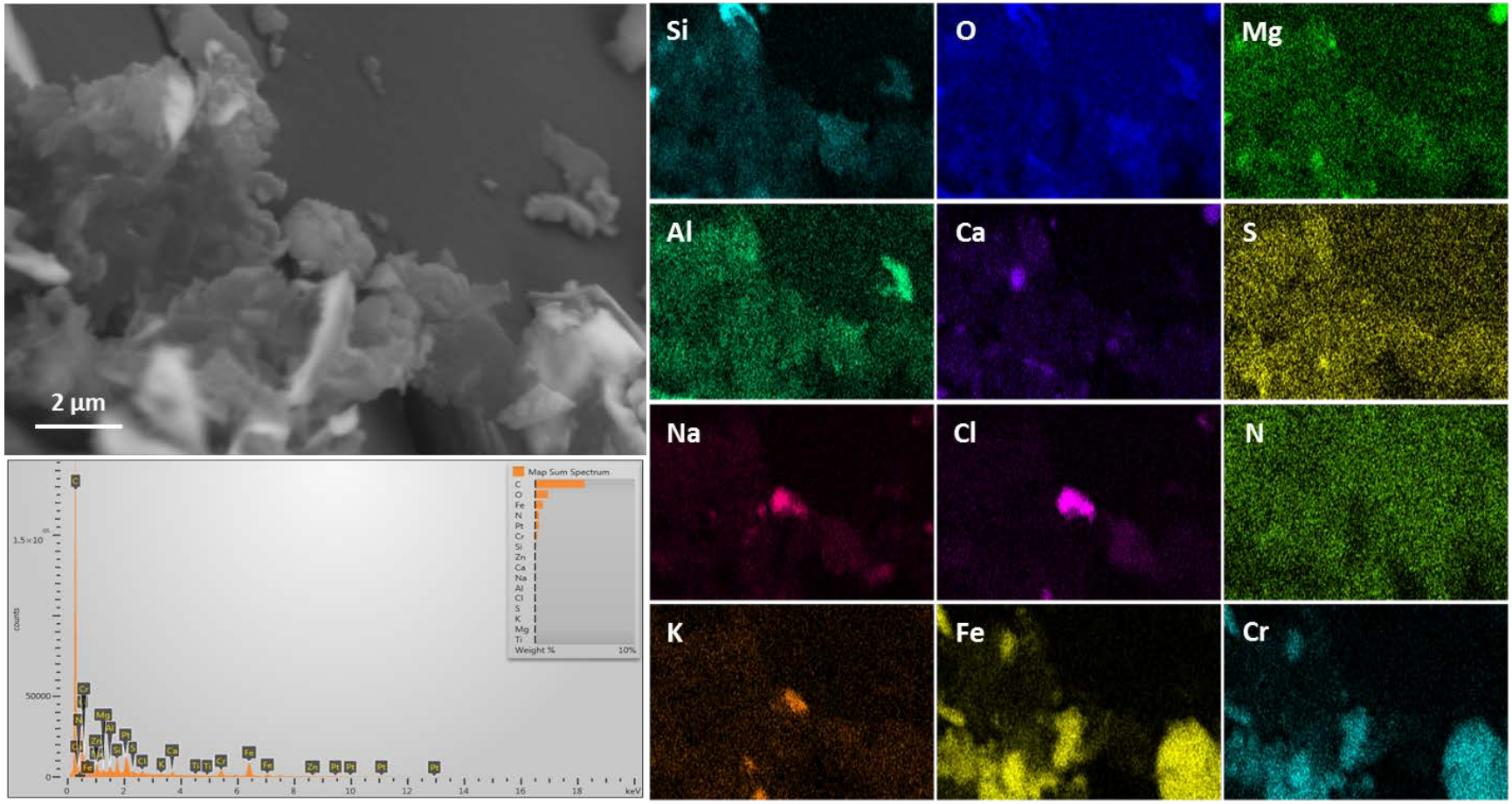

Sample 387-005, collected from the canister top, 1 foot from the edge
Map B

Notes: Particles of stainless steel, Ca-Mg-CO_3, and Ca silicate.

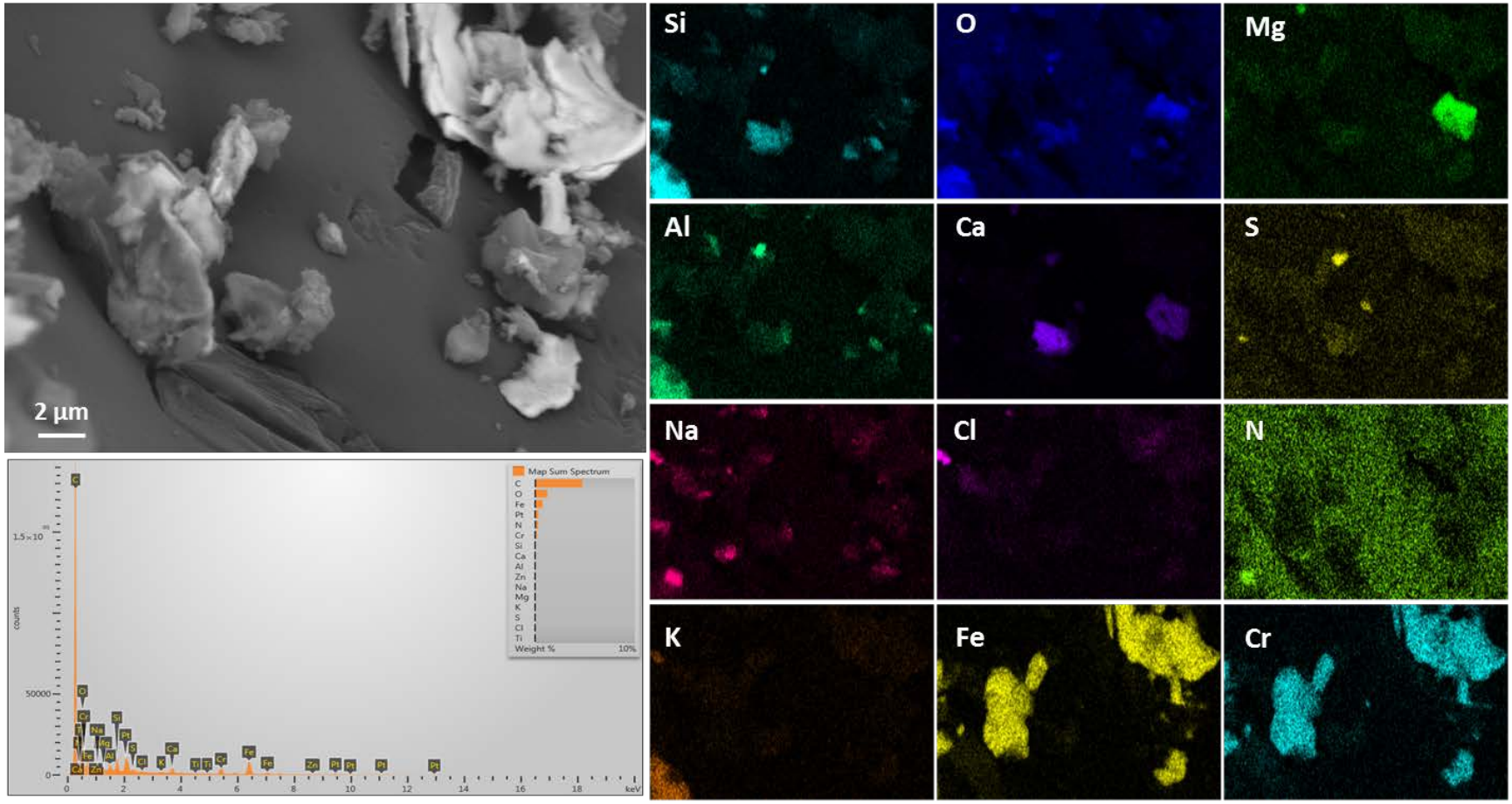

Sample 387-005, collected from the canister top, 1 foot from the edge
Map C

Notes: Sparse dust on the pad. Note NaCl grain in the center of the image.

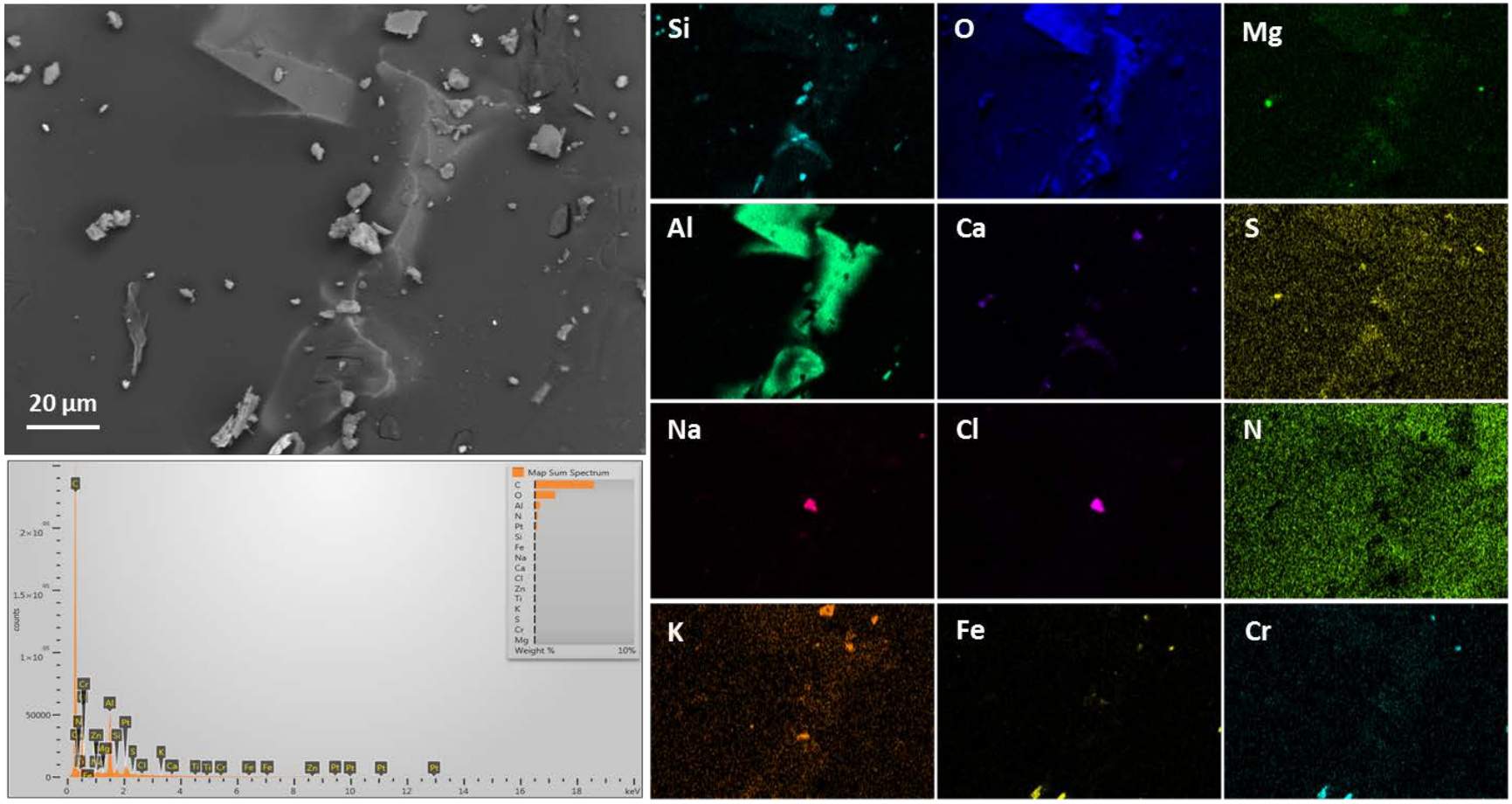

Sample 387-005, collected from the canister top, 1 foot from the edge
Map D

Notes: Magnified image of composite grain in left center of Map C. Grain contains Ca-Mg-CO_3 and Ca-SO_4 phases.

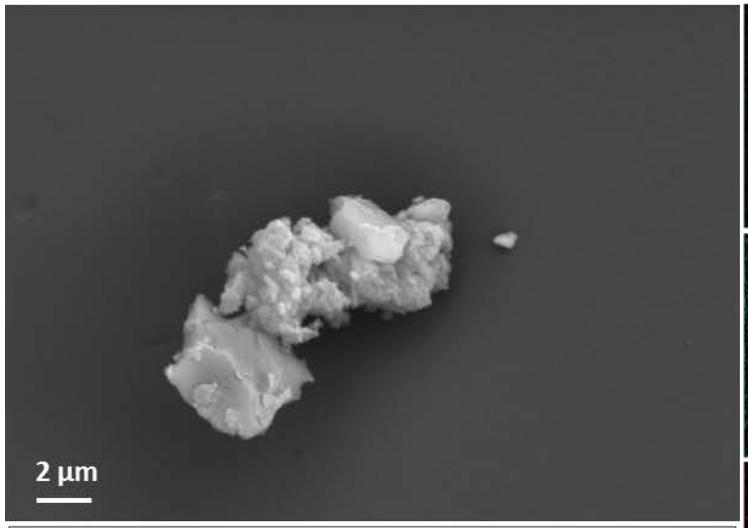

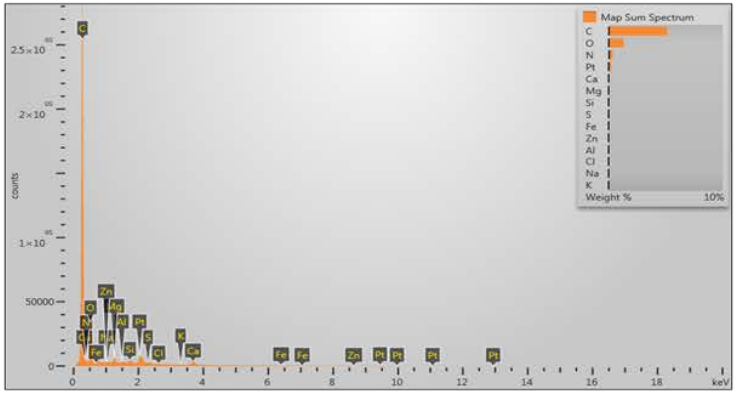

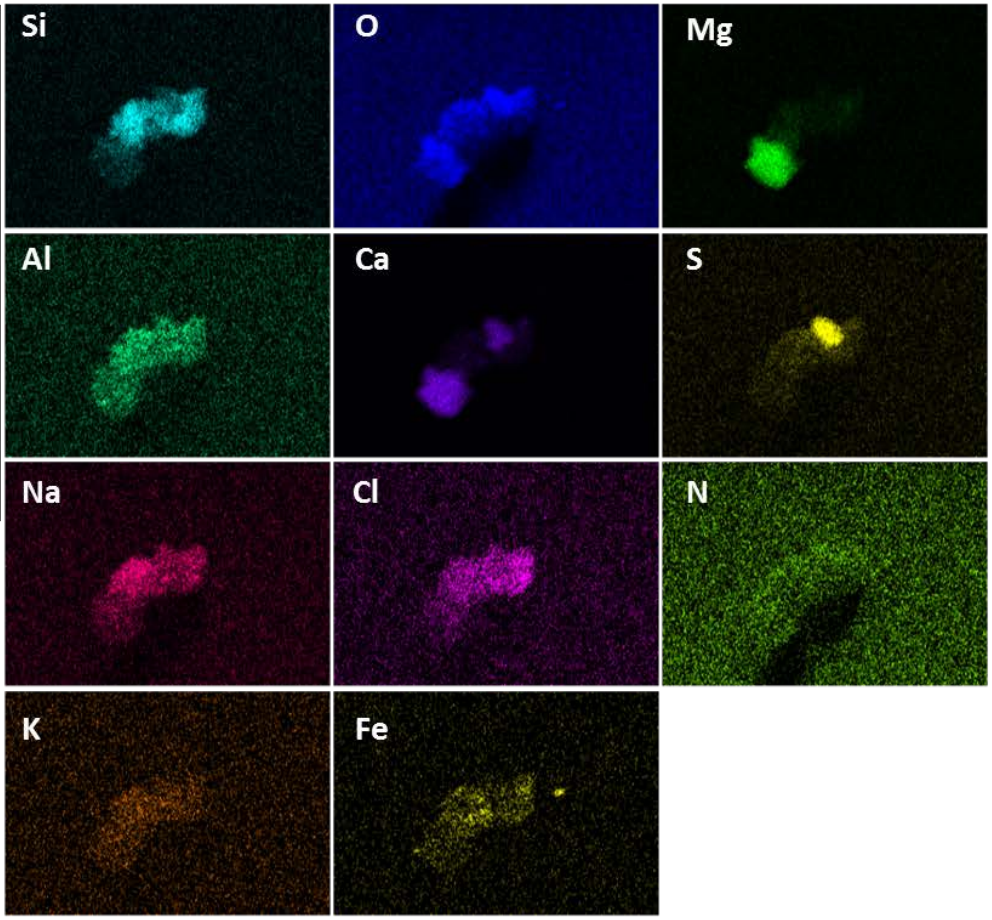

Sample 387-005, collected from the canister top, 1 foot from the edge
Map E

Notes: Most dust particles are stainless steel. Several quartz grains are also present.

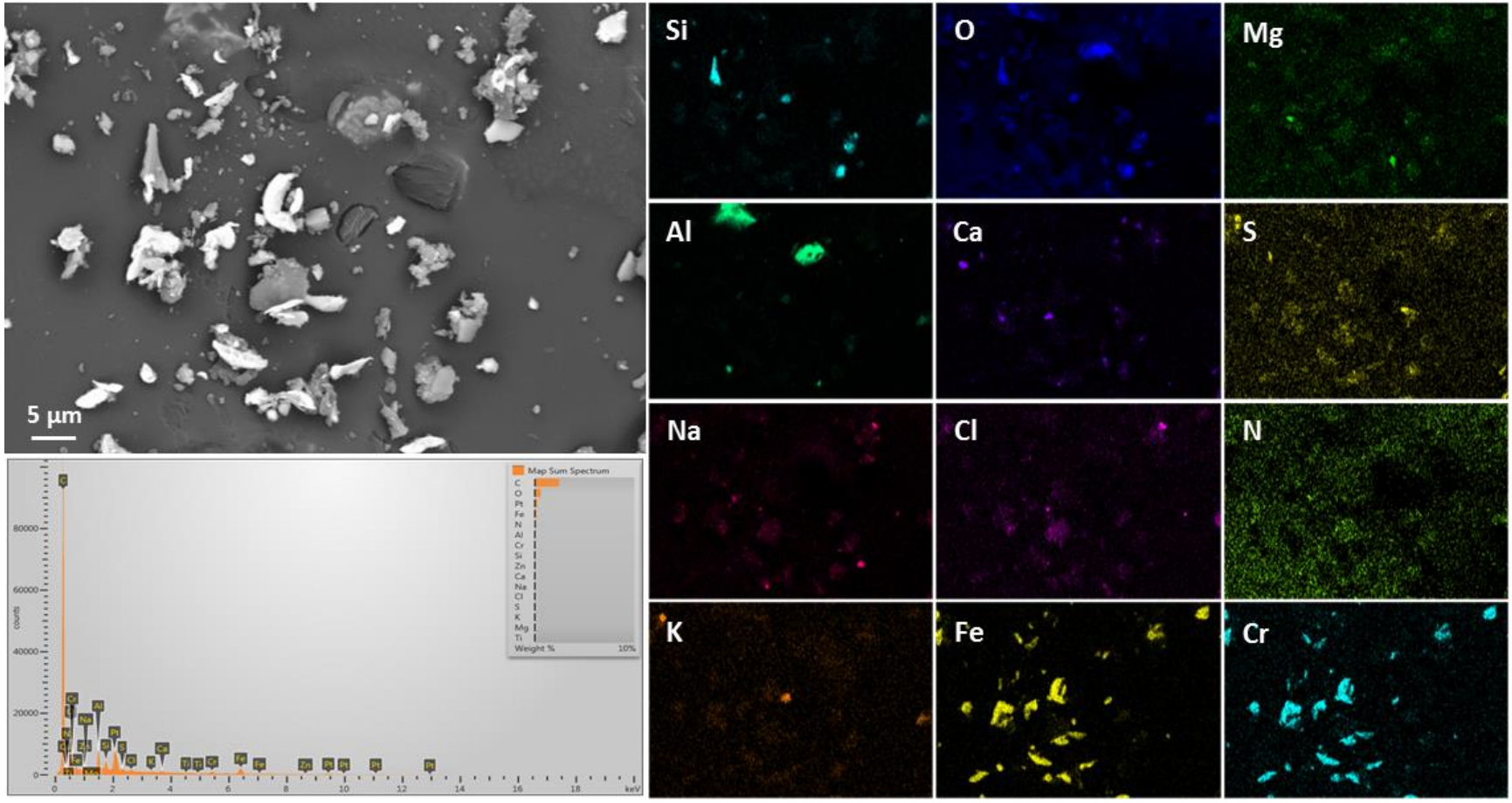

Sample 387-005, collected from the canister top, 1 foot from the edge
Map F

Notes: Dust particles are stainless steel, quartz (Si-O), Ca-CO_3, K-SO_4, Ca-SO_4.

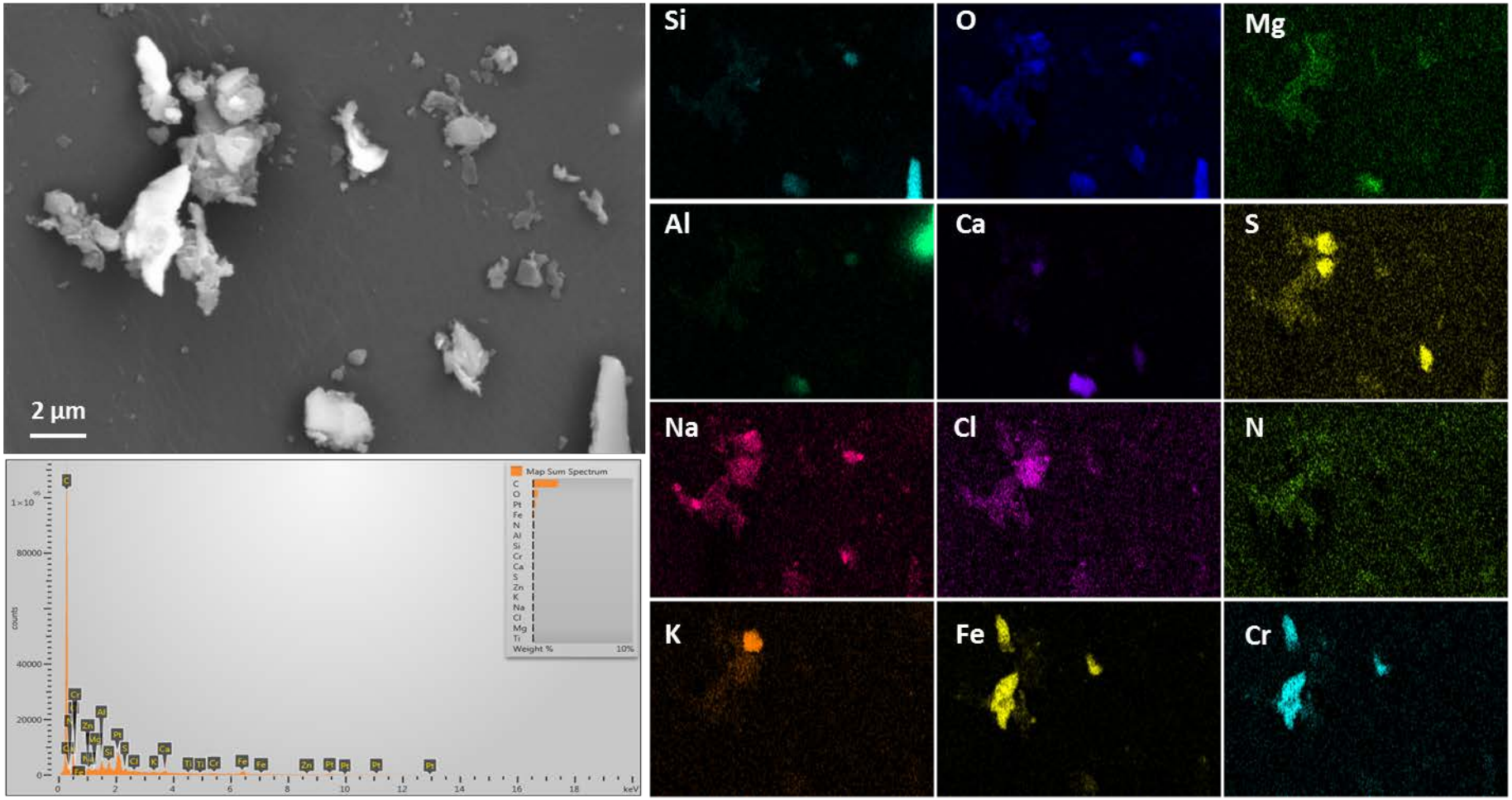

Sample 387-007, collected from the center of the canister top
Overview Image

Notes: Low magnification SEM image, showing moderate to heavy particle load adhering to the sample fibers.

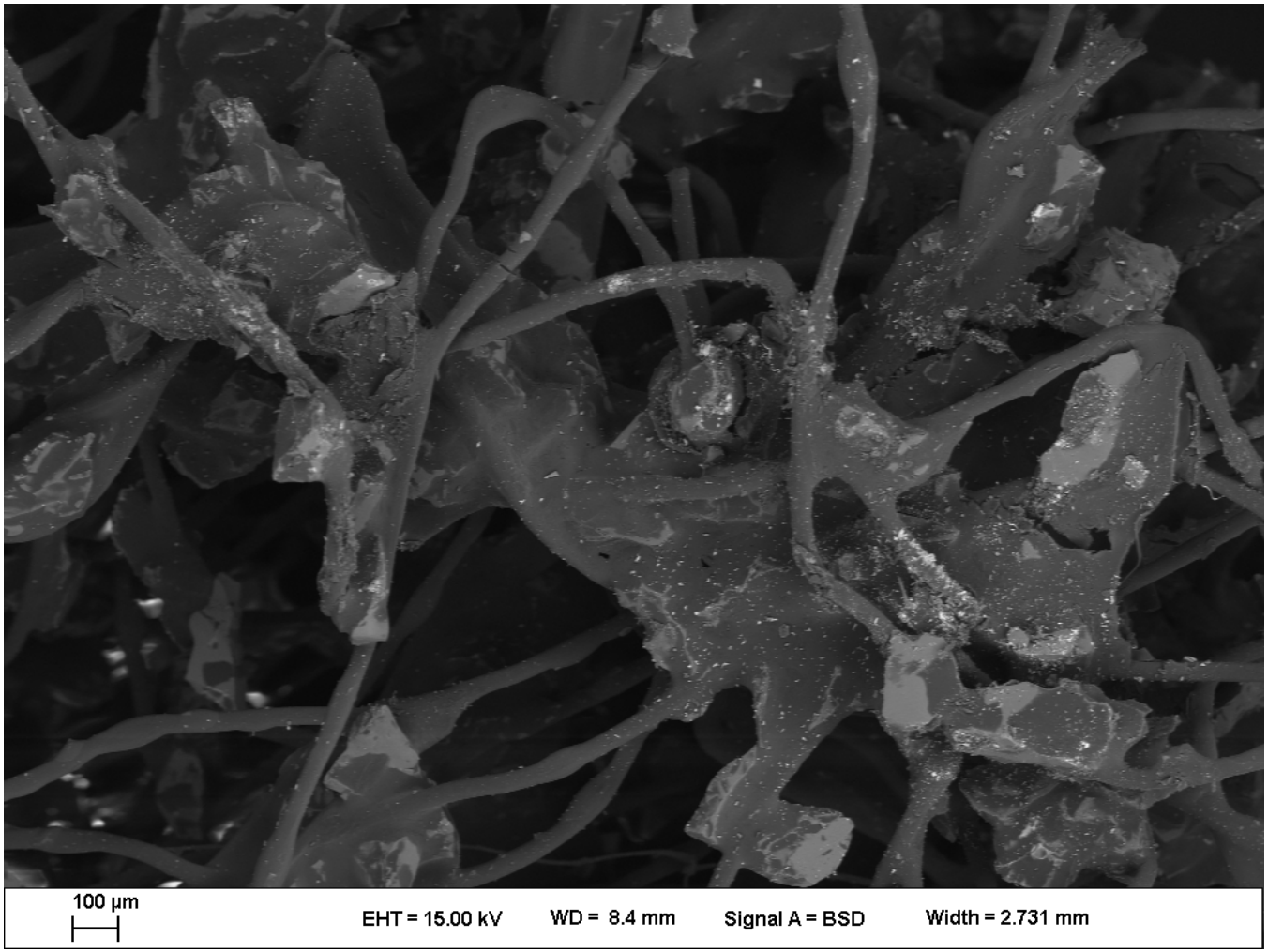

Sample 387-007, collected from the center of the canister top
Map A

Notes: Sparse dust particles are stainless steel and a large composite grain of aluminosilicates and salts.

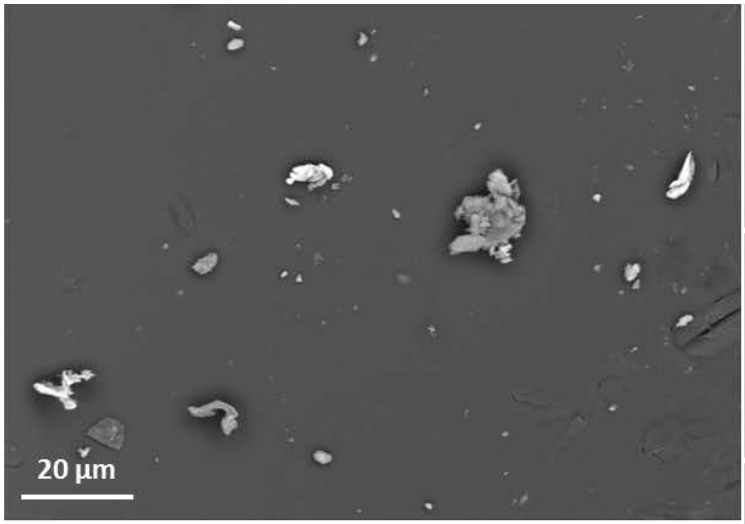

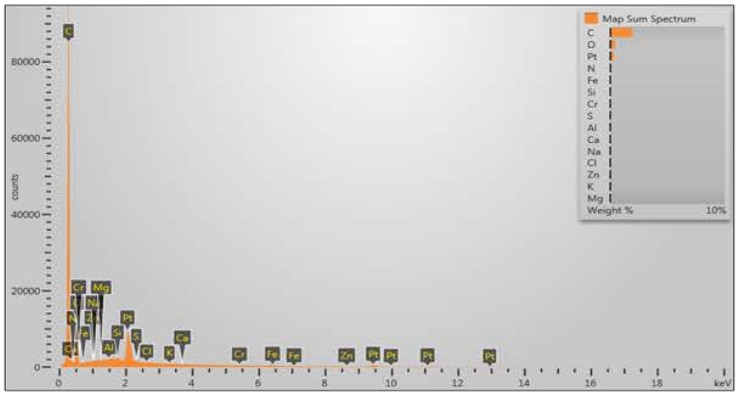

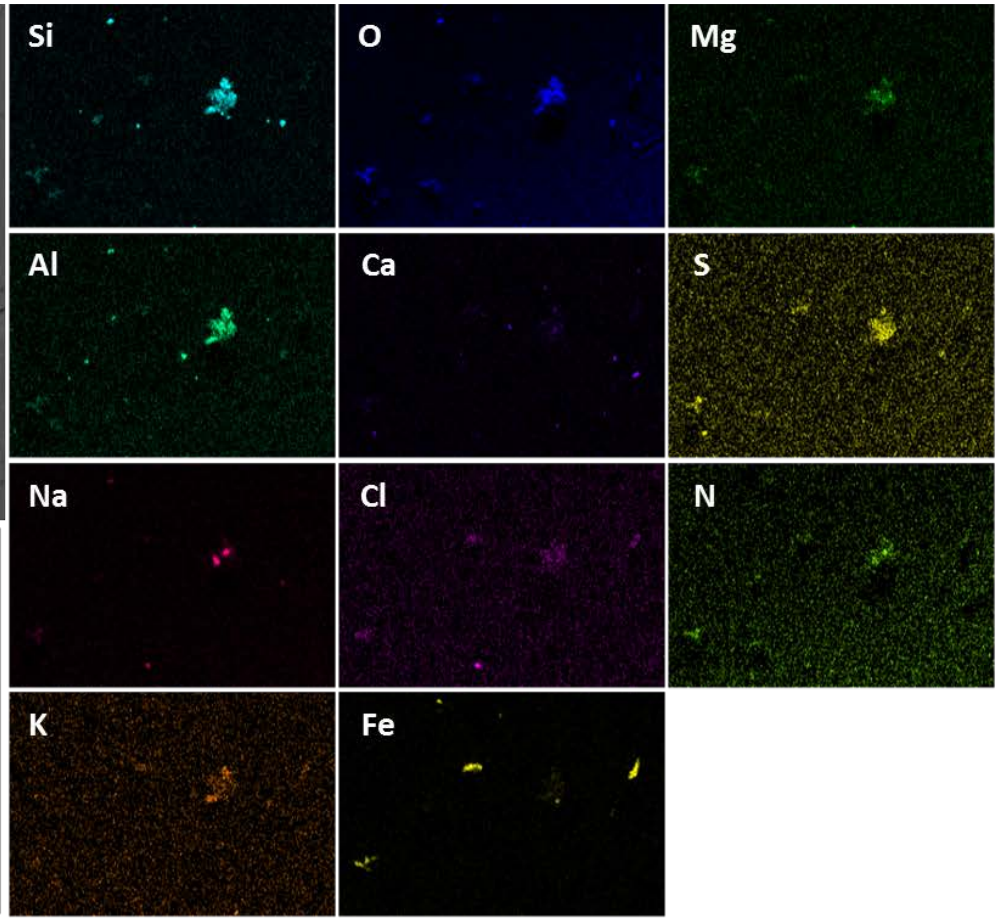

Sample 387-007, collected from the center of the canister top

Map B

Notes: Magnified composite grain in Map A. Identifiable phases in the grain are silica and aluminosilicates, and Na-NO_3. Grain also contains sulfate, although the individual phase is not readily identified.

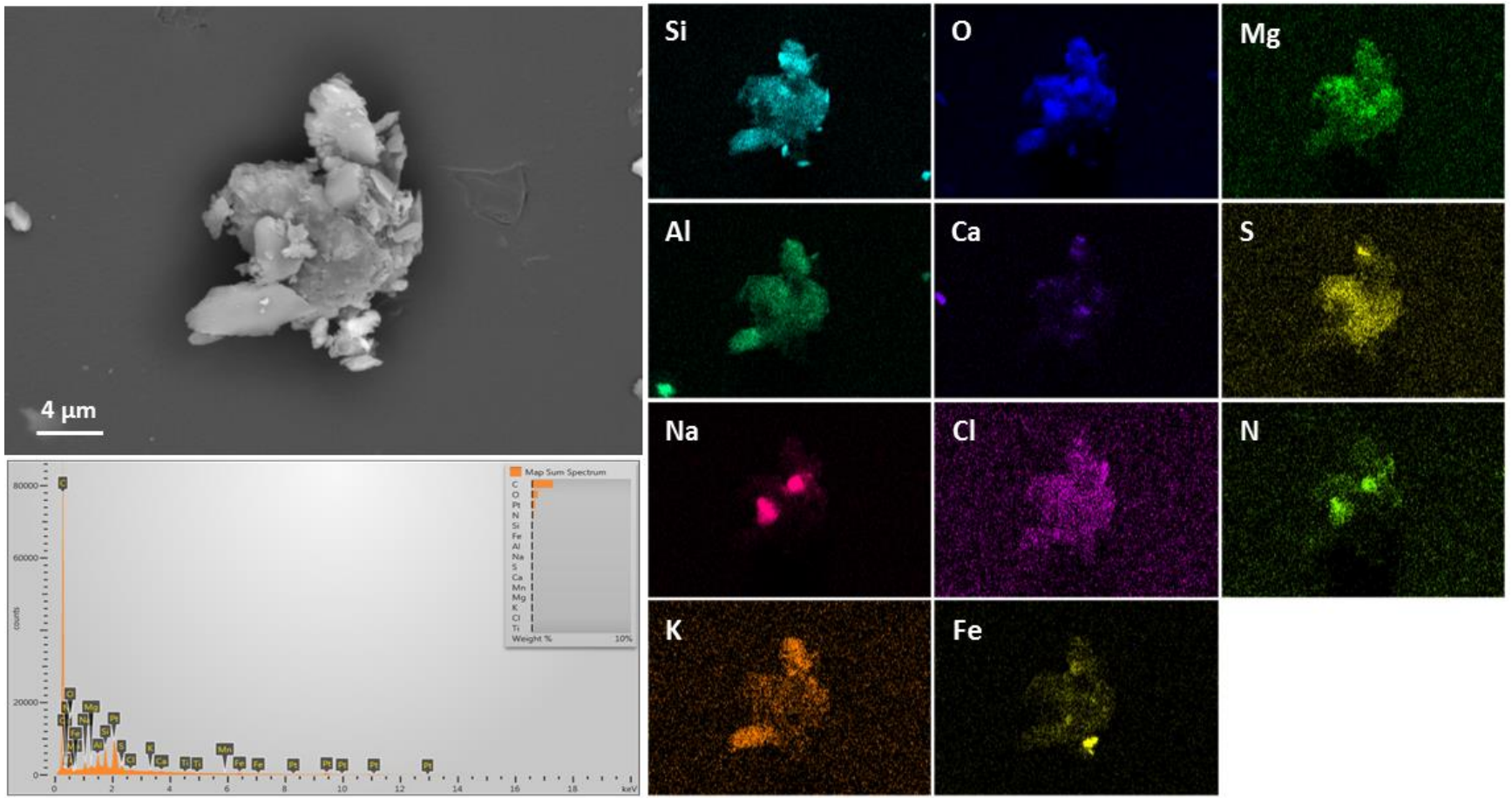

Sample 387-007, collected from the center of the canister top
Map C

Notes: Dust grains are mostly stainless steel, but Ca-SO_4 grains are also abundant, and some silica and aluminosilicate grains are also present.

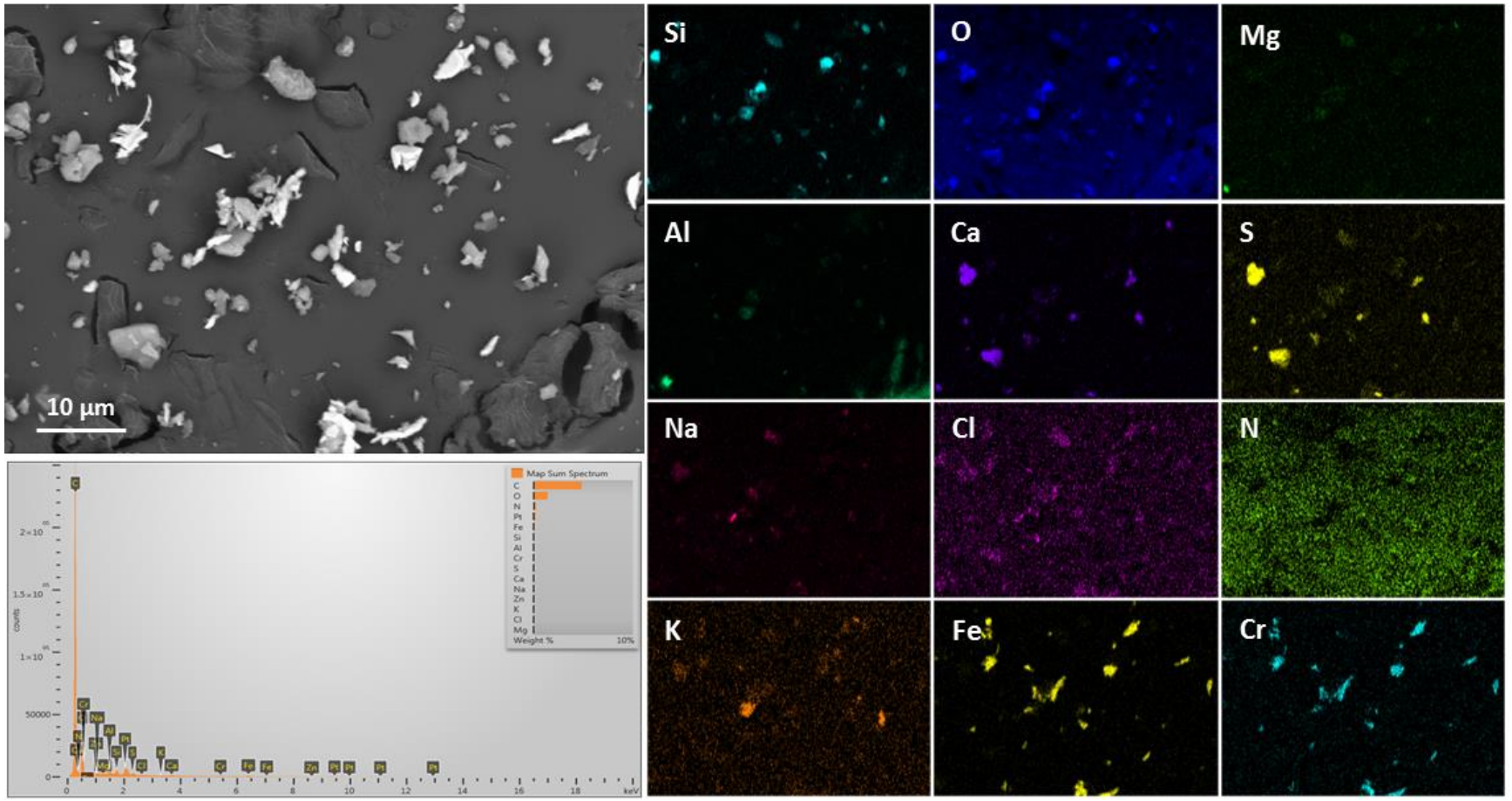

Sample 387-007, collected from the center of the canister top
Map D

Notes: Most dust particles are stainless steel, but large composite grains of silicates/aluminosilicates and salts are also present.

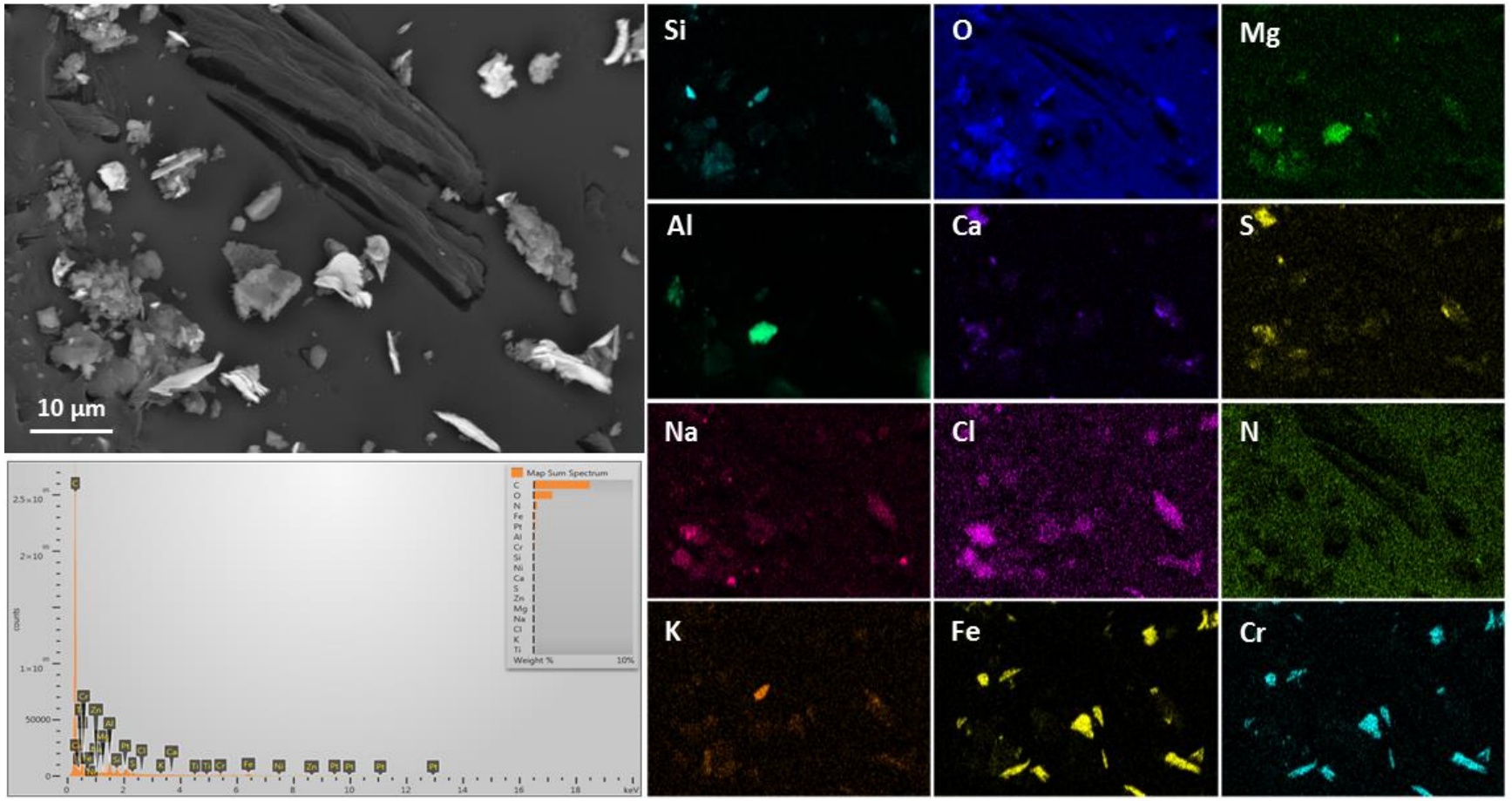

Sample 387-007, collected from the center of the canister top
Map E

Notes: Magnified view of large composite grain in Map D. Grain consists of silicates/aluminosilicates, and salts—dominantly Ca-SO_4.

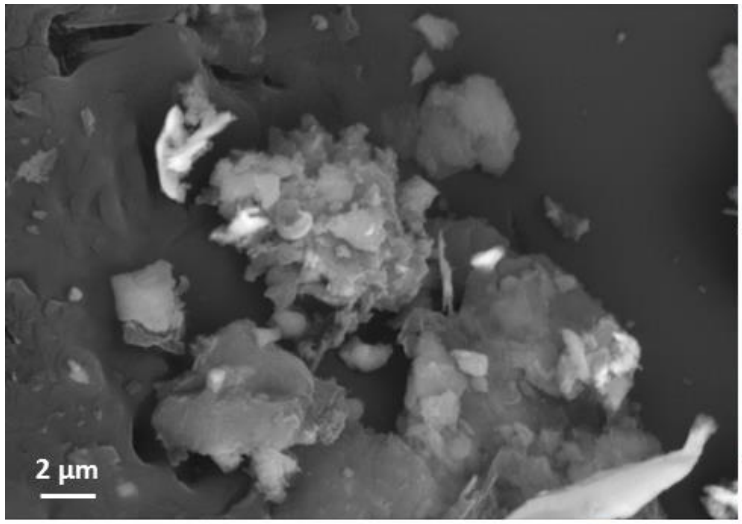

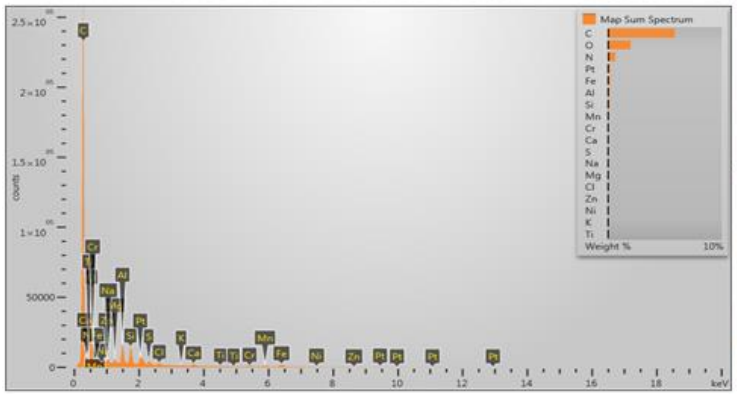

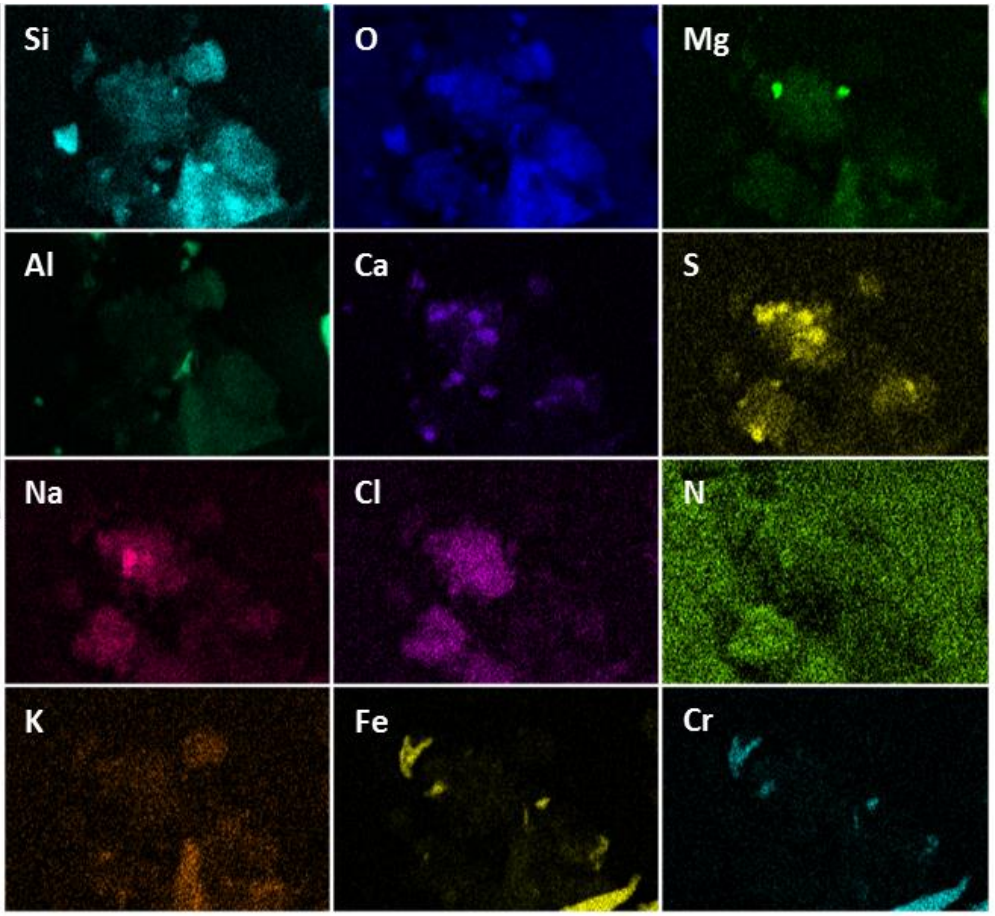

Sample 387-009, collected from the canister side, 5 feet from the base
Overview Image

Notes: Low magnification SEM image showing the light dust load on the pad.

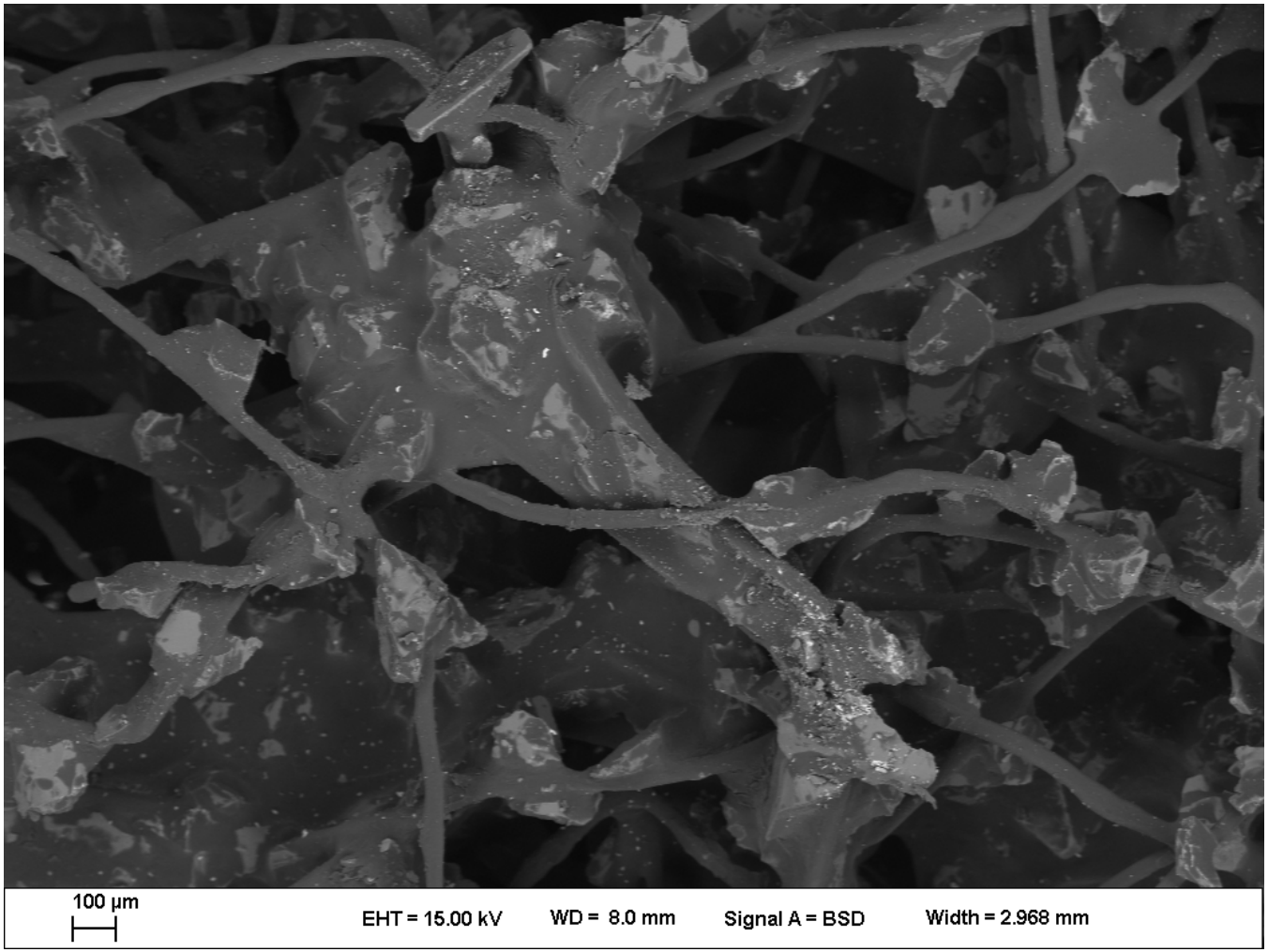

Sample 387-009, collected from the canister side, 5 feet from the base
Map A

Notes: Dust grains are almost entirely stainless steel. A single Ca-SO_4 grain is present in the upper left of the image.

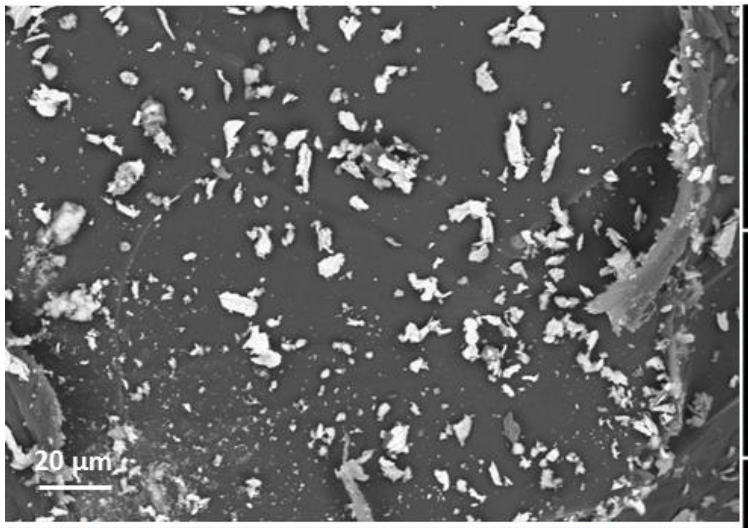

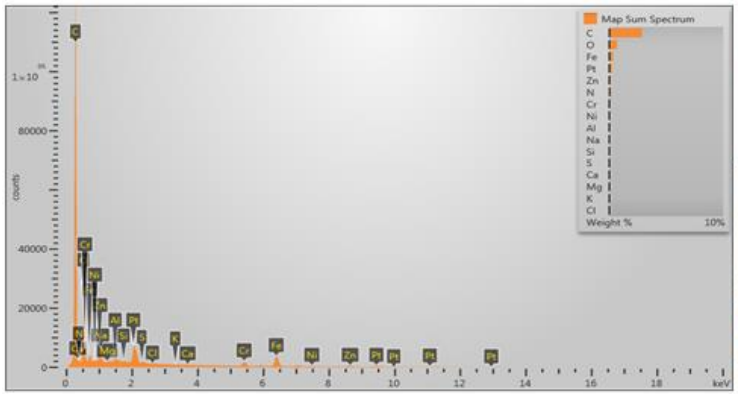

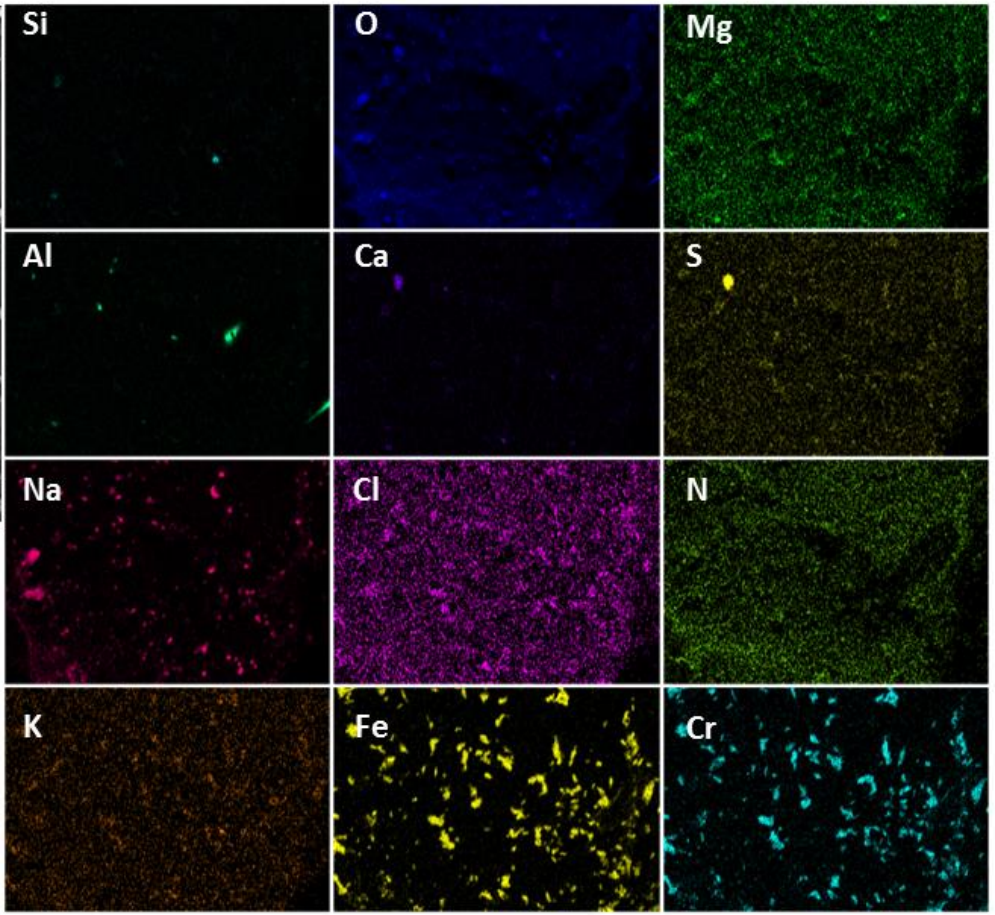

Sample 387-009, collected from the canister side, 5 feet from the base
Map B

Notes: Grains are mostly stainless steel.

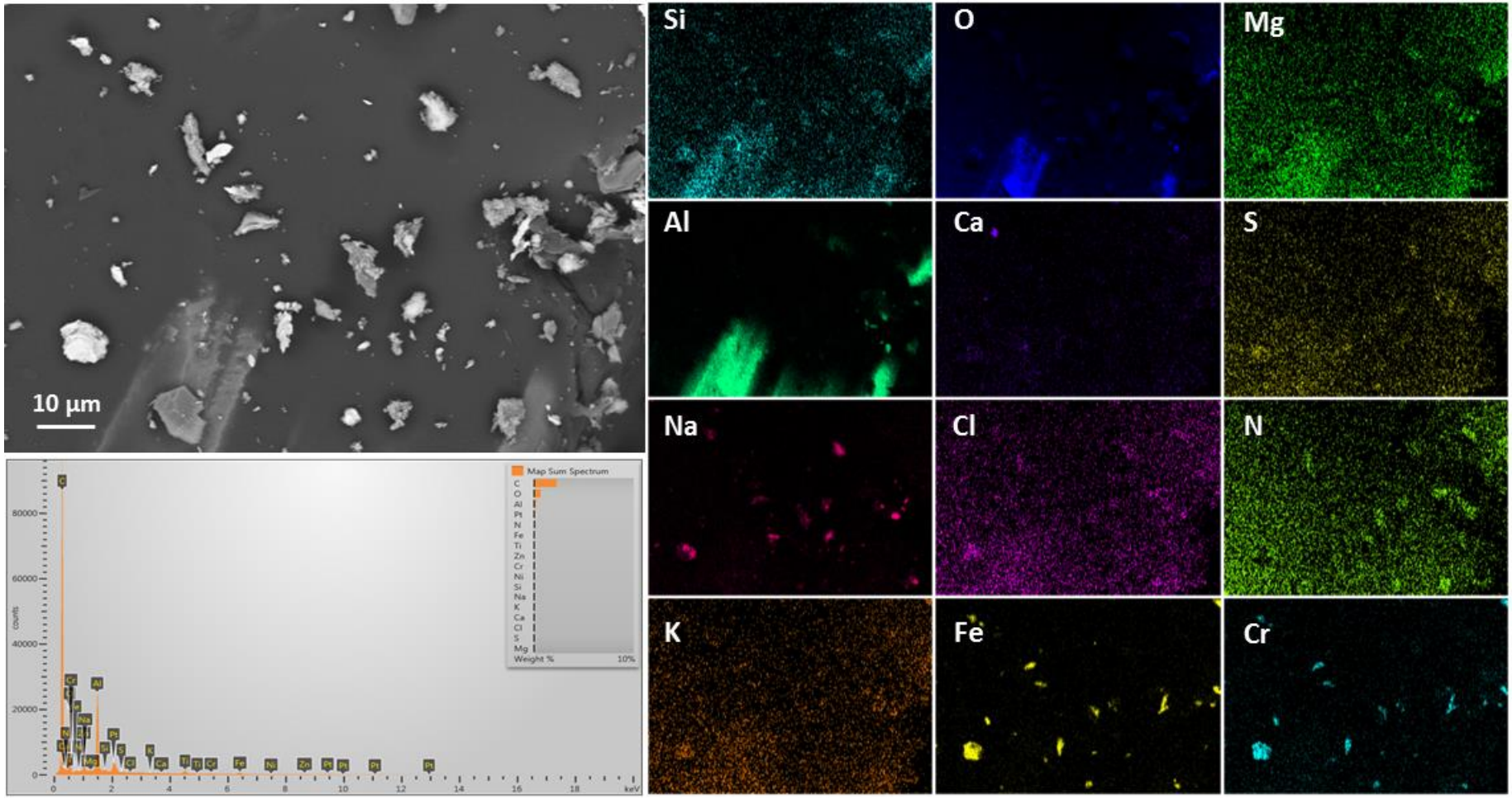

Sample 387-009, collected from the canister side, 5 feet from the base
Map C

Notes: Single Al-oxide or hydroxide grain on the pad, with associated nitrate. The particle, with a basic surface, may have adsorbed nitric acid from the atmosphere.

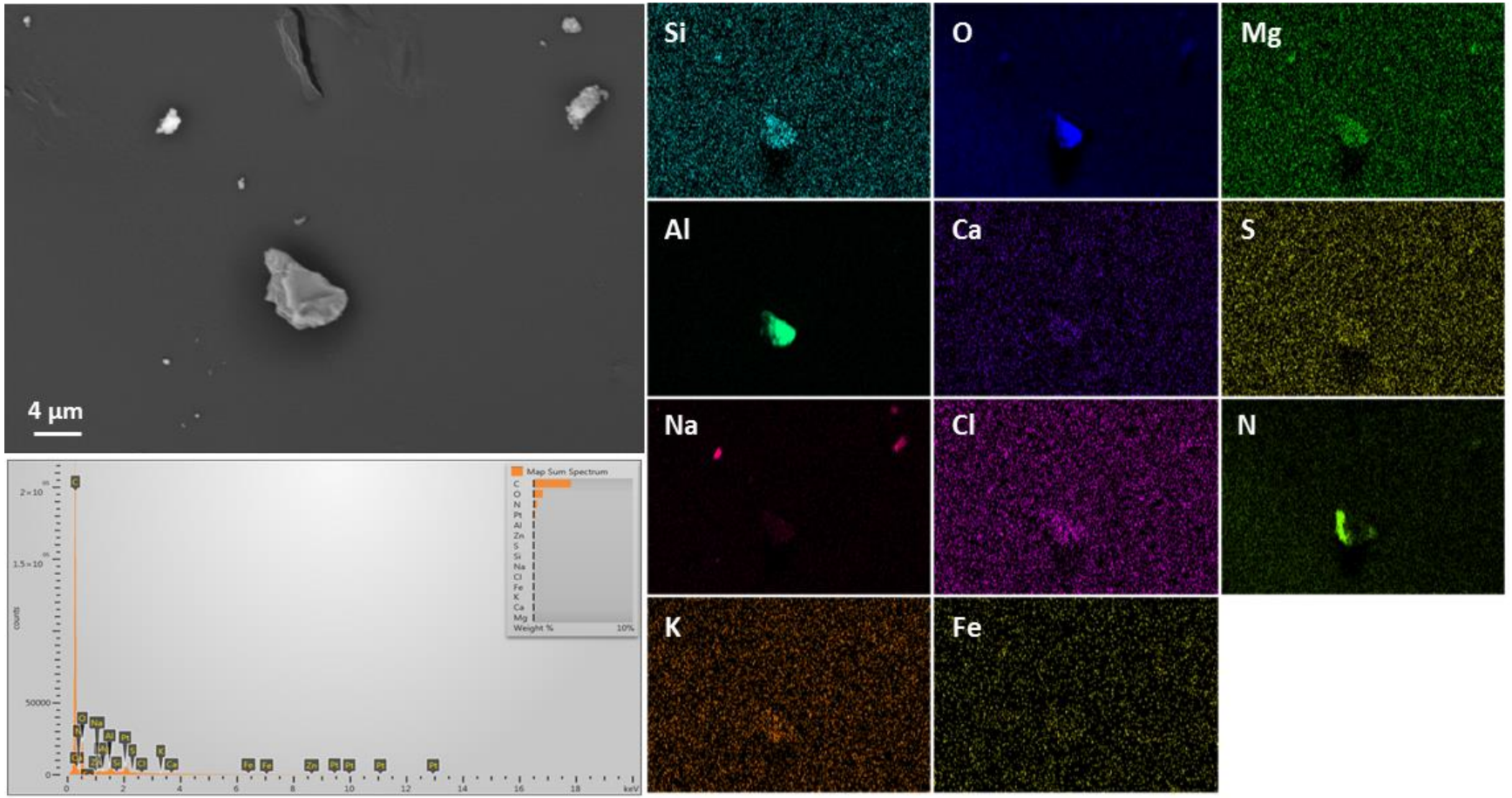

Sample 387-011, from the FME cover, 1 foot from the edge
Overview Image

Notes: Low magnification SEM image of the dry pad 387-011, showing moderate to heavy particle load adhering to the sample fibers.

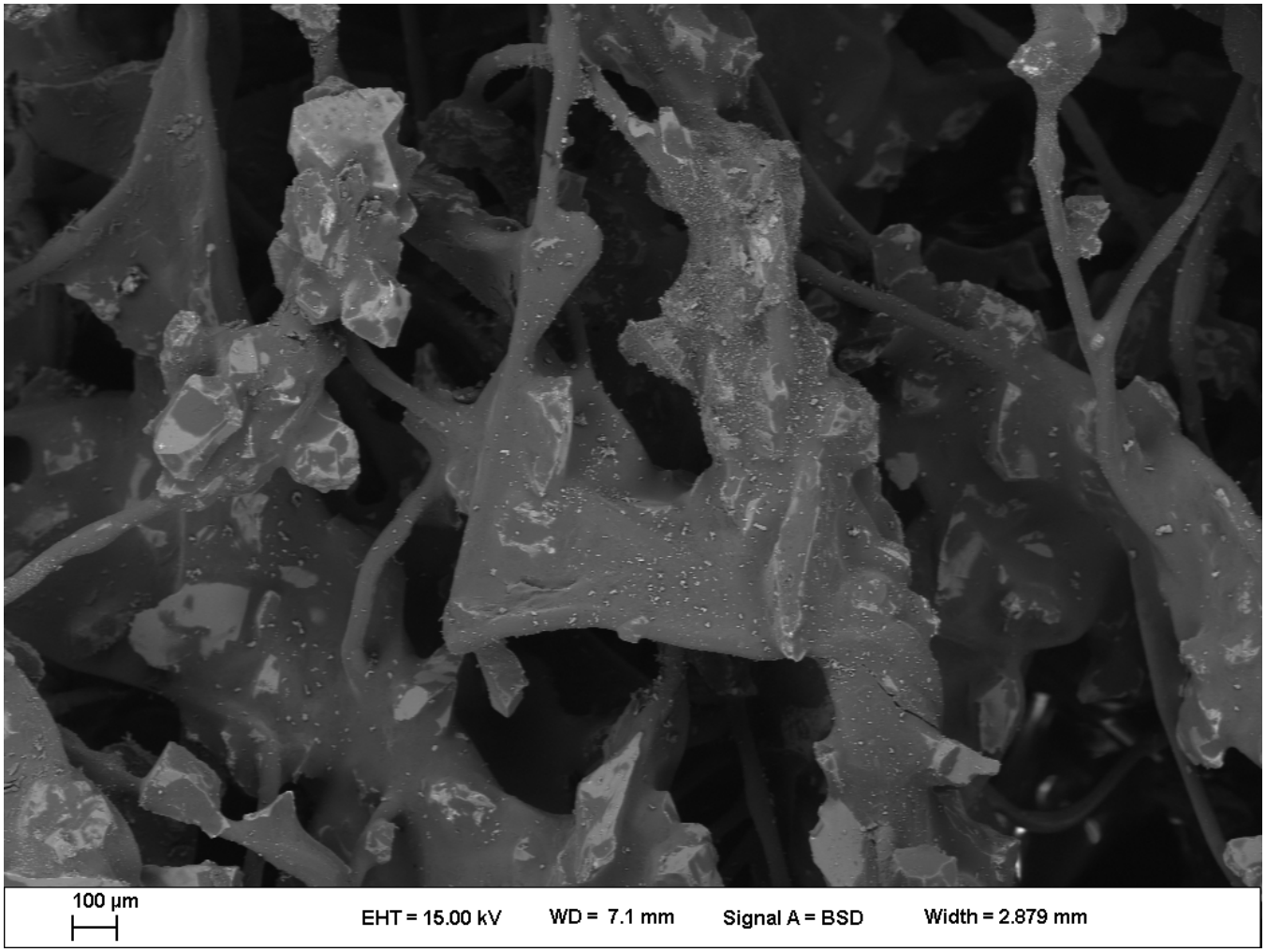

Sample 387-011, from the FME cover, 1 foot from the edge
Map A

Notes: Dust is dominantly silicates/aluminosilicates and Na-Al-SO_4. Some Ca-Mg-CO_3 is also present.

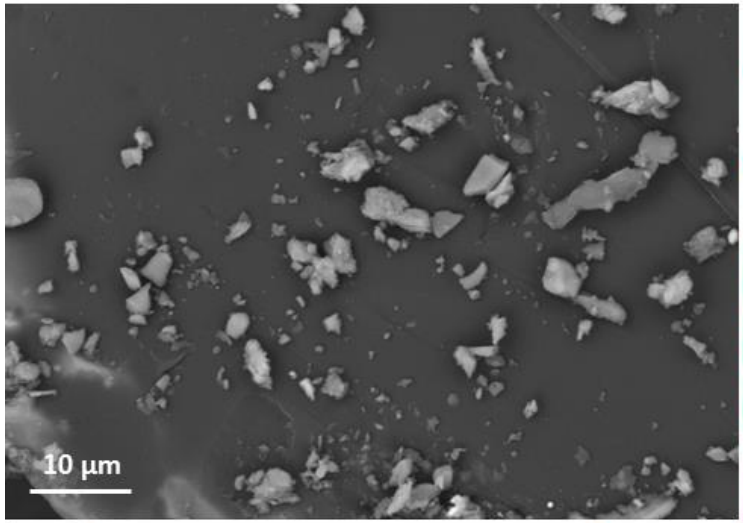

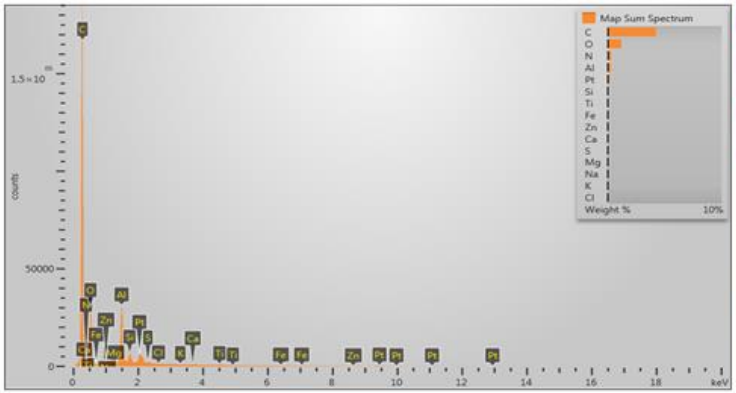

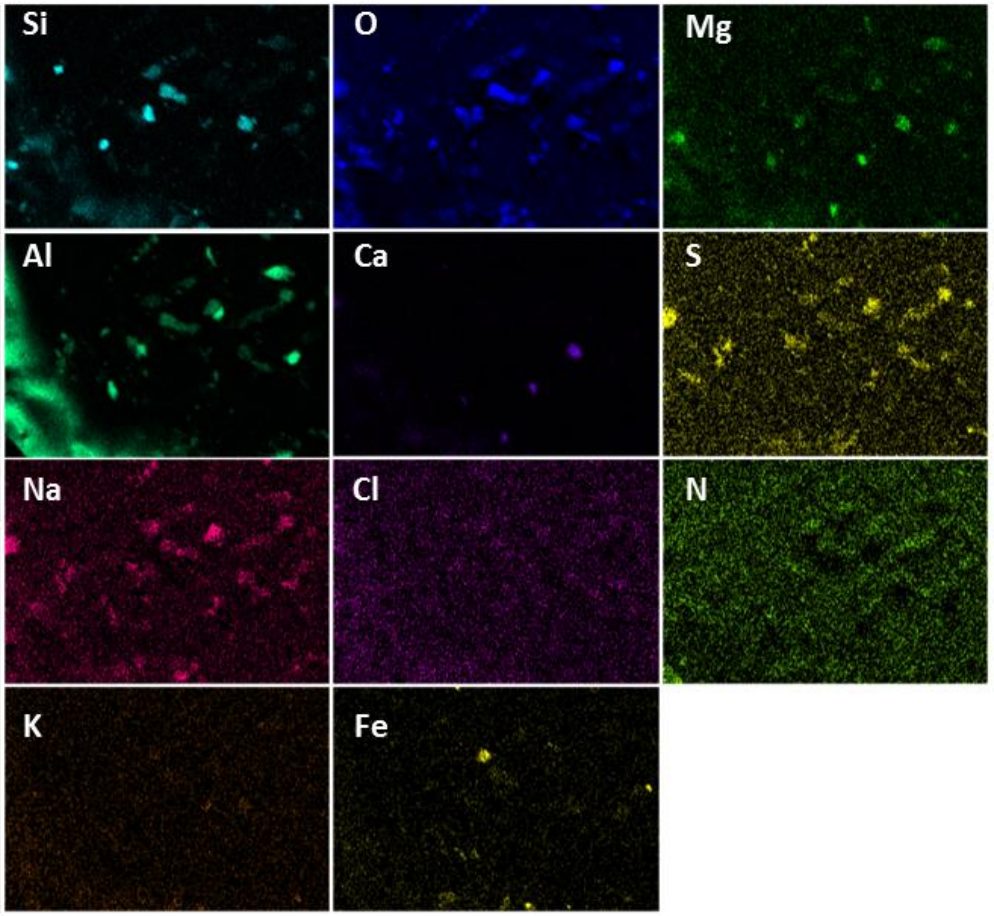

Sample 387-011, from the FME cover, 1 foot from the edge
Map B

Notes: Dust grains are mostly aluminosilicates, including a Ca-Mg aluminosilicate. Central grain is Na-Al-SO_4.

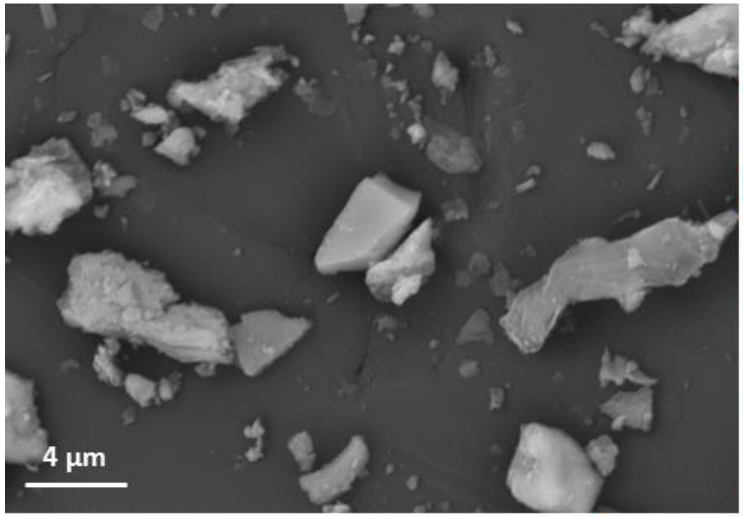

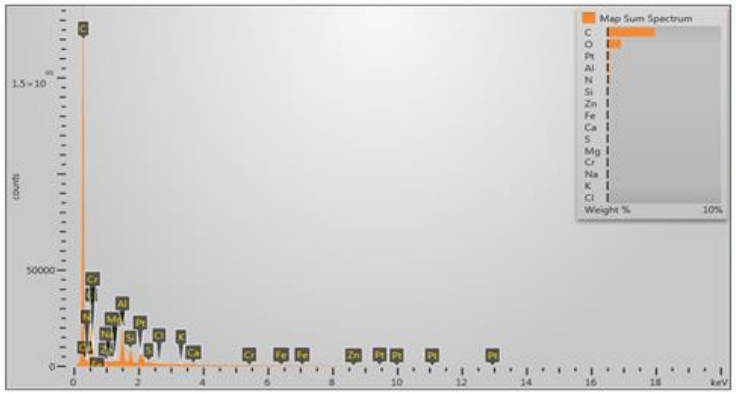

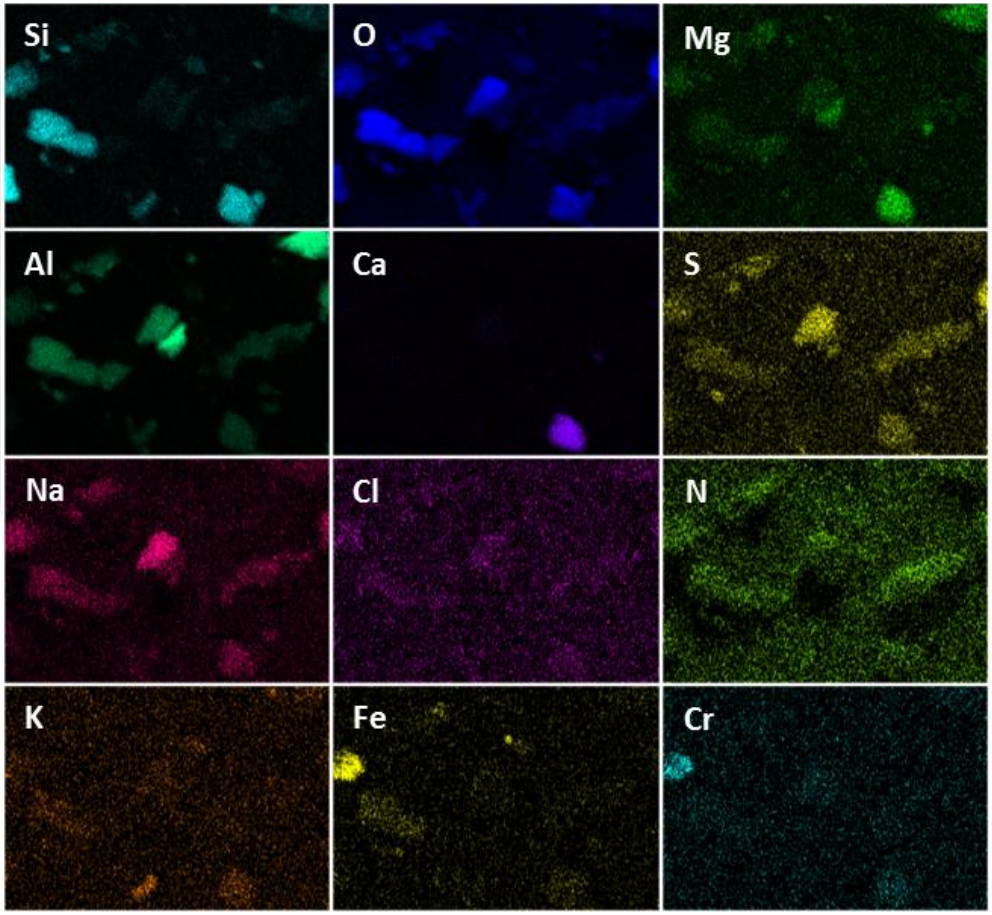

Sample 387-011, from the FME cover, 1 foot from the edge
Map C

Notes: Grains are dominantly silicates/aluminosilicates. Several grains of Na-Al-SO_4 are also present.

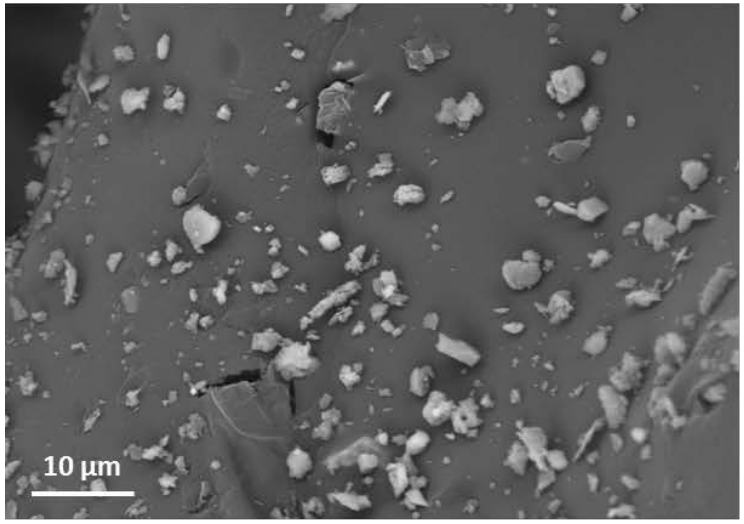

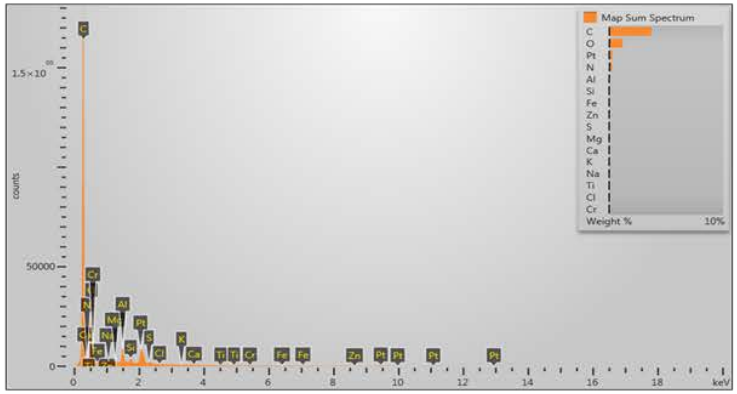

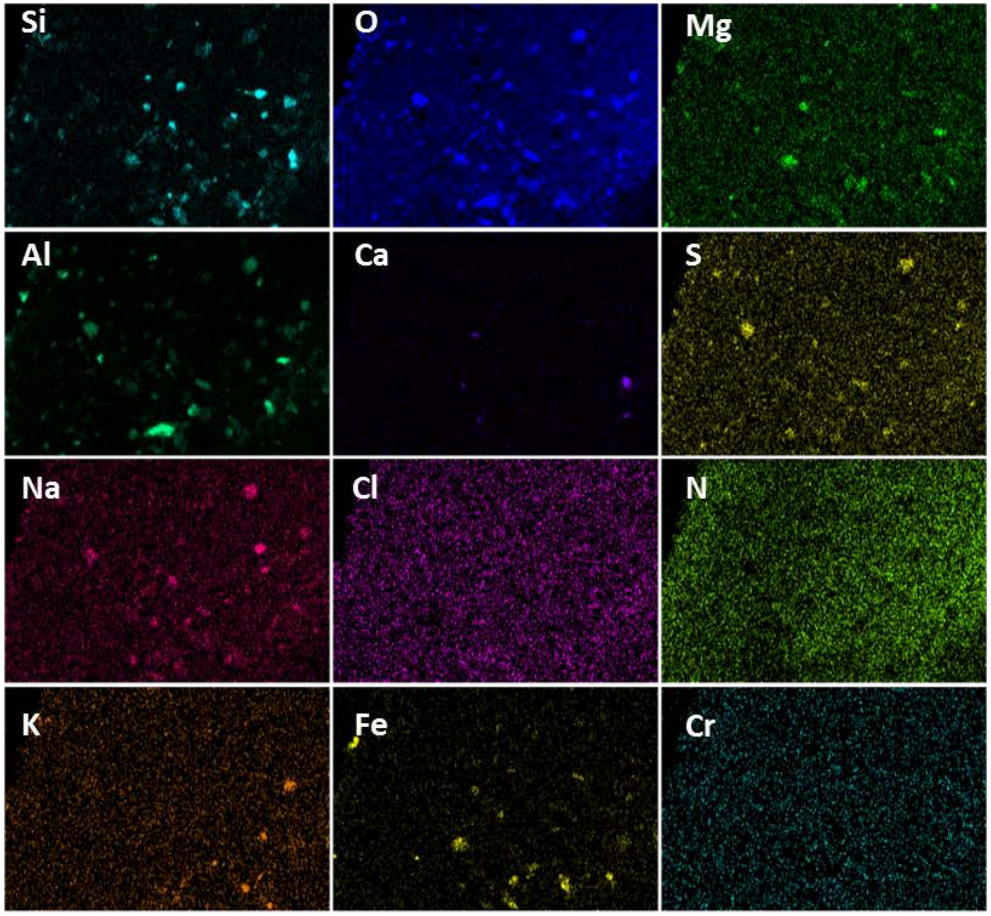

Sample 387-011, from the FME cover, 1 foot from the edge
Map D

Notes: Magnified view of Na-Al-SO_4 grain in Map C.

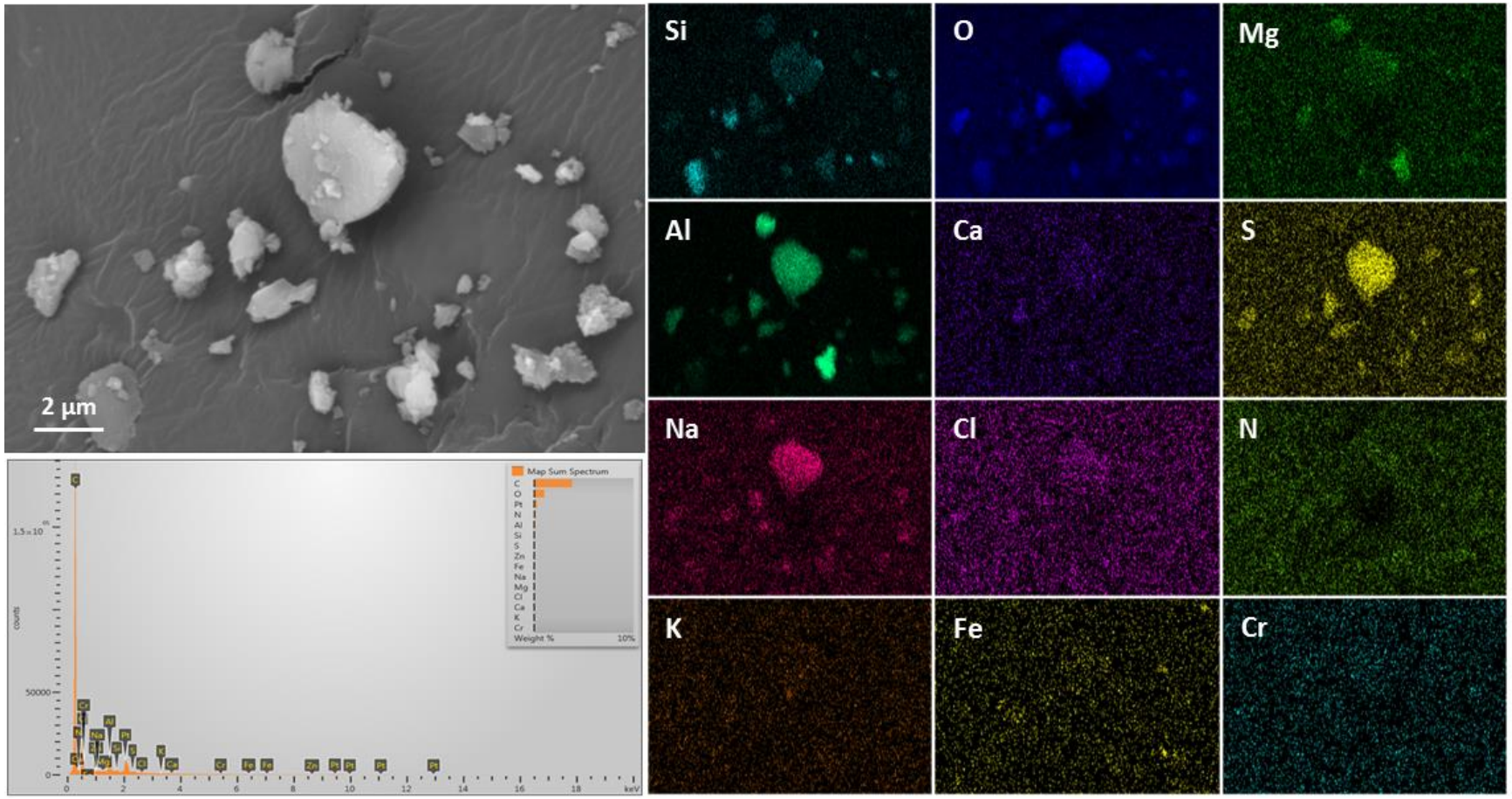

Sample 387-011, from the FME cover, 1 foot from the edge
Map E

Notes: Grains are dominantly silicates/aluminosilicates. Several grains of Na-Al-SO_4 are also present.

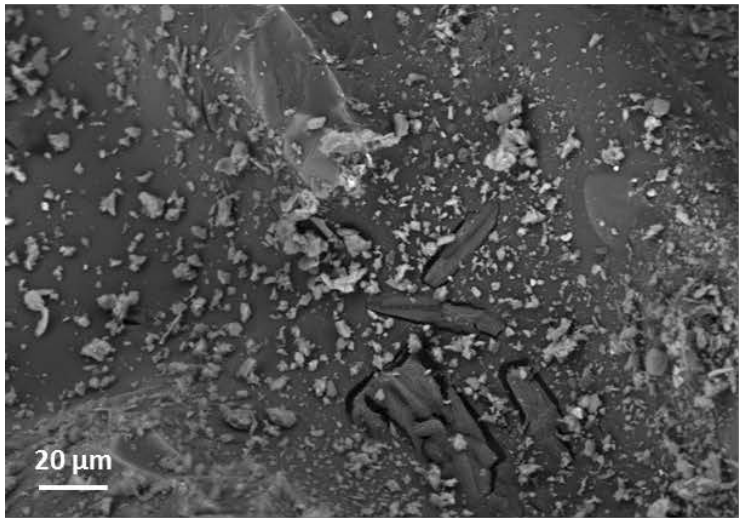

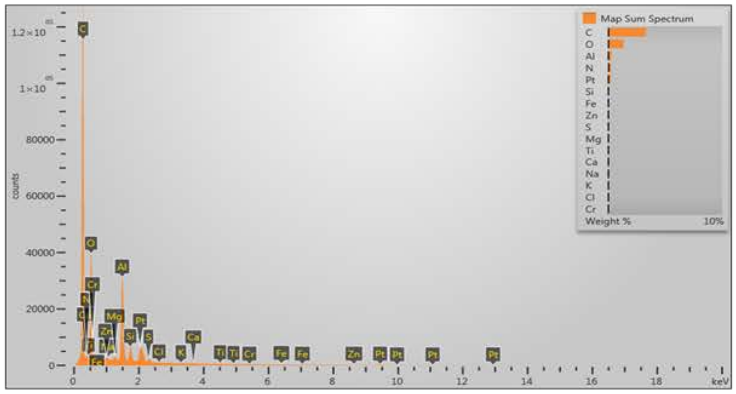

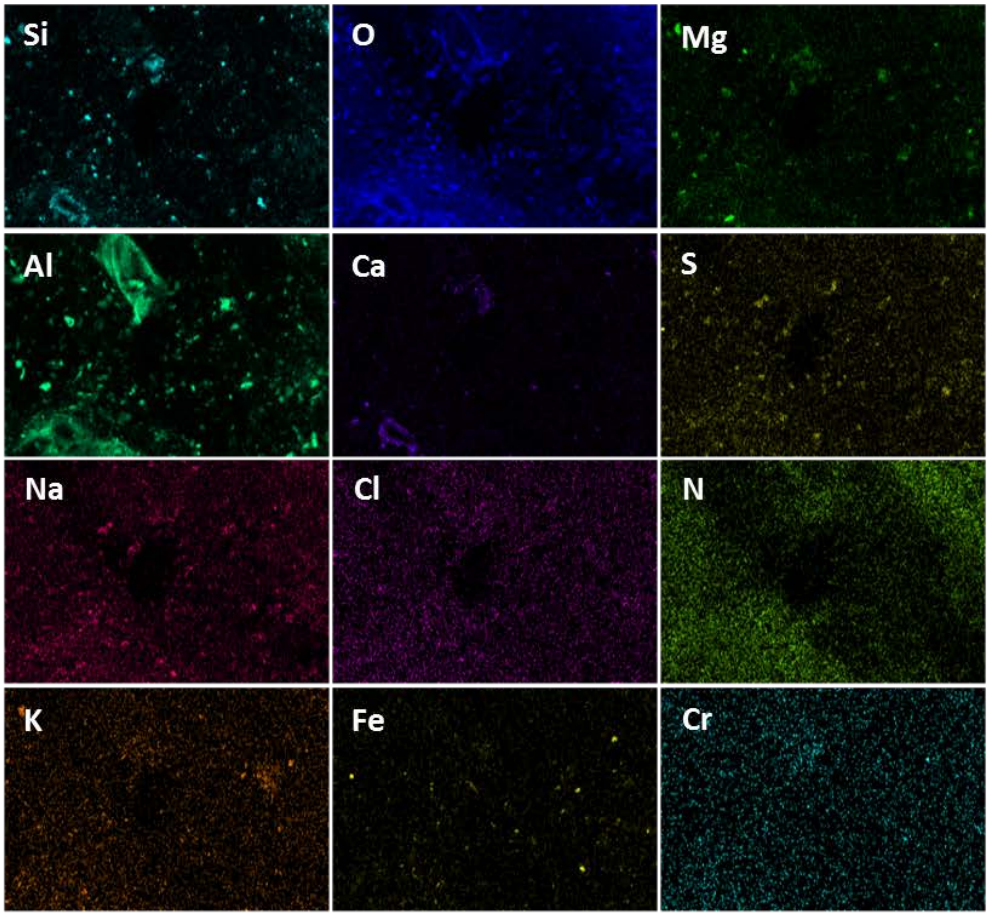

Sample 387-013, from the center of the FME cover
Overview Image

Notes: Low magnification SEM image, showing heavy particle load adhering to the sample fibers.

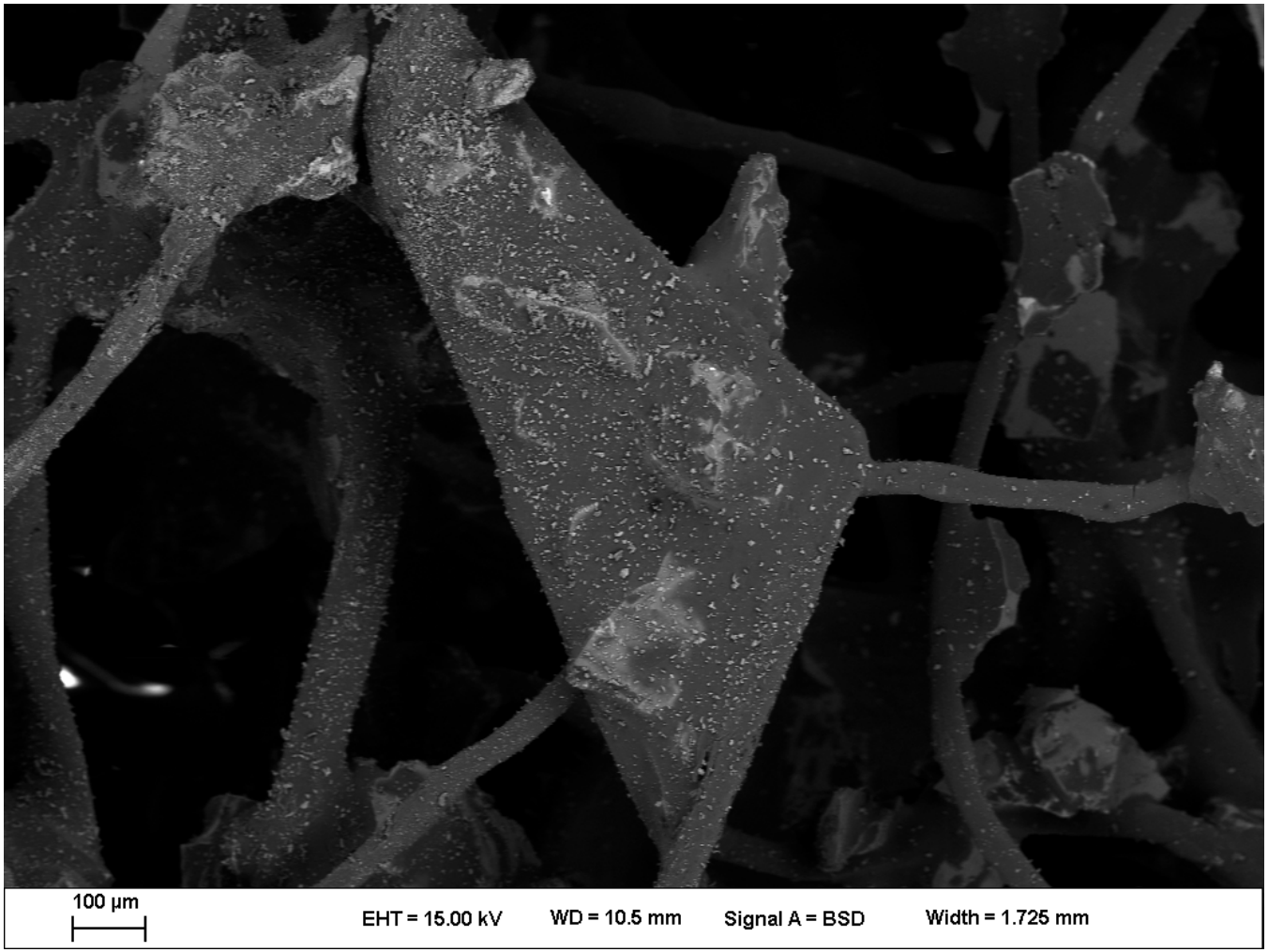

Sample 387-013, from the center of the FME cover
Map A

Notes: Dust grains are dominantly silicates/aluminosilicates.

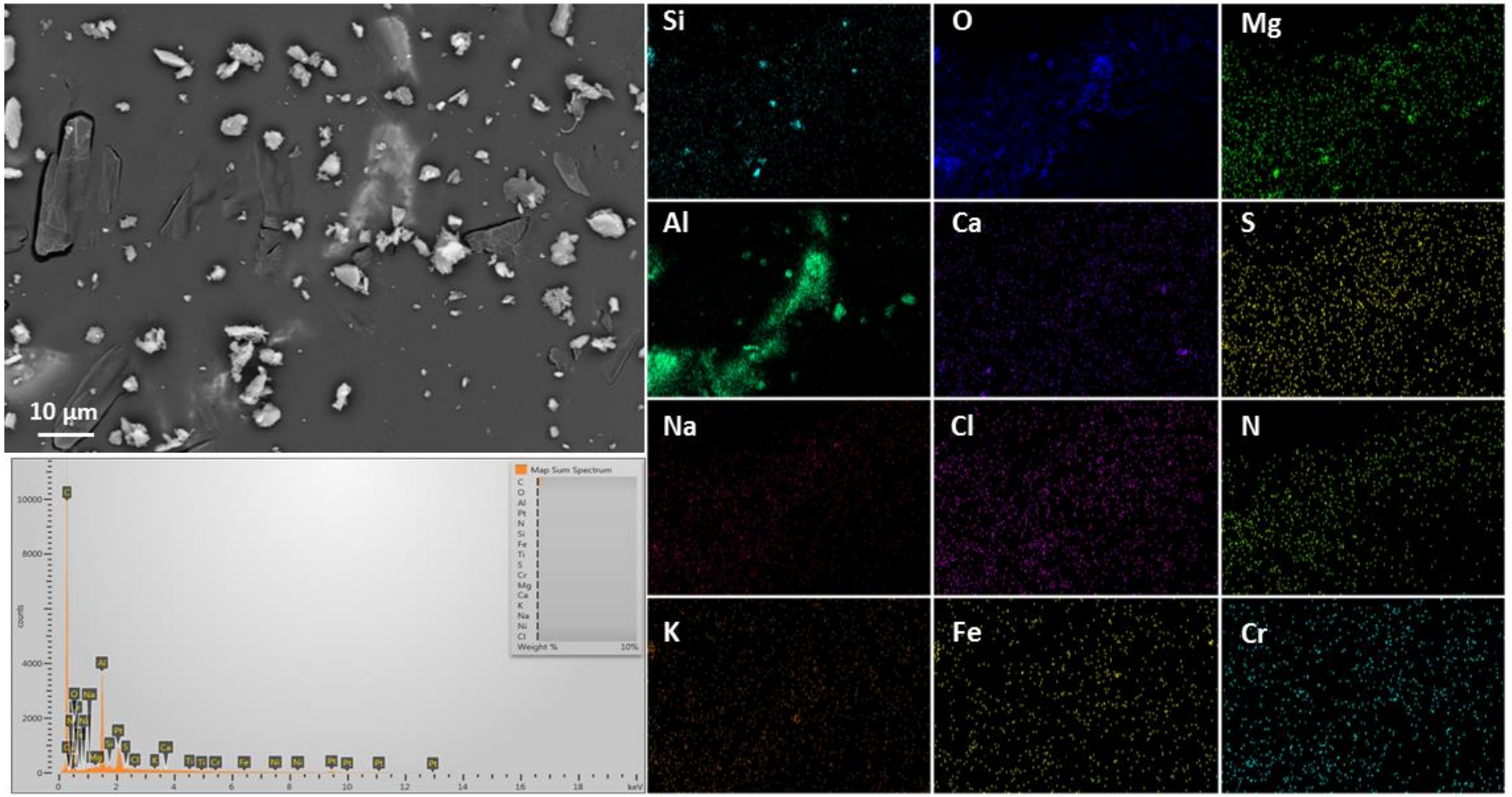

Sample 387-013, from the center of the FME cover
Map B

Notes: Grains are dominantly silicates/aluminosilicates.

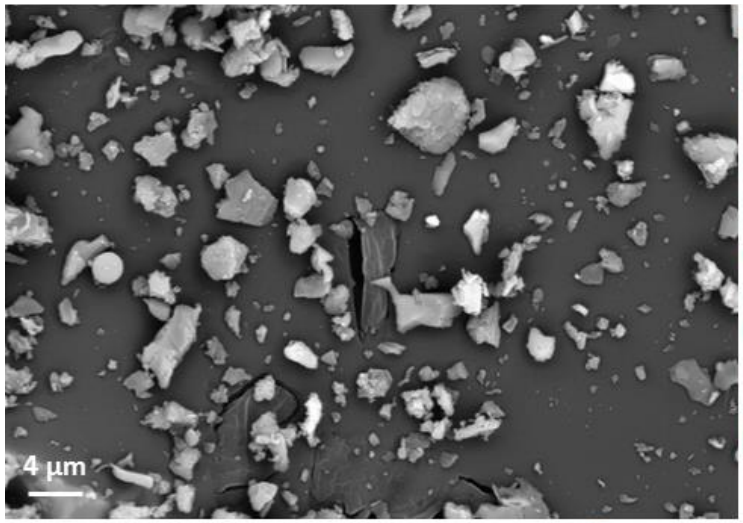

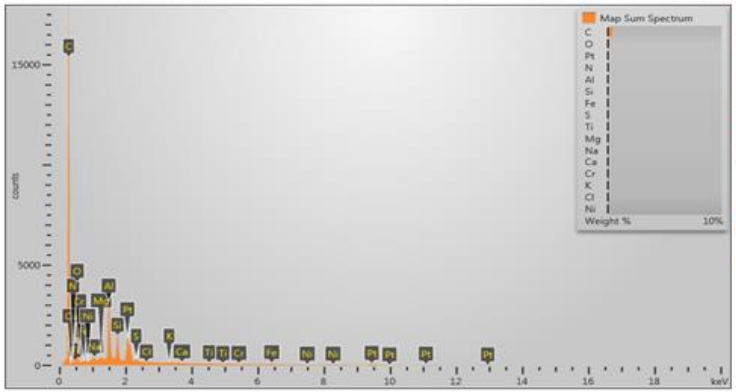

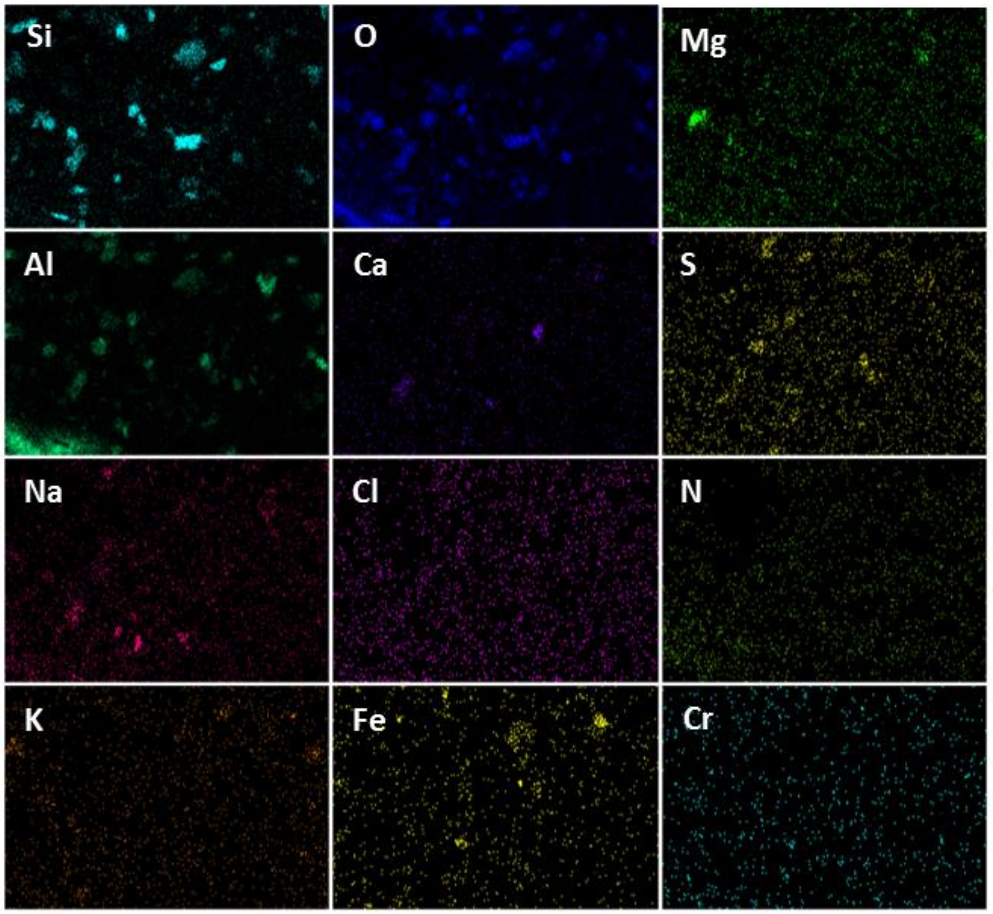

Sample 387-013, from the center of the FME cover
Map C

Notes: Grains are dominantly silicates/aluminosilicates.

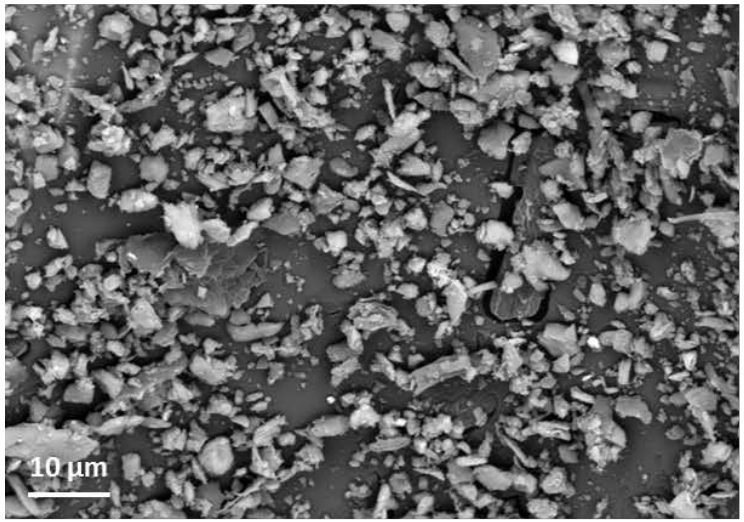

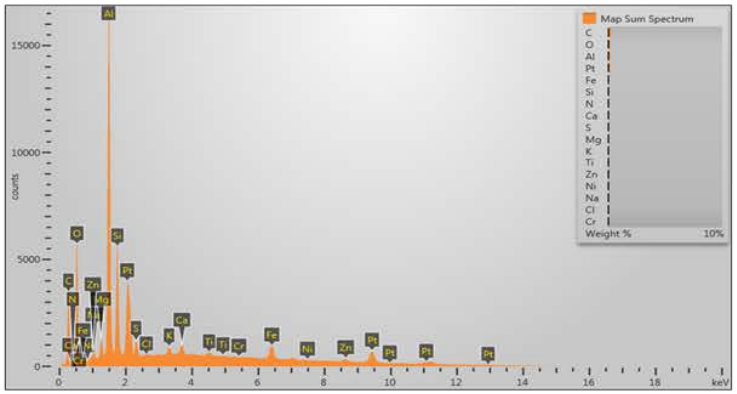

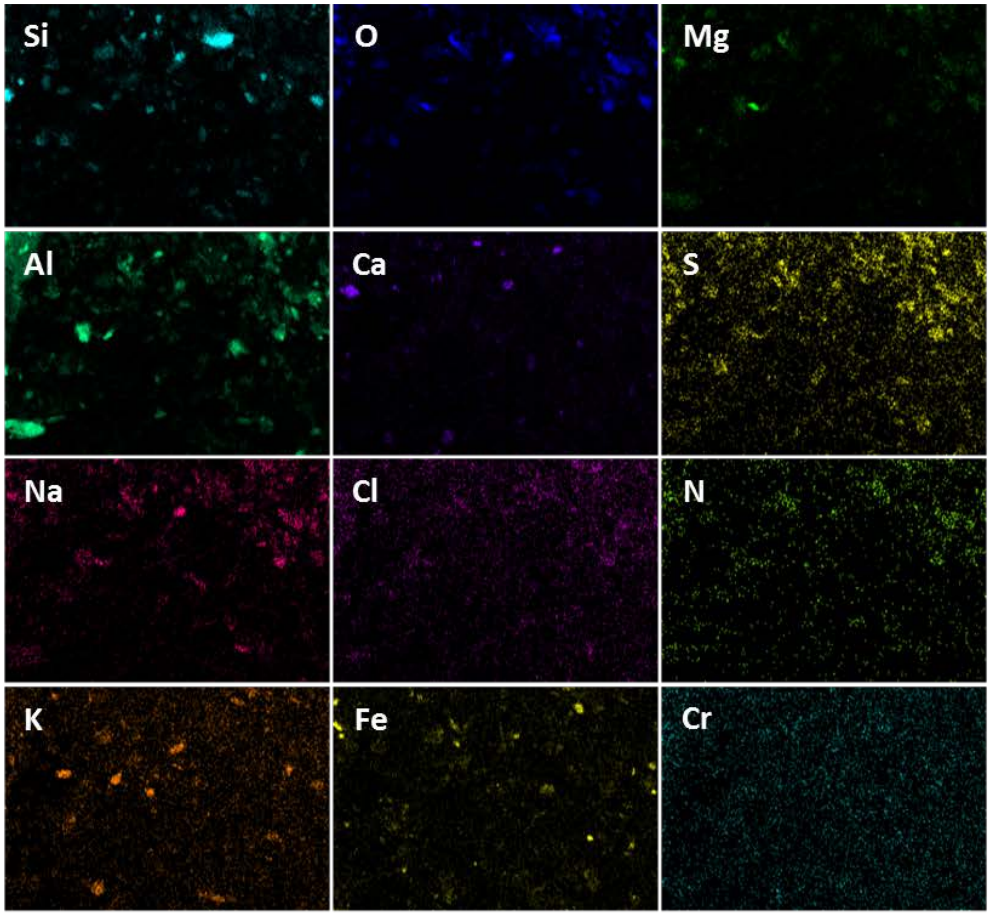

Sample 387-013, from the center of the FME cover
Map D

Notes: Grains are dominantly silicates/aluminosilicates. Some fibrous material, possibly plant matter, is present.

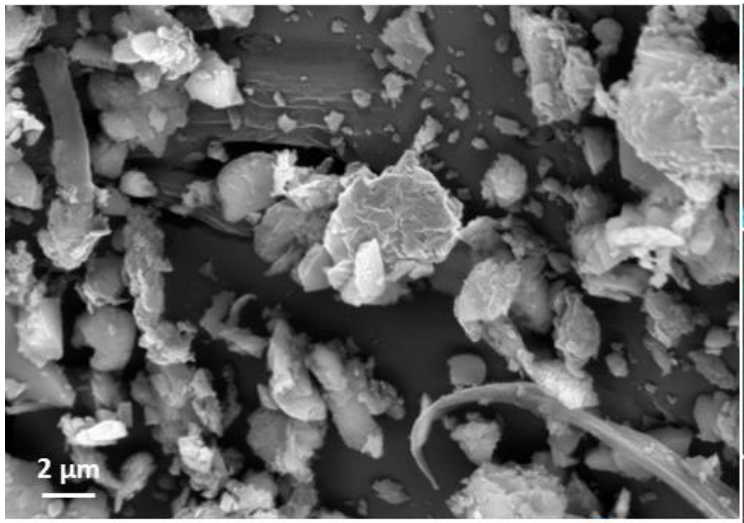

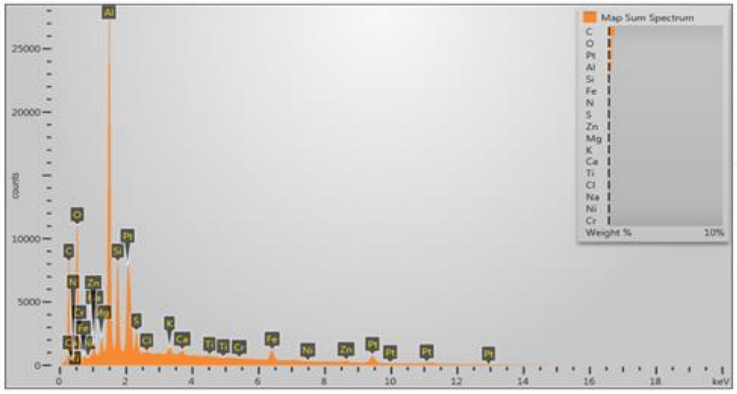

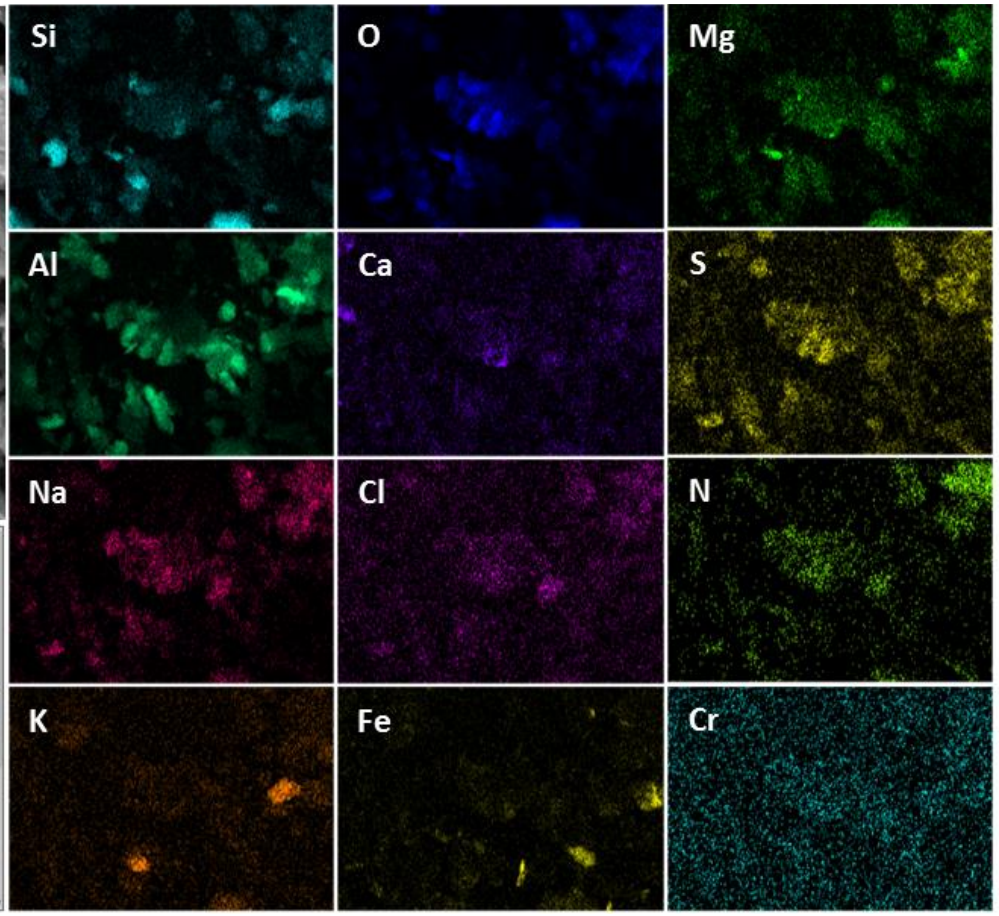

Sample 387-013, from the center of the FME cover
Map E

Notes: Grains are dominantly silicates/aluminosilicates. Large iron-rich grain may be biotite. Some fibrous material, possibly plant matter, is present.

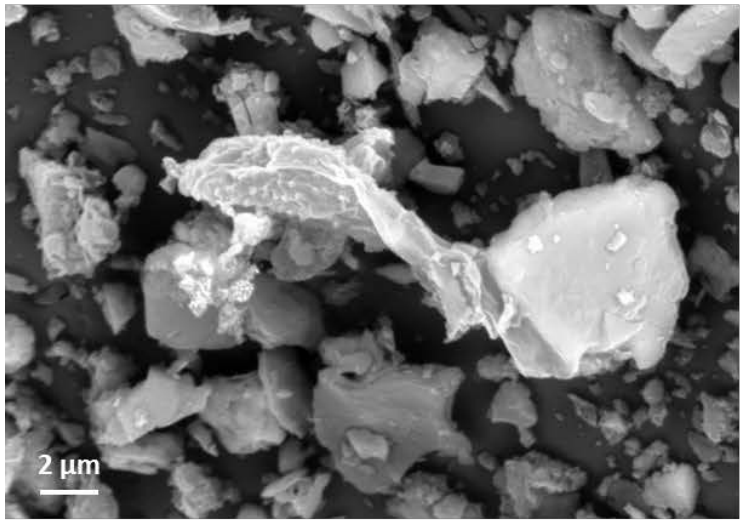

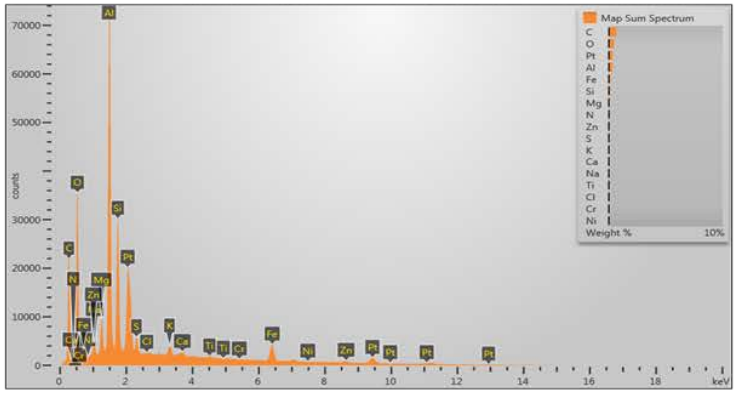

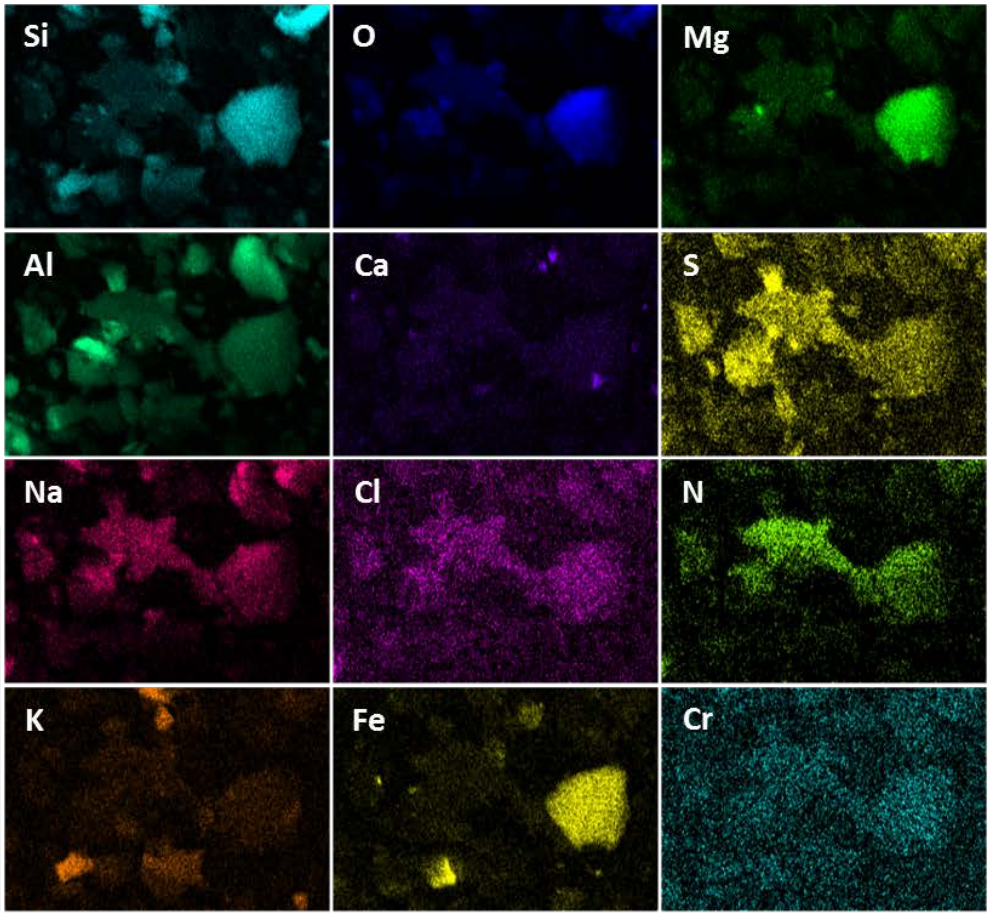

Sample 387-013, from the center of the FME cover
Map F

Notes: Grains are silicates/aluminosilicates and Na-Al-SO_4 particles. A single grain of Ca-CO_3 is present.

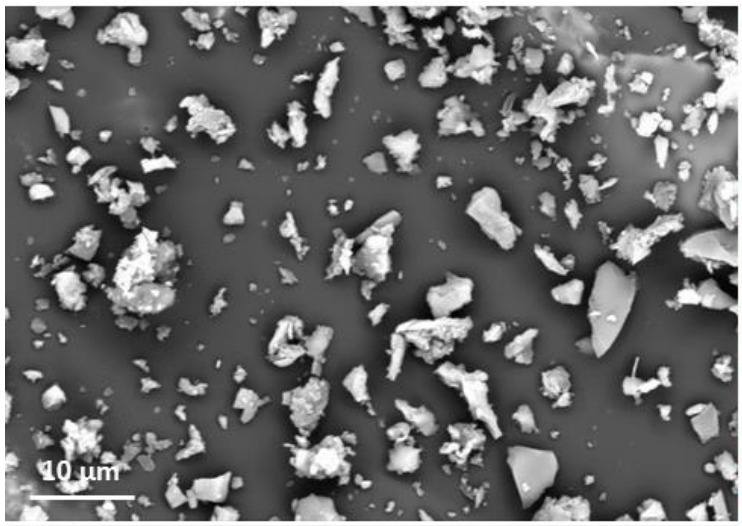

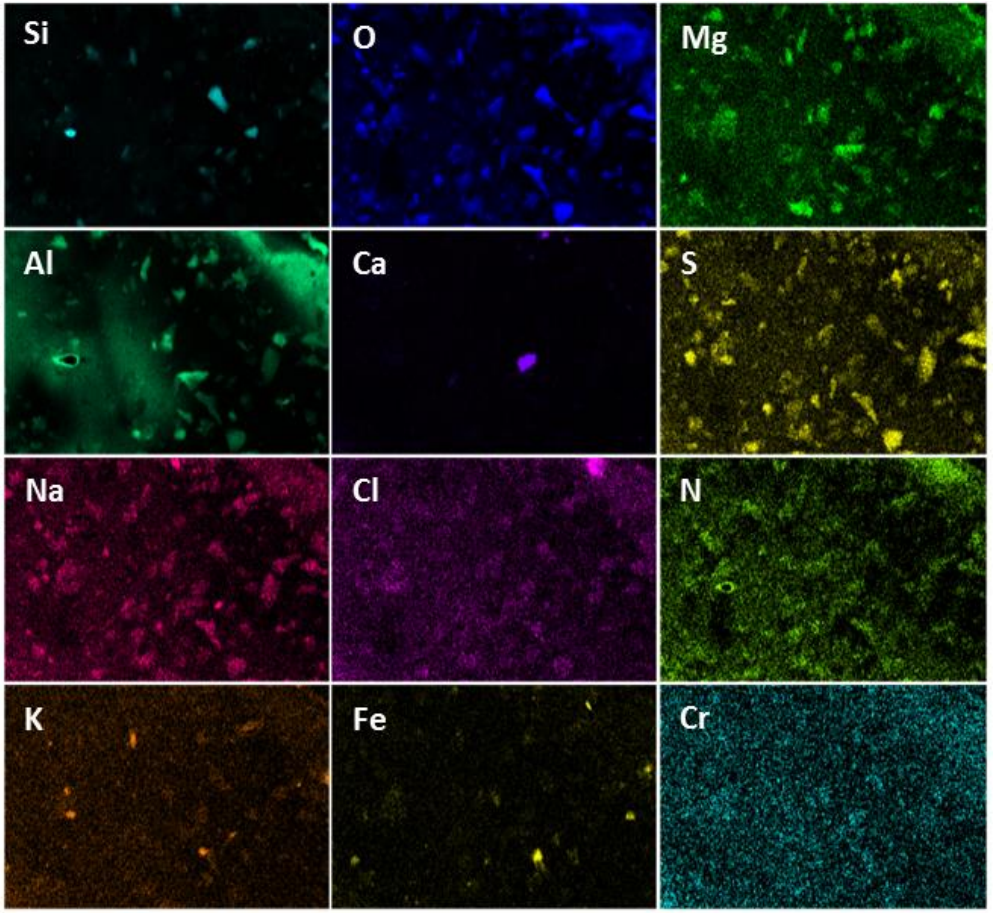

Sample 387-013, from the center of the FME cover
Map G

Notes: Grains are silicates/aluminosilicates and Na-Al-SO_4 particles. A few grains of Ca-CO_3 are present.

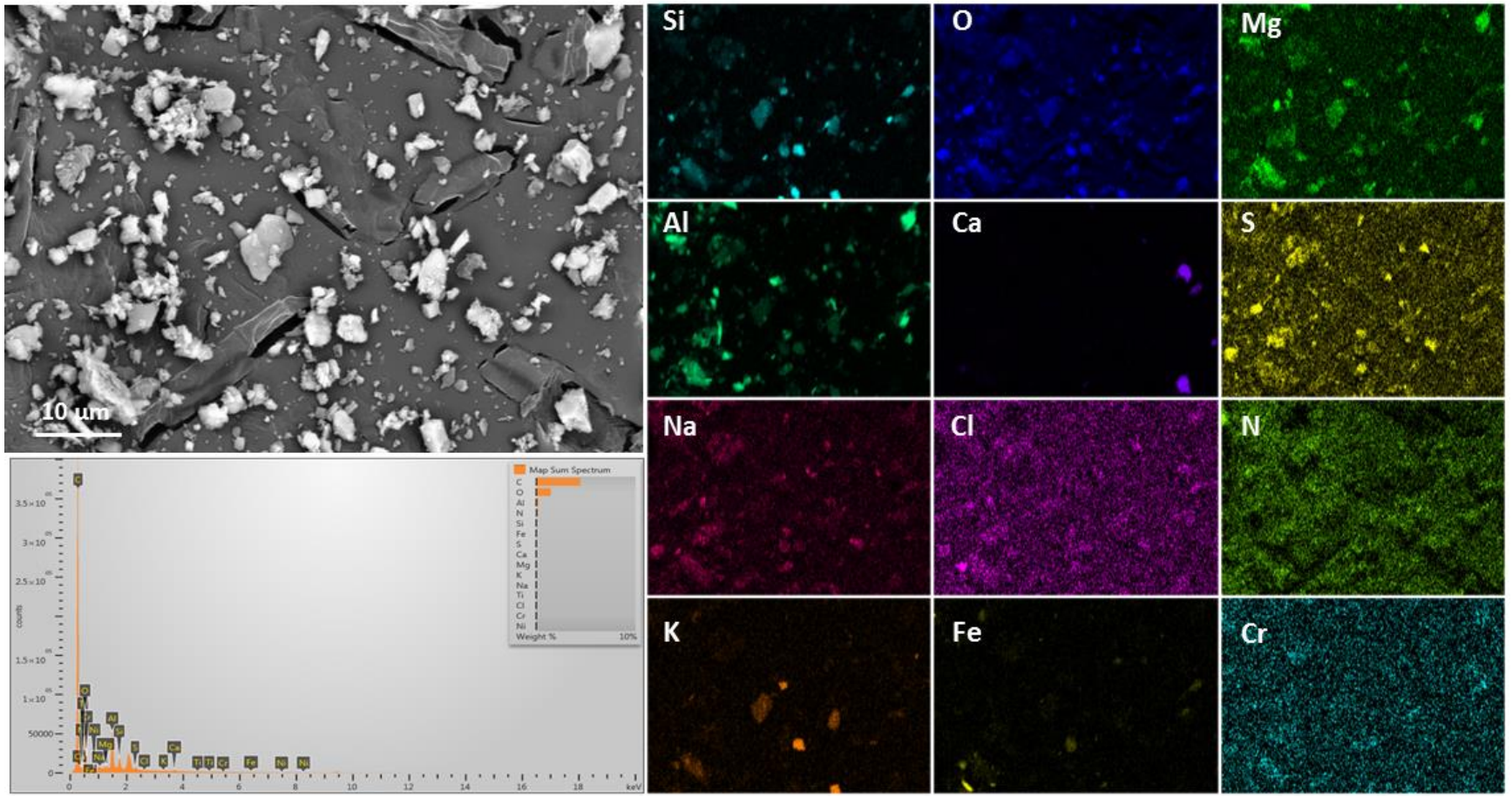

Sample 387-013, from the center of the FME cover
Map H

Notes: Grains are mostly silicates/aluminosilicates and sulfates.

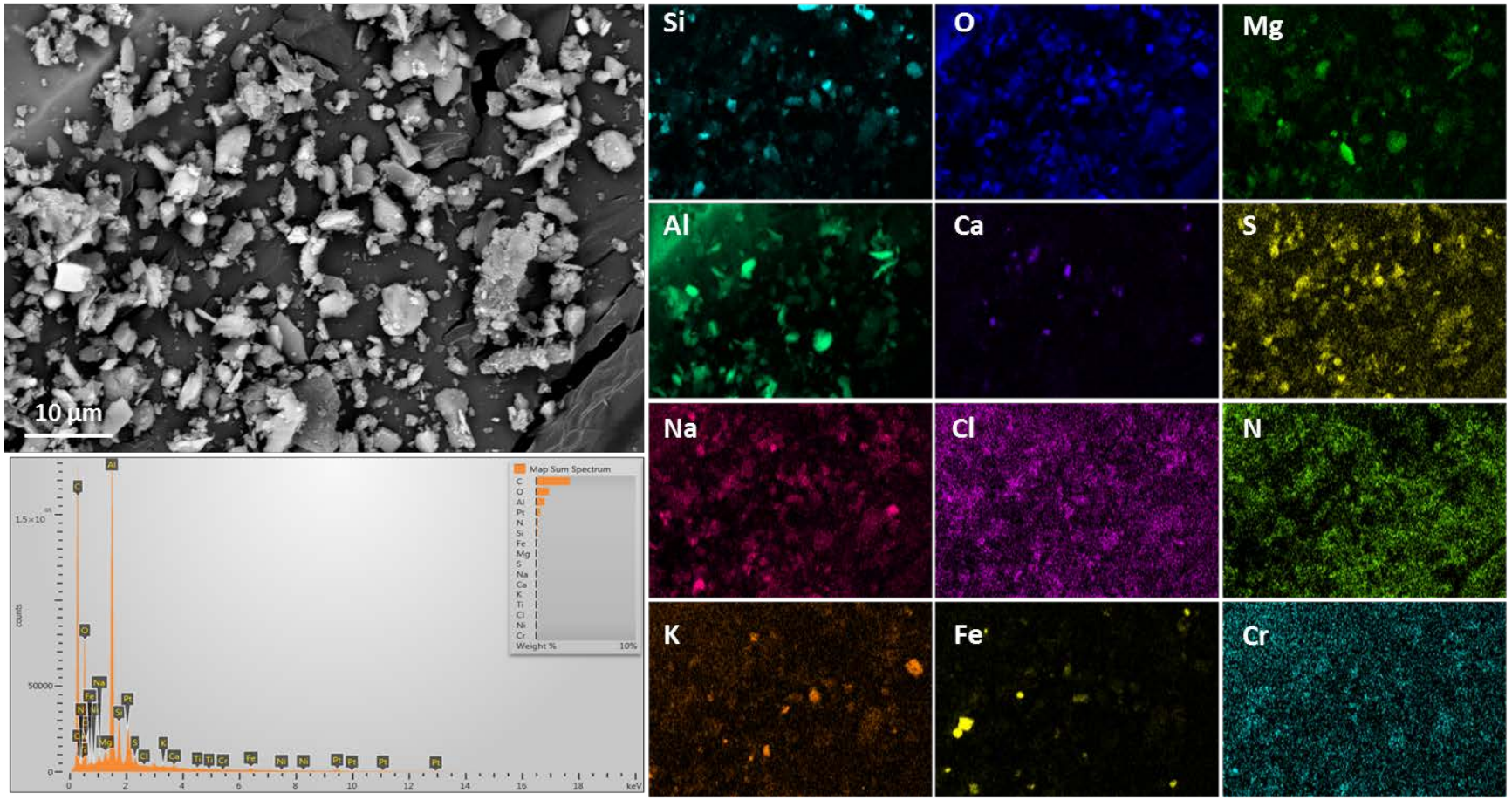

Sample 387-015, collected 1 foot from the edge of the second FME cover

Overview Image

Notes: Low magnification SEM image of the dry pad sample 387-015, showing a heavy particle load on the fibers.

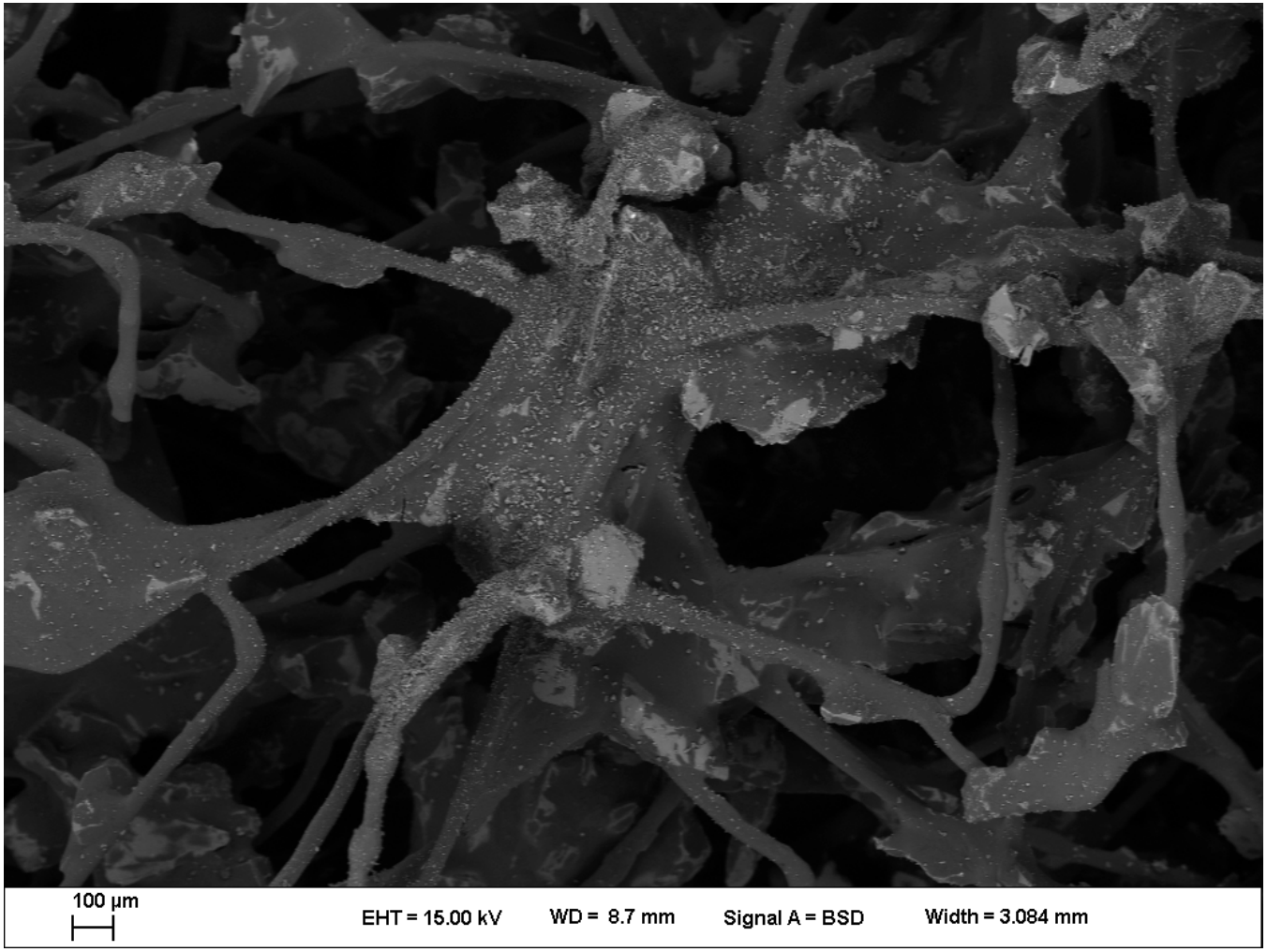

Sample 387-015, collected 1 foot from the edge of the second FME cover
Map A

Notes: Grains are dominantly silicates/aluminosilicates.

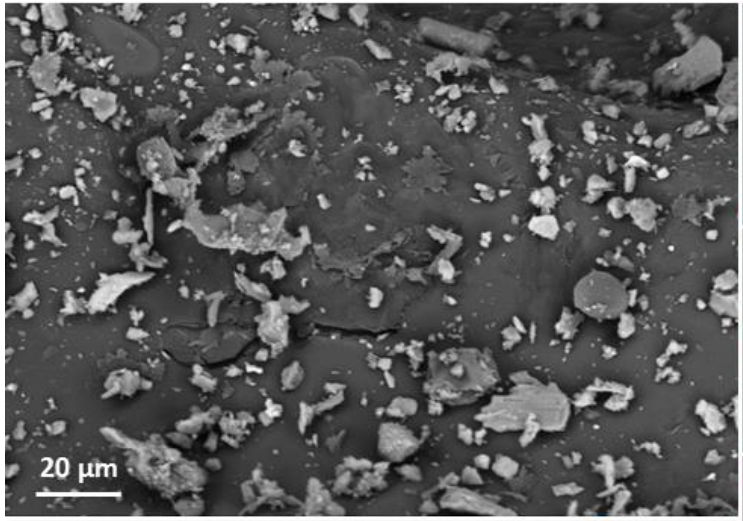

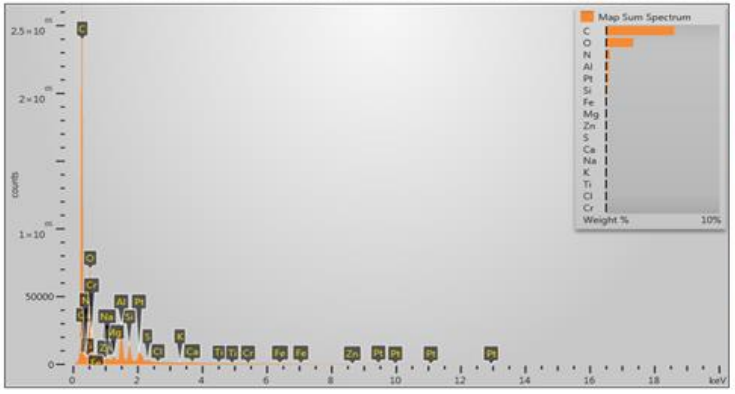

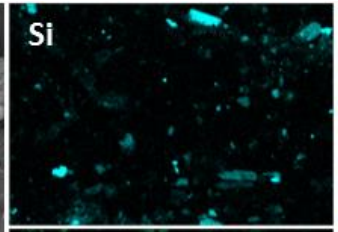

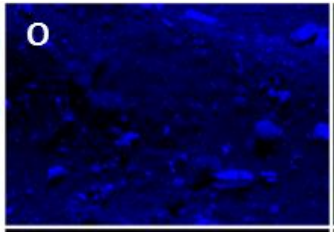

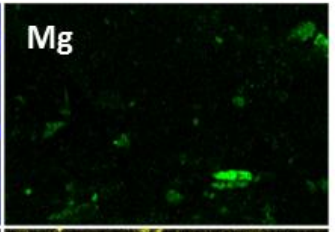

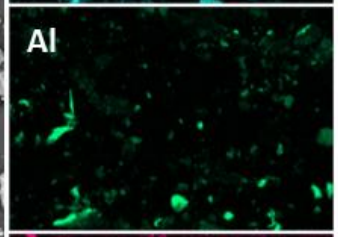

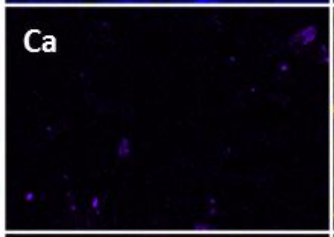

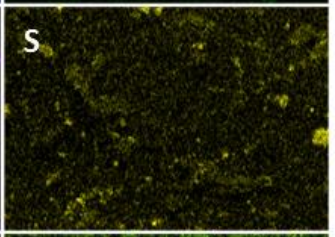

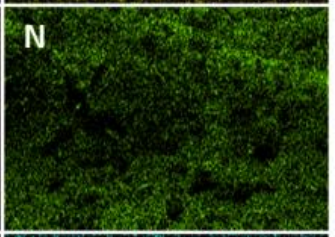

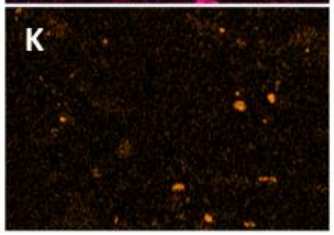

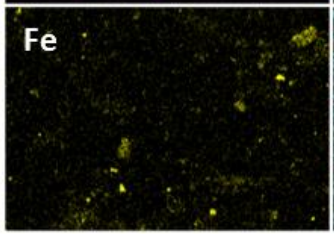

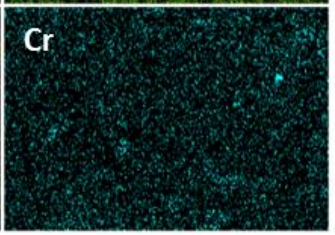

Sample 387-015, collected 1 foot from the edge of the second FME cover
Map B

Notes: Grains are dominantly silicates/aluminosilicates. Very small iron oxide grains are also present.

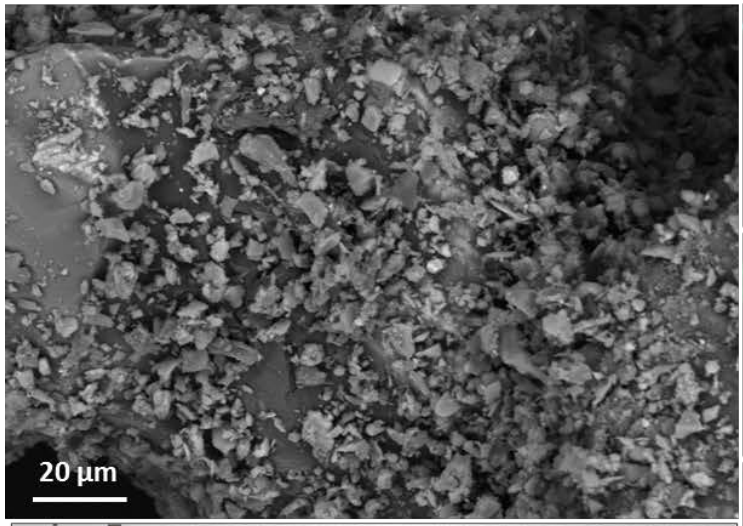

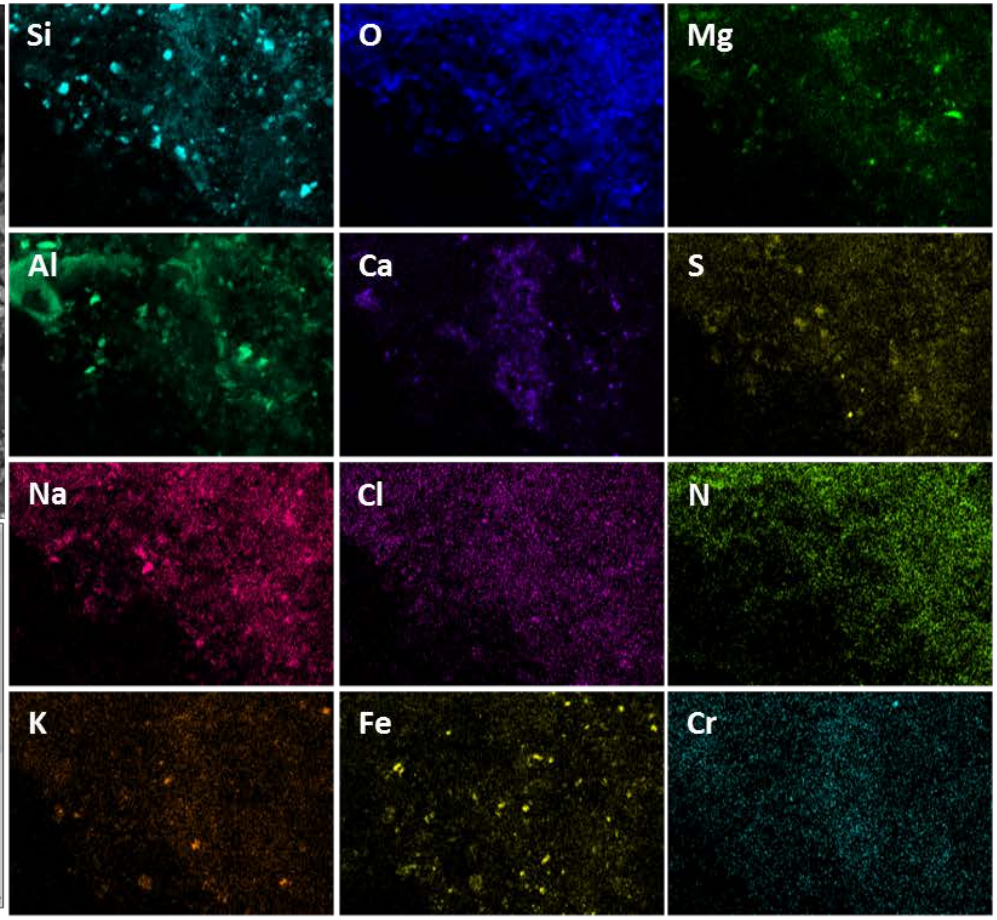

Sample 387-015, collected 1 foot from the edge of the second FME cover
Map C

Notes: Grains are silicates/aluminosilicates and Na-Al-SO_4. Note iron oxide sphere in lower right.

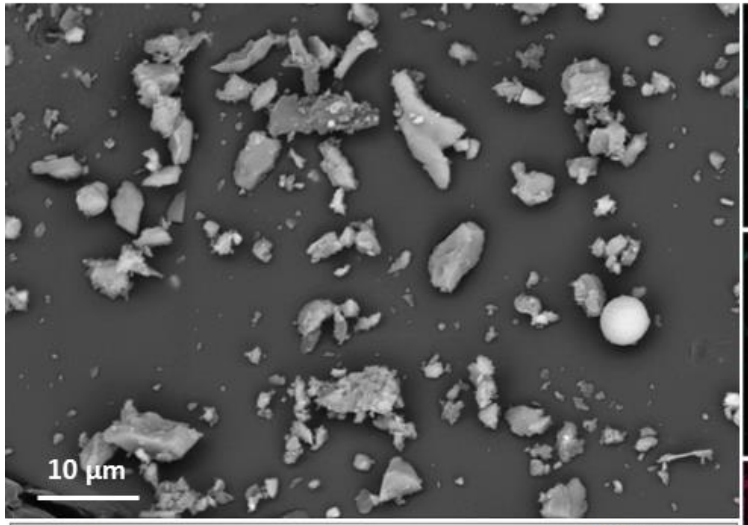

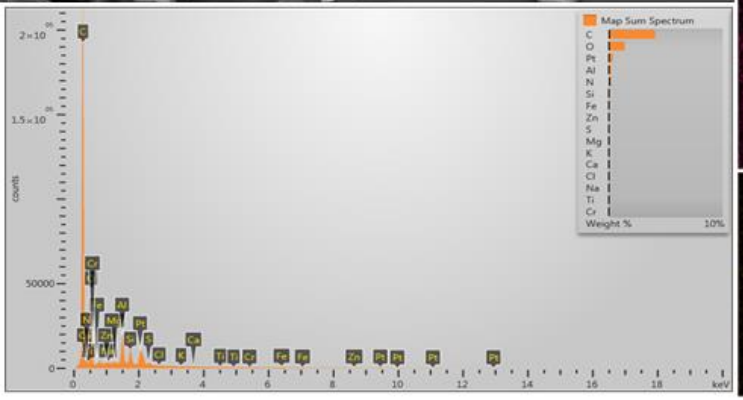

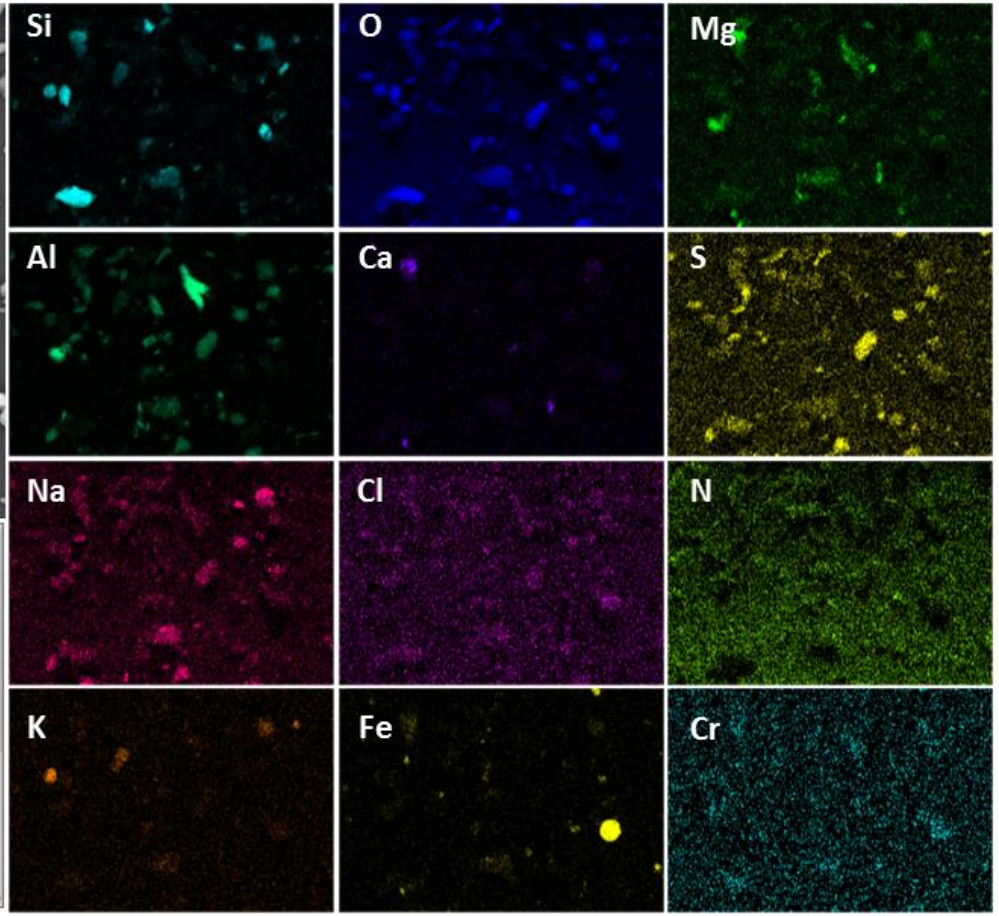

Sample 387-015, collected 1 foot from the edge of the second FME cover
Map D

Notes: Magnified image of Na-Al-SO_4 grains in Map C. These appear to contain less Na than other example

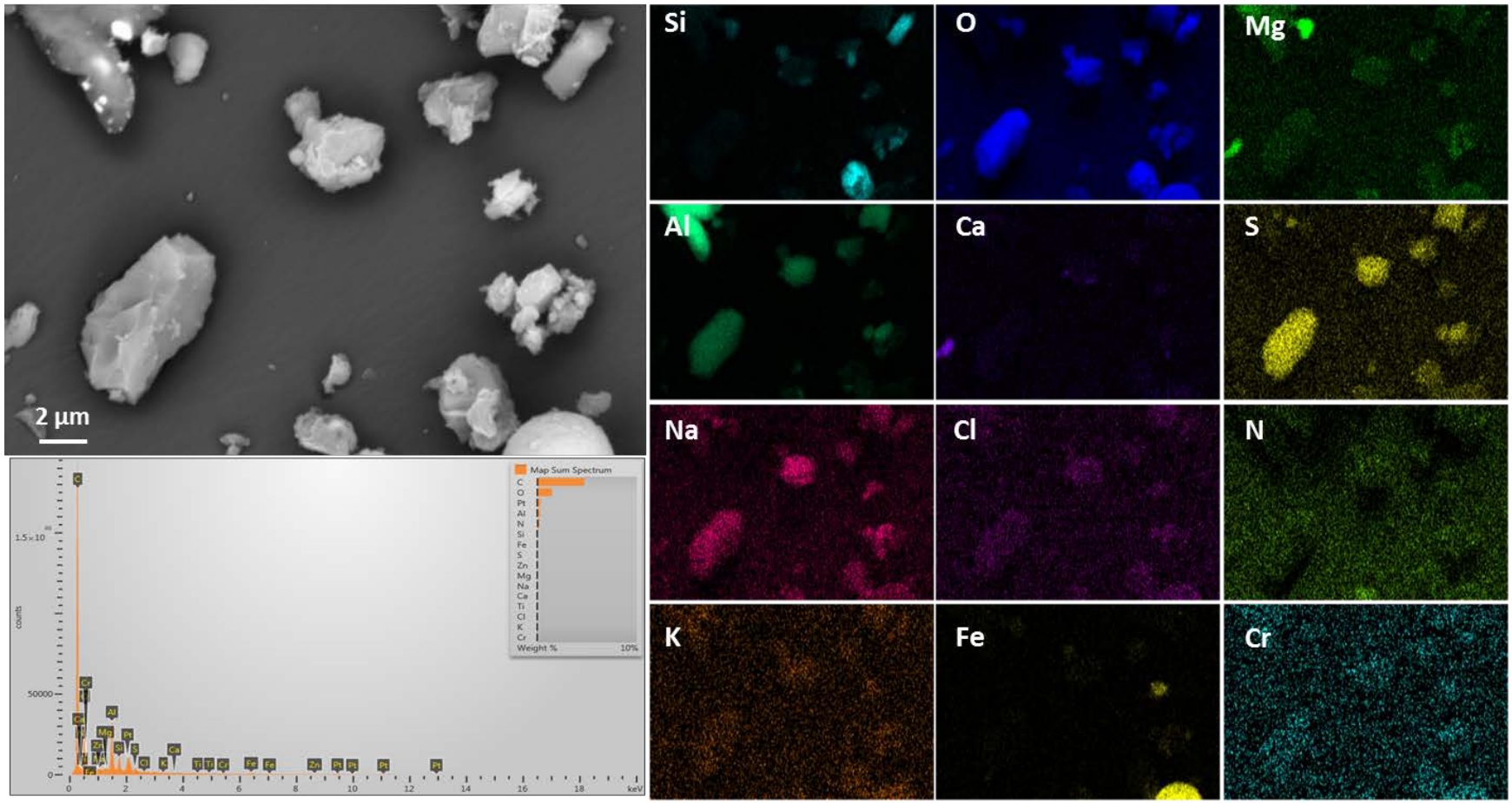

APPENDIX B: XRF DATA

XRF data for the Hope Creek and Diablo Canyon dust samples are discussed in Section 3.2, and a subset of the results is presented. This appendix contains the complete suite of analyses collected for these samples, allowing the reader to better evaluate the representativeness of the results provided in Section 3.2.

Sample: Pad Blank

micro-XRF for: **Blank** "XRF Spectrum"

Scan Area
22mm x 8mm (Width x Height)
31min scan (deviation depends on detector dead time)

Full Spectrum (5cps/eV)

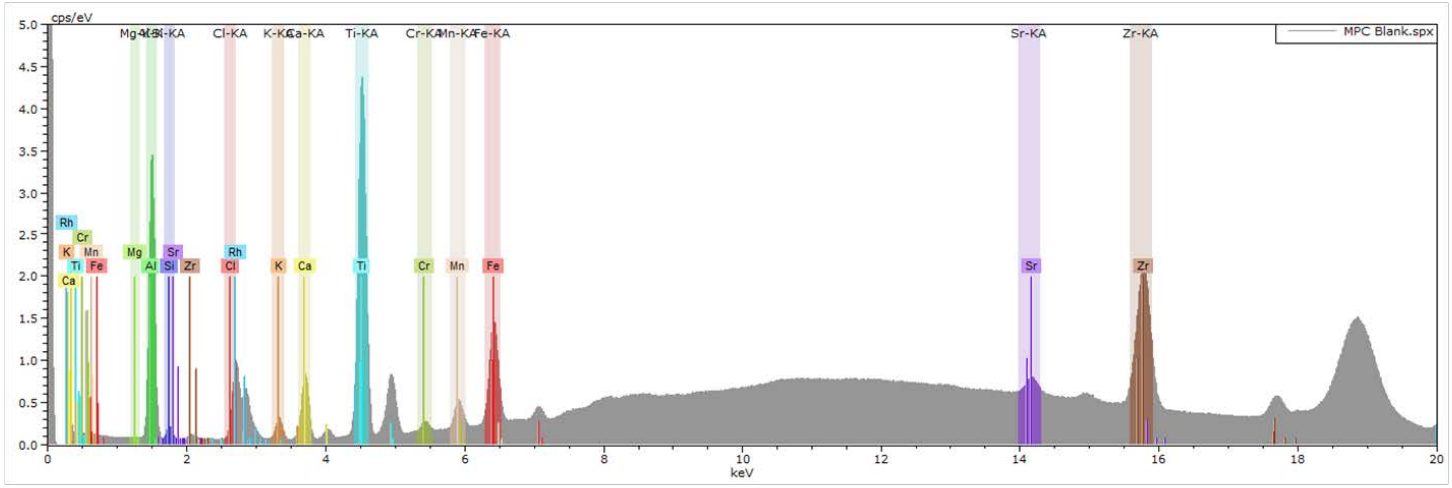

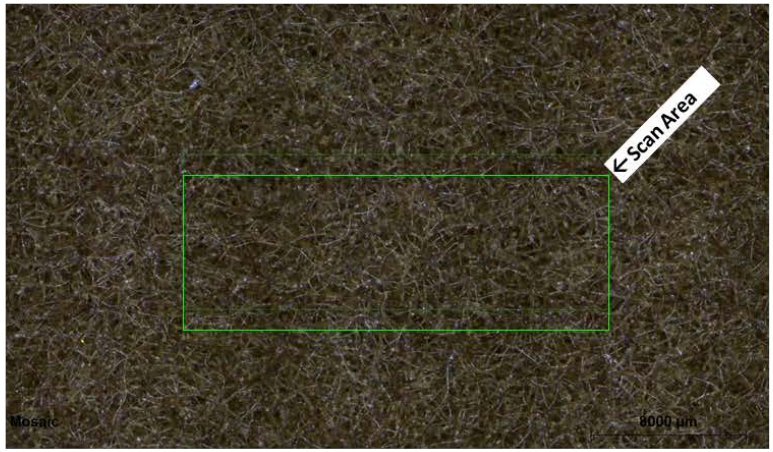

Semi-Quantitative Results

Element	AN	Net	norm. C. [wt.%]	Atom C. [at.%]	Error (1 Sigma) [wt.%]
Chlorine	17	35754	1.77	1.53	0.00
Aluminium	13	415926	70.32	80.14	0.13
Silicon	14	17743	3.19	3.49	0.00
Titanium	22	867811	11.36	7.29	0.00
Zirconium	40	626056	4.97	1.68	0.00
Calcium	20	142628	3.52	2.70	0.00
Potassium	19	42840	1.92	1.51	0.01
Strontium	38	81396	0.53	0.19	0.01
Manganese	25	72984	0.50	0.28	0.01
Chromium	24	26051	0.22	0.13	0.01
Magnesium	12	343	0.18	0.23	0.01
Iron	26	273307	1.51	0.83	0.01
		Total	**100.00**	**100.00**	

Sample: Hope Creek 387-001

micro-XRF for: **MPC-387-001** "XRF Spectrum"

Scan Area
23mm x 8mm (Width x Height)
31min scan (deviation depends on detector dead time)

Full Spectrum (5cps/eV)

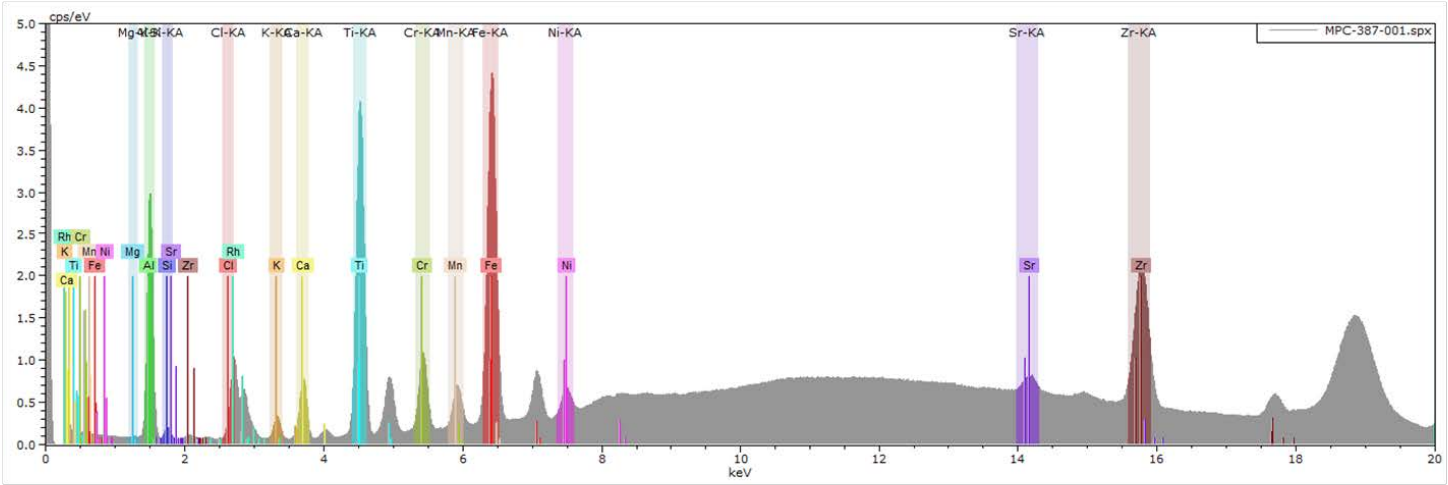

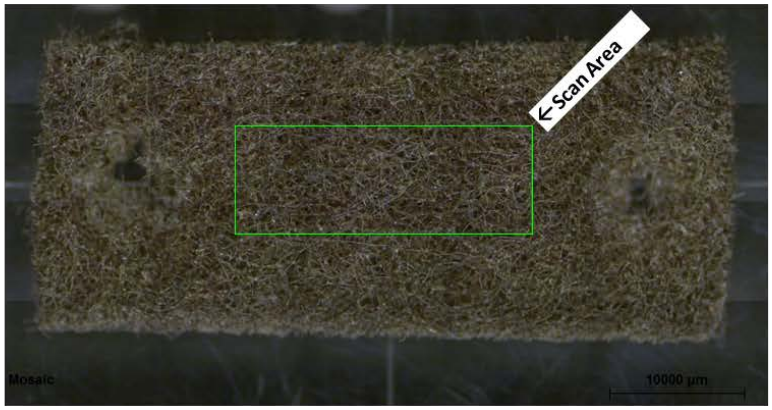

Semi-Quantitative Results

Element	AN	Net	norm. C. [wt.%]	Atom C. [at.%]	Error (1 Sigma) [wt.%]
Chlorine	17	0	0.00	0.00	
Aluminium	13	352582	66.69	78.48	0.12
Silicon	14	16348	2.97	3.36	0.00
Titanium	22	802368	10.53	6.98	0.00
Zirconium	40	628818	5.99	2.08	0.00
Calcium	20	130856	3.23	2.56	0.00
Potassium	19	37315	1.68	1.36	0.01
Rhodium	45	119339	0.00	0.00	
Strontium	38	82321	0.64	0.23	0.01
Manganese	25	86651	0.61	0.35	0.01
Chromium	24	194542	1.67	1.02	0.01
Magnesium	12	407	0.24	0.31	0.01
Iron	26	924817	5.37	3.05	0.00
Nickel	28	82757	0.39	0.21	0.01
		Total	**100.00**	**100.00**	

Sample: Hope Creek 1387-001 vs. Blank

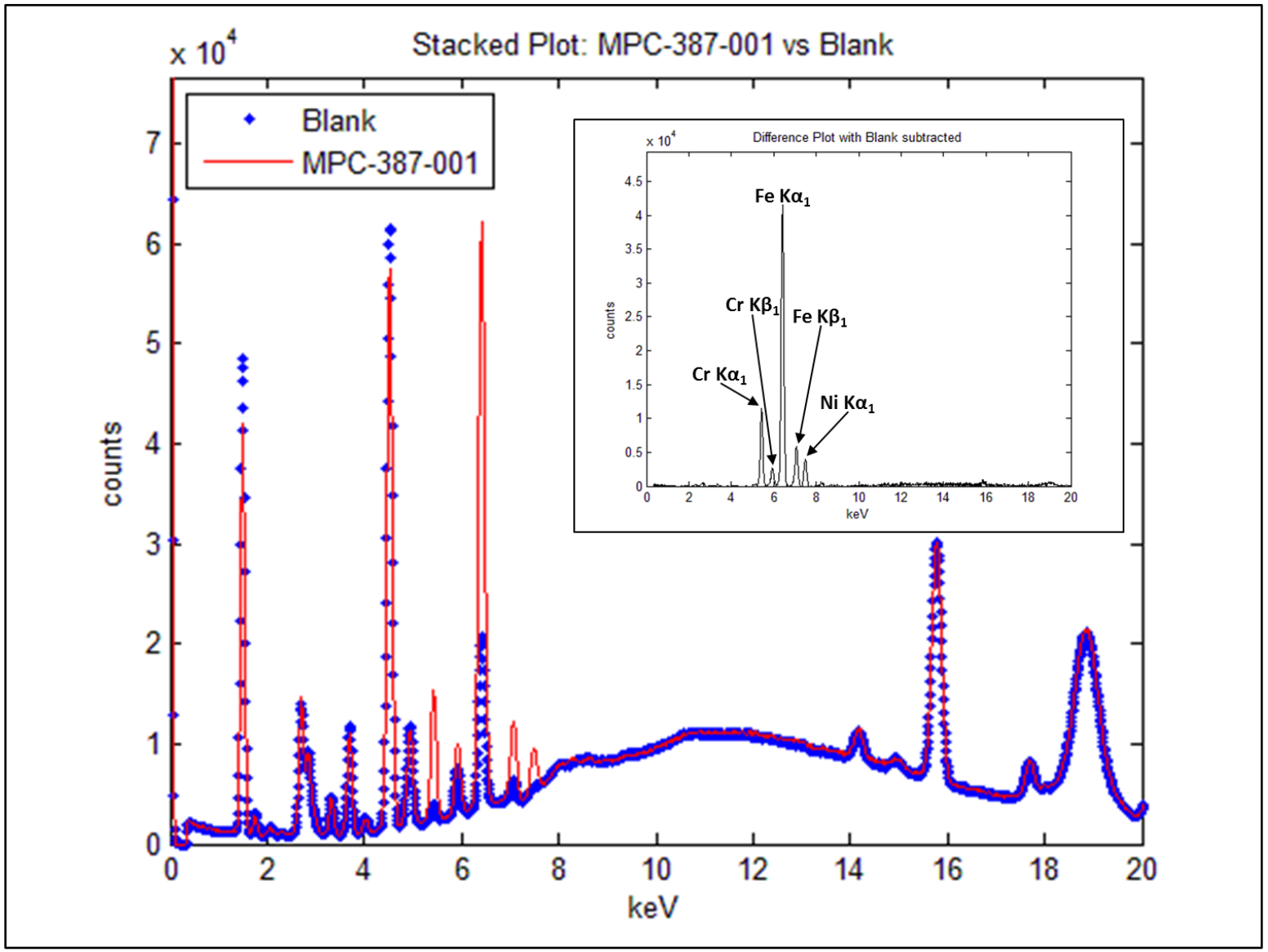

Sample: Hope Creek 387-003

micro-XRF for: **MPC-387-003** "XRF Spectrum"

Scan Area
22mm x 8mm (Width x Height)
31min scan (deviation depends on detector dead time)

Full Spectrum (5cps/eV)

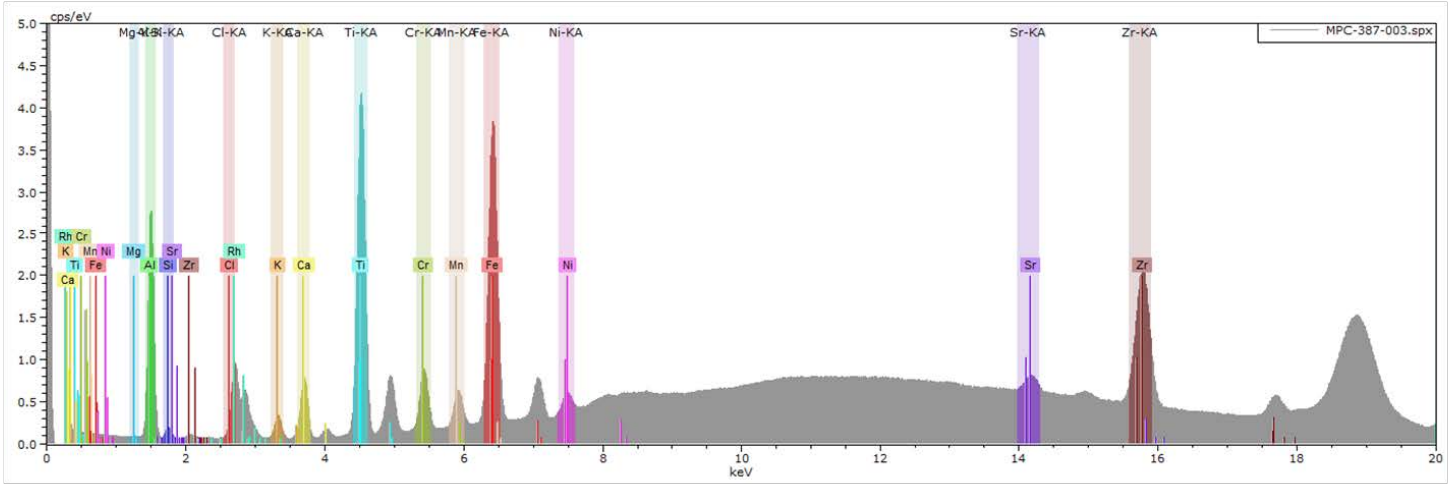

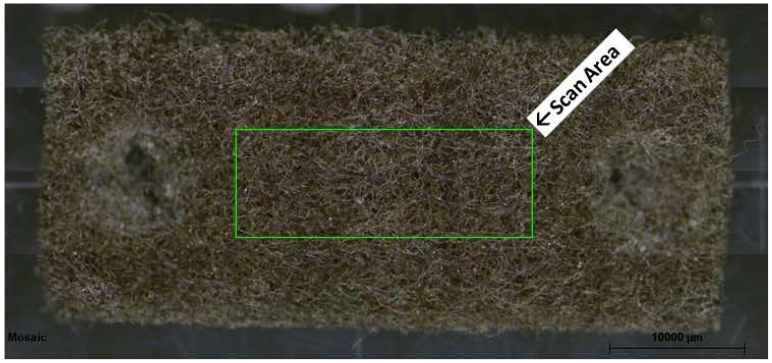

Semi-Quantitative Results

Element	AN	Net	norm. C. [wt.%]	Atom C. [at.%]	Error (1 Sigma) [wt.%]
Chlorine	17	0	0.00	0.00	
Aluminium	13	331541	66.11	77.91	0.10
Silicon	14	16286	3.11	3.53	0.00
Titanium	22	818042	11.44	7.60	0.00
Zirconium	40	594753	5.98	2.09	0.00
Calcium	20	130604	3.42	2.71	0.00
Potassium	19	38589	1.83	1.49	0.01
Rhodium	45	116624	0.00	0.00	
Strontium	38	78945	0.65	0.24	0.01
Manganese	25	76864	0.58	0.34	0.01
Chromium	24	153131	1.42	0.87	0.01
Magnesium	12	305	0.19	0.25	0.01
Iron	26	791129	4.92	2.80	0.00
Nickel	28	65108	0.33	0.18	0.01
		Total	**100.00**	**100.00**	

Sample: Hope Creek 387-003 vs. Blank

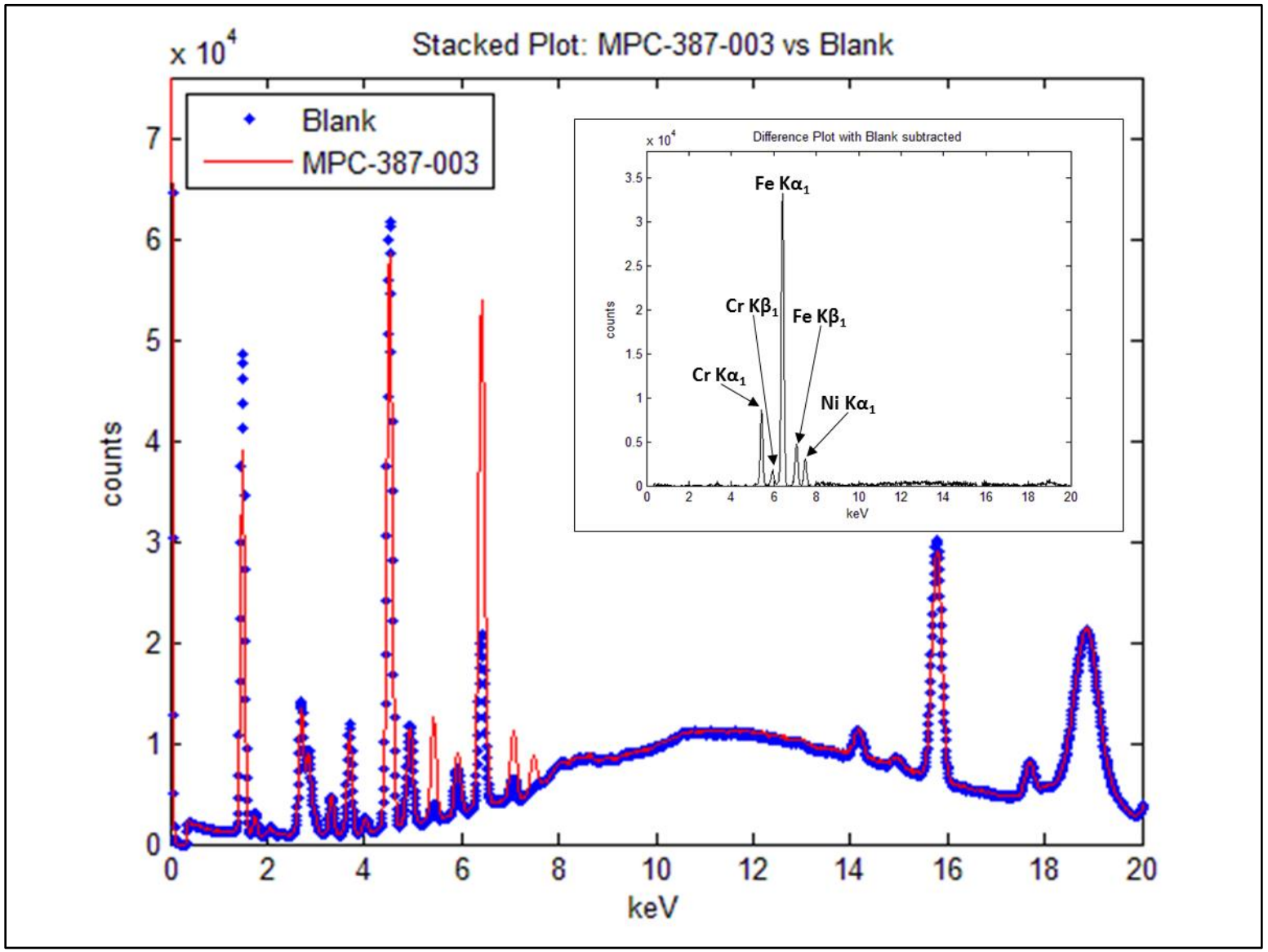

Sample: Hope Creek 387-005

micro-XRF for: **MPC-387-005** "XRF Spectrum"

Scan Area
22mm x 8mm (Width x Height)
31min scan (deviation depends on detector dead time)

Full Spectrum (5cps/eV)

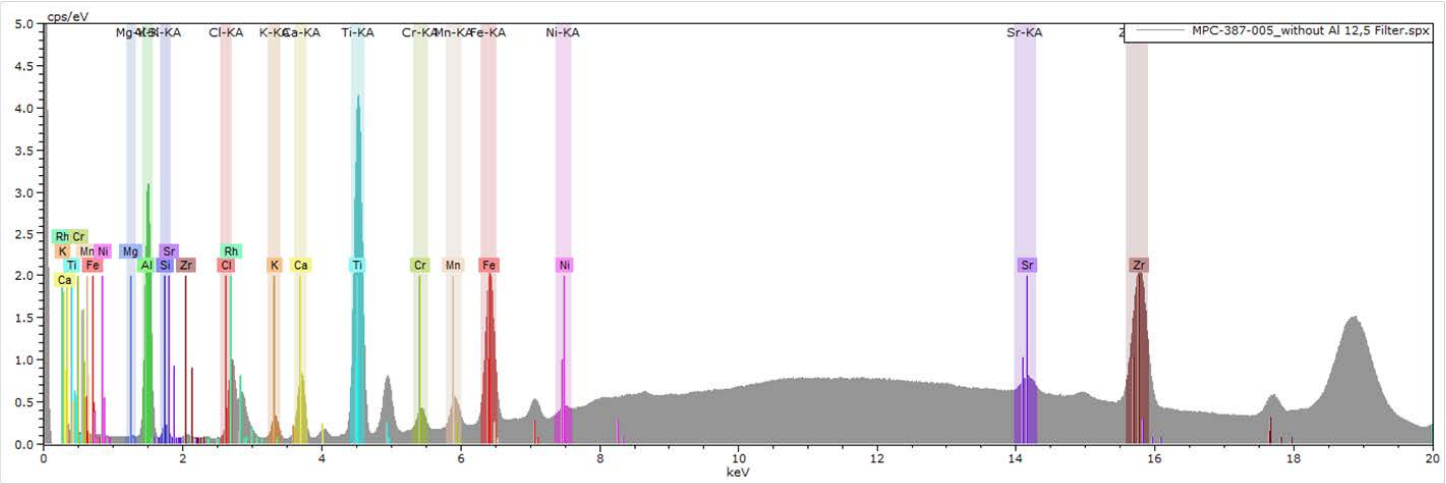

Semi-Quantitative Results

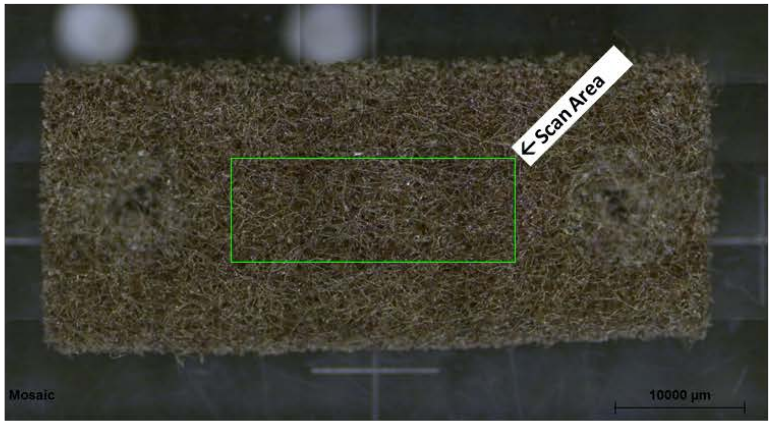

Element	AN	Net	norm. C. [wt.%]	Atom C. [at.%]	Error (1 Sigma) [wt.%]
Chlorine	17	38041	1.98	1.74	0.00
Aluminium	13	366043	67.48	77.87	0.11
Silicon	14	19904	3.71	4.11	0.00
Titanium	22	812294	11.31	7.36	0.00
Zirconium	40	605654	5.36	1.83	0.00
Calcium	20	139735	3.65	2.84	0.00
Potassium	19	43806	2.08	1.65	0.01
Strontium	38	80188	0.58	0.21	0.01
Manganese	25	74463	0.55	0.31	0.01
Chromium	24	58498	0.53	0.32	0.01
Magnesium	12	532	0.30	0.39	0.01
Iron	26	394596	2.34	1.31	0.01
Nickel	28	25793	0.12	0.06	0.01
		Total	**100.00**	**100.00**	

Sample: Hope Creek 387-005 vs. Blank

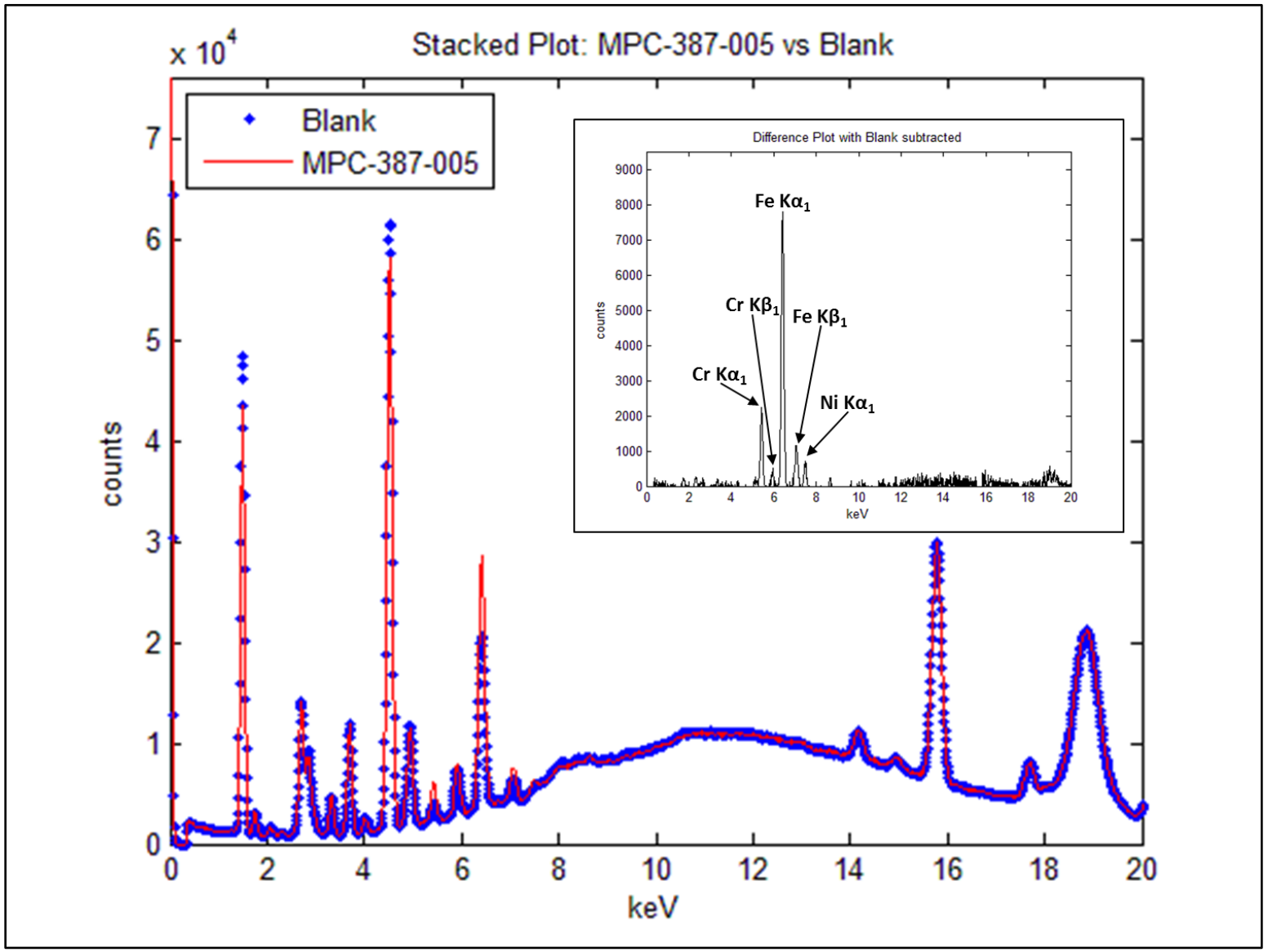

Sample: Hope Creek 387-007

micro-XRF for: **MPC-387-007** "XRF Spectrum"

Scan Area
22mm x 8mm (Width x Height)
31min scan (deviation depends on detector dead time)

Full Spectrum (5cps/eV)

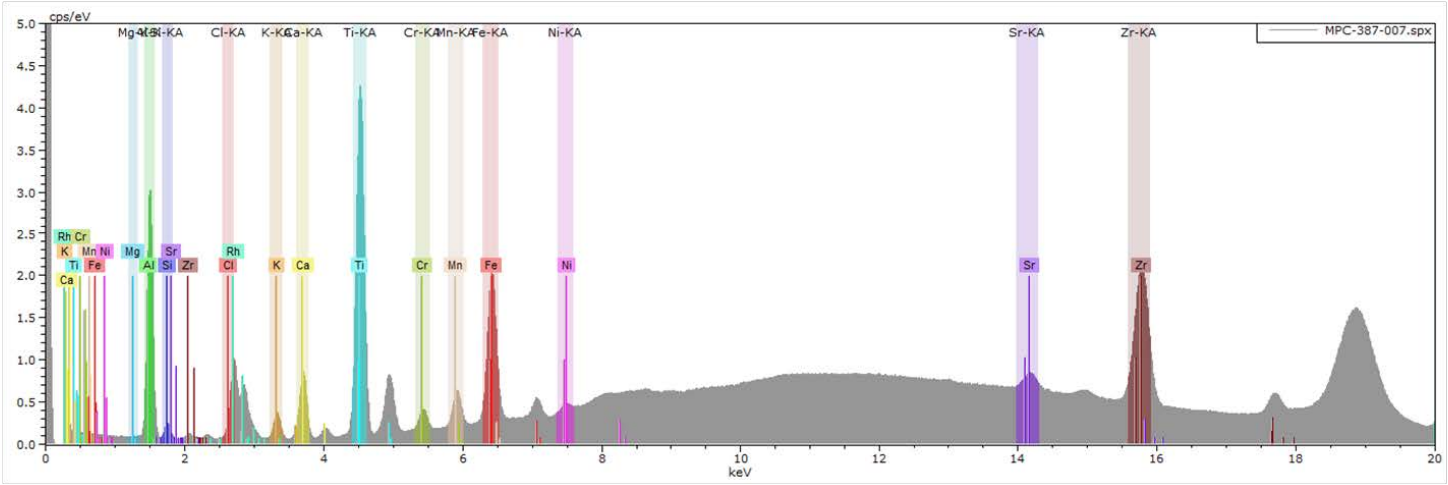

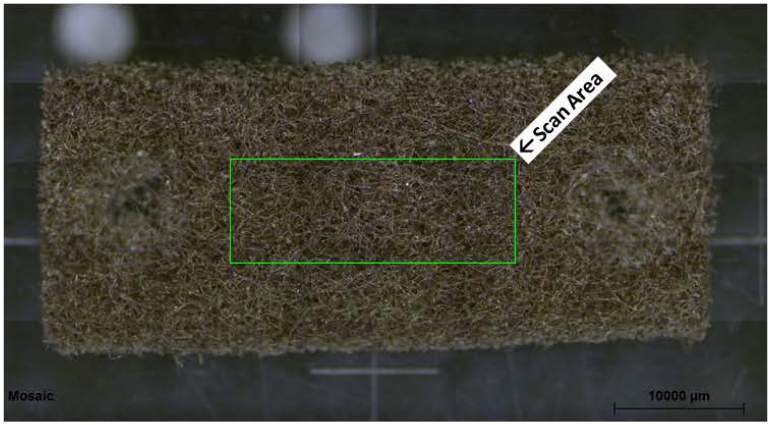

Semi-Quantitative Results

Element	AN	Net	norm. C. [wt.%]	Atom C. [at.%]	Error (1 Sigma) [wt.%]
Chlorine	17	0	0.00	0.00	
Aluminium	13	358795	68.00	78.60	0.11
Silicon	14	21914	4.22	4.68	0.00
Titanium	22	833079	11.82	7.70	0.00
Zirconium	40	608868	5.62	1.92	0.00
Calcium	20	141924	3.77	2.93	0.00
Potassium	19	43955	2.11	1.68	0.00
Rhodium	45	121080	0.00	0.00	
Strontium	38	83257	0.63	0.22	0.01
Manganese	25	90093	0.68	0.39	0.01
Chromium	24	50865	0.48	0.29	0.01
Magnesium	12	227	0.13	0.17	0.01
Iron	26	392426	2.40	1.34	0.01
Nickel	28	28455	0.13	0.07	0.01
		Total	**100.00**	**100.00**	

Sample: Hope Creek 387-007 vs. Blank

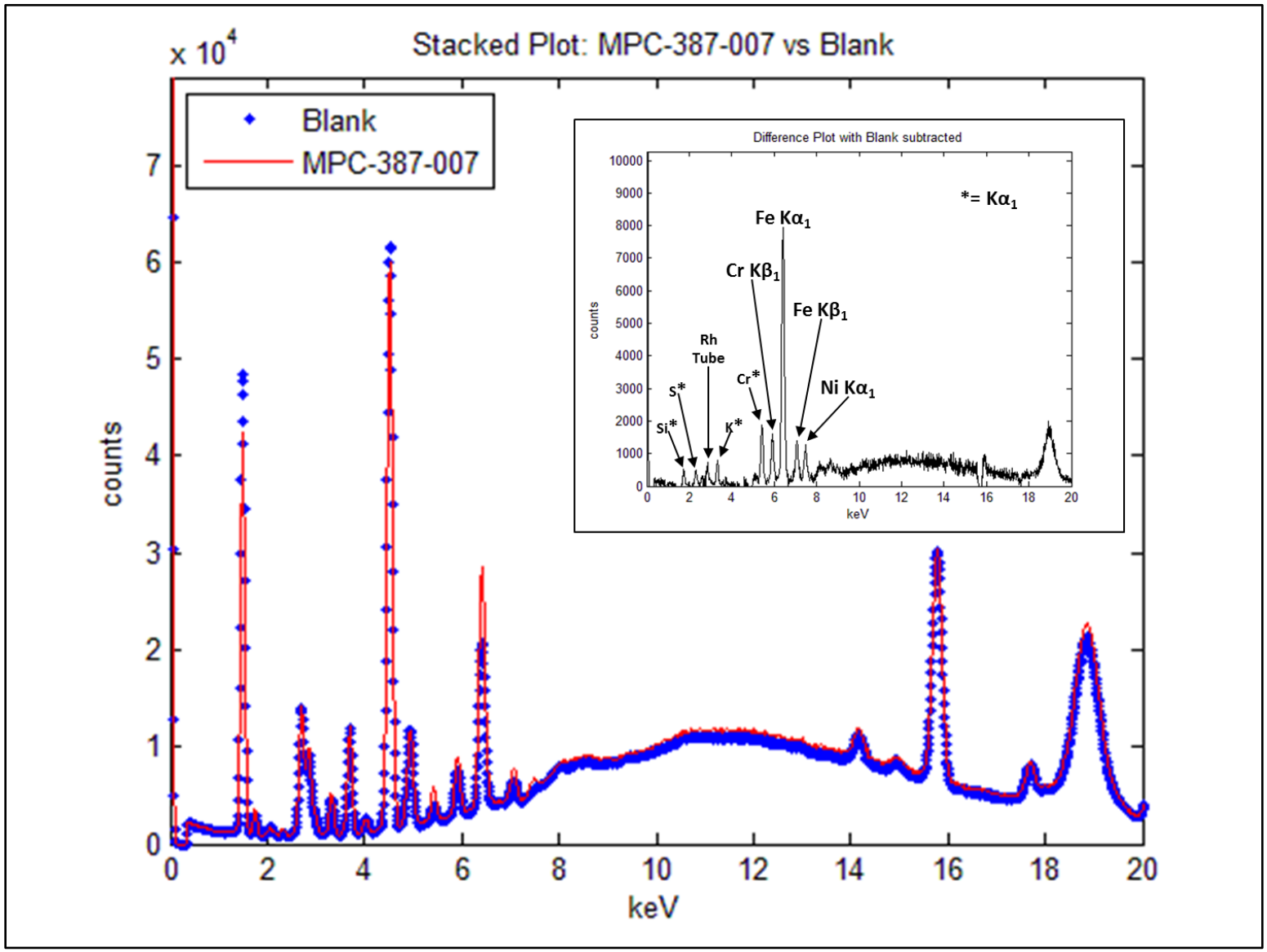

Sample: Hope Creek 387-009

micro-XRF for: **MPC-387-009** "XRF Spectrum"

Scan Area
22mm x 8mm (Width x Height)
31min scan (deviation depends on detector dead time)

Full Spectrum (5cps/eV)

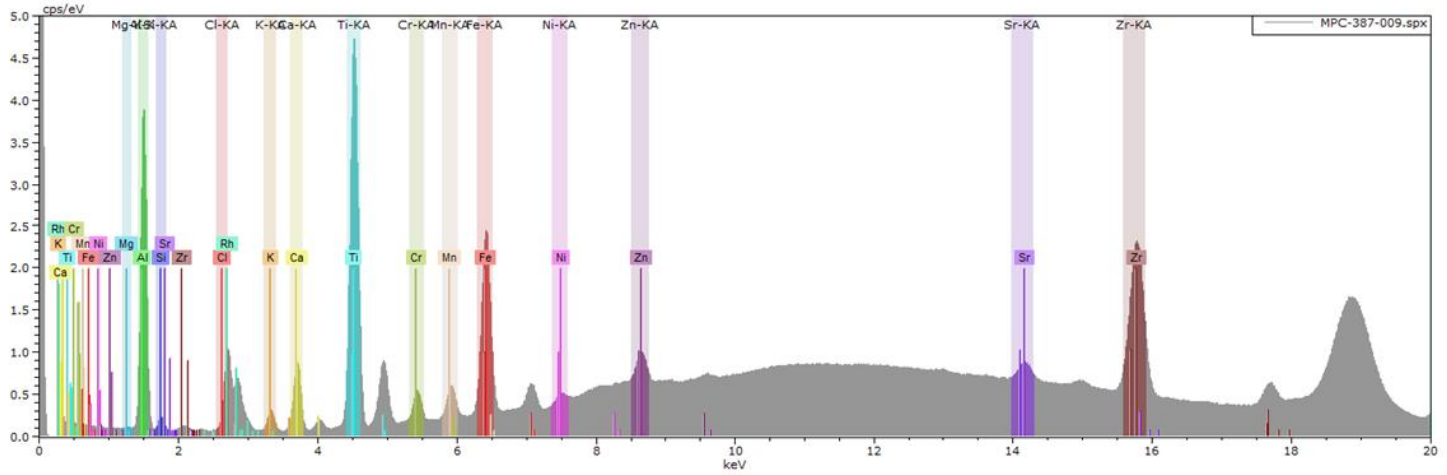

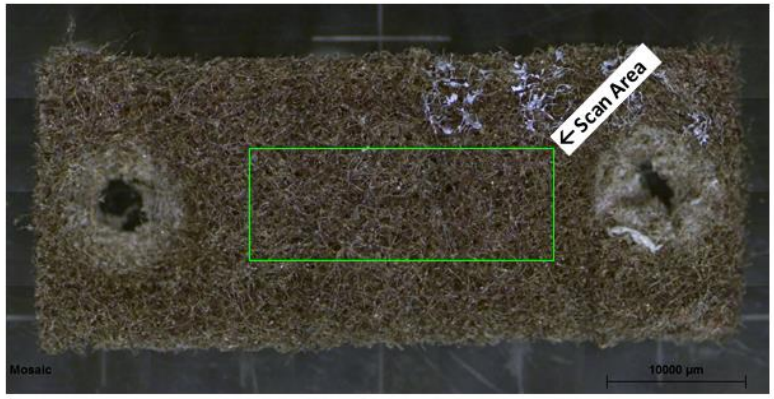

Semi-Quantitative Results

Element	AN	Net	norm. C. [wt.%]	Atom C. [at.%]	Error (1 Sigma) [wt.%]
Chlorine	17	0	0.00	0.00	
Aluminium	13	464376	72.32	82.25	0.18
Silicon	14	17489	2.91	3.17	0.00
Titanium	22	921195	10.61	6.80	0.00
Zirconium	40	672338	4.95	1.67	0.00
Calcium	20	147307	3.21	2.46	0.00
Potassium	19	32554	1.30	1.02	0.01
Rhodium	45	129065	0.00	0.00	
Strontium	38	86439	0.53	0.18	0.01
Manganese	25	78371	0.48	0.27	0.01
Chromium	24	77559	0.58	0.34	0.01
Magnesium	12	477	0.23	0.29	0.01
Iron	26	490319	2.40	1.32	0.01
Nickel	28	34566	0.13	0.07	0.01
Zinc	30	109790	0.37	0.17	0.01
		Total	**100.00**	**100.00**	

Sample: Hope Creek 387-009 vs. Blank

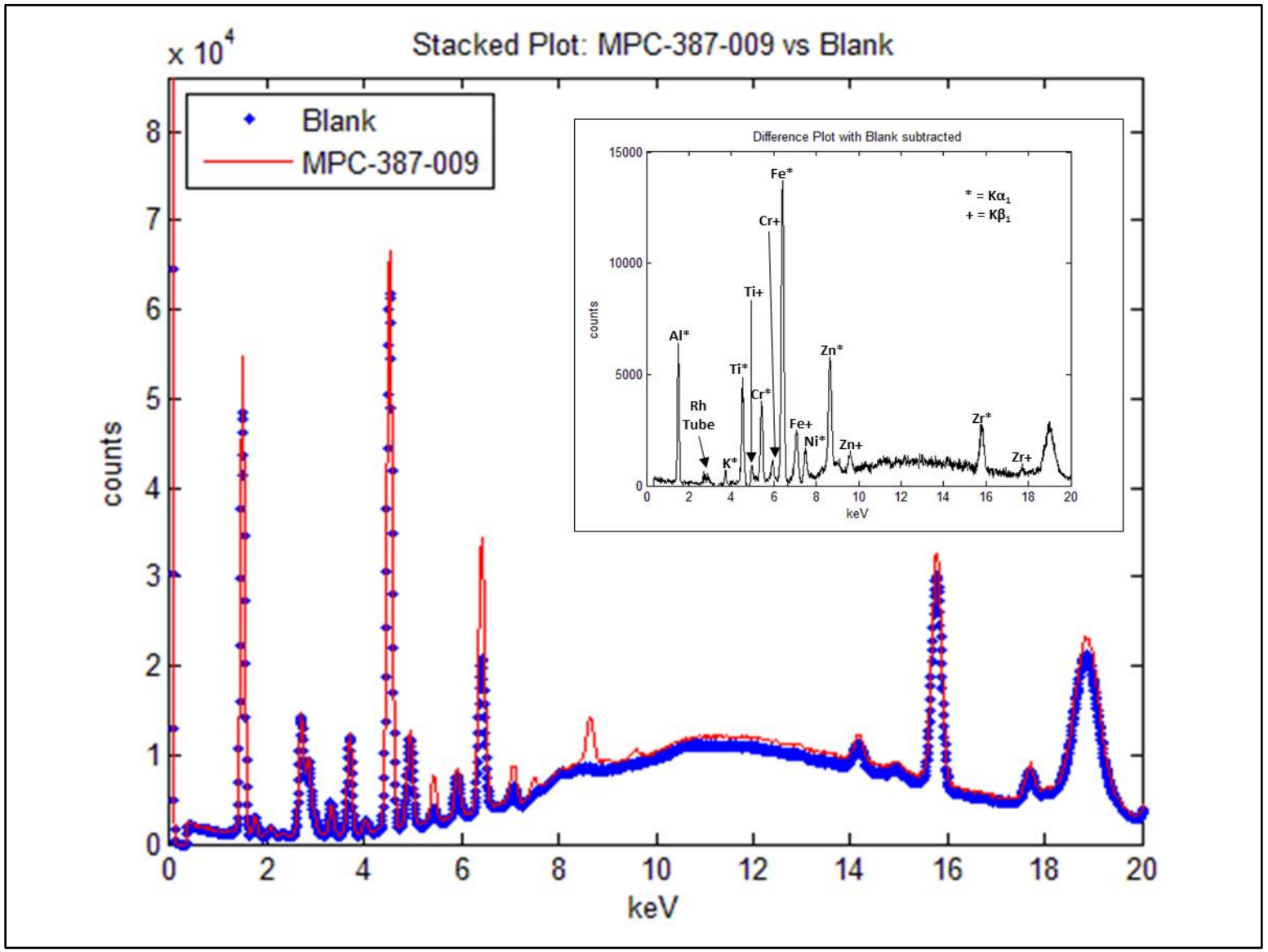

Distribution

1 Keith Waldrop (electronic copy)
Used Fuel and HLW Management Program
Electric Power Research Institute
1300 West WT Harris Blvd.
Charlotte, NC 28262

1 John Kessler (electronic copy)
Manager, Used Fuel and HLW Management Program
Electric Power Research Institute
1300 West WT Harris Blvd.
Charlotte, NC 28262

1 Shannon Chu (electronic copy)
Senior Technical Leader, Spent Fuel and High Level Waste
Electric Power Research Institute
3420 Hillview Avenue.
Palo Alto, CA 94304

1 Ned Larson (electronic copy)
M/S NSF 165, Room B119
U.S. Department of Energy
232 Energy Way
North Las Vegas, NV 89030

1	MS0115	OFA/NFE Agreements	10012
1	MS0736	P. Swift	6220 (electronic copy)
1	MS0747	K. Sorenson	6223 (electronic copy)
1	MS0779	S. Saltzstein	6225 (electronic copy)
1	MS0899	Technical Library	9536 (electronic copy)


Sandia National Laboratories